

การสังเคราะห์สารประกอบกลูตาไทโอน-/กรดลิพอิก-พอร์เฟรินเพื่อเป็นสารต้านออกซิเดชันชนิดใหม่
ที่เข้ากันได้ทางชีวภาพ



บทคัดย่อและแฟ้มข้อมูลฉบับเต็มของวิทยานิพนธ์ตั้งแต่ปีการศึกษา 2554 ที่ให้บริการในคลังปัญญาจุฬาฯ (CUIR)
เป็นแฟ้มข้อมูลของนิสิตเจ้าของวิทยานิพนธ์ ที่ส่งผ่านทางบัณฑิตวิทยาลัย

The abstract and full text of theses from the academic year 2011 in Chulalongkorn University Intellectual Repository (CUIR)
are the thesis authors' files submitted through the University Graduate School.

วิทยานิพนธ์นี้เป็นส่วนหนึ่งของการศึกษาตามหลักสูตรปริญญาวิทยาศาสตรดุษฎีบัณฑิต

สาขาวิชาเคมี ภาควิชาเคมี

คณะวิทยาศาสตร์ จุฬาลงกรณ์มหาวิทยาลัย

ปีการศึกษา 2559

ลิขสิทธิ์ของจุฬาลงกรณ์มหาวิทยาลัย

SYNTHESIS OF GLUTATHIONE-/LIPOIC ACID-
PORPHYRIN COMPOUNDS AS NOVEL BIOCOMPATIBLE ANTIOXIDANTS

Mr. Apiratt Thitimon



A Dissertation Submitted in Partial Fulfillment of the Requirements
for the Degree of Doctor of Philosophy Program in Chemistry

Department of Chemistry

Faculty of Science

Chulalongkorn University

Academic Year 2016

Copyright of Chulalongkorn University

อภิรัตน์ ฐิติมัน : การสังเคราะห์สารประกอบกลูตาไทโอน-/กรดลิโปอิก-พอร์ไฟรินเพื่อเป็นสารต้านออกซิเดชันชนิดใหม่ที่เข้ากันได้ทางชีวภาพ (SYNTHESIS OF GLUTATHIONE- / LIPOIC ACID- PORPHYRIN COMPOUNDS AS NOVEL BIOCOMPATIBLE ANTIOXIDANTS) อ.ที่ปรึกษาวิทยานิพนธ์หลัก: ผศ. ดร.โรจน์ฤทธิ์ โรจนธเนศ, อ.ที่ปรึกษาวิทยานิพนธ์ร่วม: รศ. ดร.พัชณิดา ธรรมยงค์กิจ, 131 หน้า.

อนุพันธ์ของสารประกอบพอร์ไฟรินซึ่งต่อกับกรดลิโปอิกที่ละลายน้ำได้ชนิดใหม่และสารประกอบเชิงซ้อนแมงกานีสของสารประกอบนี้ถูกสังเคราะห์สำเร็จด้วยใช้ปฏิกิริยาการเกิดเอไมด์เป็นหลัก ได้ผลิตภัณฑ์ P-4Lp และ Mn-P-4Lp ที่ต้องการจากสารตั้งต้นที่สามารถหาซื้อได้ในร้อยละผลผลิตเท่ากับ 5 และ 4 ตามลำดับ สารประกอบชนิดใหม่ทั้งหมดถูกพิสูจน์เอกลักษณ์ของด้วยเทคนิคนิวเคลียร์แมกเนติกเรโซแนนซ์ สเปกโทรสโคปี และแมสสเปกโทรเมทรี สมบัติทางกายภาพเชิงแสงของสารประกอบตรวจสอบด้วยเทคนิคยูวี-วิสิเบิล และฟลูออเรสเซนส์สเปกโทรโฟโตเมทรี จากการทดสอบหาความเป็นพิษในเซลล์ ความเข้มข้นของ P-4Lp และ Mn-P-4Lp ที่ออกฤทธิ์ยับยั้งการเจริญเติบโตของเซลล์ได้ร้อยละ 50 ของ มีค่าอยู่ในช่วง 50 ถึง 100 มิลลิกรัมต่อลิตร และมากกว่า 150 มิลลิกรัมต่อลิตร ในเซลล์ HaCaT และ HDFa ตามลำดับ ดังนั้นผลิตภัณฑ์ทั้งสองจึงจัดเป็นสารที่มีความเป็นพิษต่ำ อย่างไรก็ตาม จากการทดสอบฤทธิ์การต้านออกซิเดชันของสารประกอบนี้ไม่ปรากฏในเซลล์ทั้งสองชนิด นอกเหนือจากนั้น การประเมินผลในไมโทคอนเดรียเป้าหมายบ่งชี้ว่าอนุพันธ์ของสารประกอบพอร์ไฟรินเป้าหมายสามารถถูกสะสมอย่างจำเพาะในไมโทคอนเดรียของเซลล์ HaCaT ได้

ภาควิชา เคมี
สาขาวิชา เคมี
ปีการศึกษา 2559

ลายมือชื่อนิสิต

ลายมือชื่อ อ.ที่ปรึกษาหลัก

ลายมือชื่อ อ.ที่ปรึกษาร่วม

5373930323 : MAJOR CHEMISTRY

KEYWORDS: WATER SOLUBLE PORPHYRIN / LIPOIC ACID / CYTOTOXICITY / ANTIOXIDANT ACTIVITY / MITOCHONDRIAL TARGETING COMPOUND

APIRATT THITIMON: SYNTHESIS OF GLUTATHIONE-/LIPOIC ACID-PORPHYRIN COMPOUNDS AS NOVEL BIOCOMPATIBLE ANTIOXIDANTS. ADVISOR: ASST. PROF. ROJRIT ROJANATHANES, Ph.D., CO-ADVISOR: ASSOC. PROF. PATCHANITA THAMYONGKIT, Dr.rer.nat., 131 pp.

A novel water-soluble porphyrin derivative bearing lipoic acid and manganese complex of this compound were successfully synthesized based primarily on the amidation reaction. The desired products, P-4Lp and Mn-P-4Lp, were achieved in the overall yields of 5% and 4% respectively from commercially available starting material. All new compounds were characterized by NMR spectroscopy and mass spectrometry. Their optical properties were also investigated by UV-visible and fluorescence spectrophotometry. According to cell cytotoxicity test, IC_{50} of P-4Lp and Mn-P-4Lp were found in the range of 50 to 100 mg/L and more than 150 mg/L against HaCaT and HDFa cells, respectively. Thus, both products were considered to be low cytotoxicity compounds. However, based on the antioxidant activity test, no antioxidant activity of these compounds in both kinds of cells was observed. In addition, mitochondria targeting evaluation suggested that the target porphyrin derivatives exhibited accumulation specifically in the mitochondria of the HaCaT cells.

Department: Chemistry

Field of Study: Chemistry

Academic Year: 2016

Student's Signature

Advisor's Signature

Co-Advisor's Signature

ACKNOWLEDGEMENTS

Firstly, I would like to express my deepest gratitude to my supervisors, Assistant Professor Dr. Rojrit Rojanathanes and my co-advisor, Associate Professor Dr. Patchanita Thamyomgkit for the continuous support, excellent guidances, stimulation, helpful discussions, valuable suggestions and providing me with an excellent atmosphere for doing research and writing of this thesis and also Assistant Professor Dr. Amornpun Sereemasapun, MD for his guidance and suggestions in medical data analysis. Without these persons I could not reach my goal.

Secondly, my appreciation is given to Assoc. Prof. Dr. Vudhichai Parasuk, for serving as the chairman, Assistant Professor Dr. Puttaruksa Varanusupakul and Assistant Professor Dr. Anawat Ajavakom by serving as members of thesis defense committee. Thank you for their kind attentions and advices in this thesis. I gratefully thank Assistant Professor Dr. Vachiraporn Ajavakom, the external examiner from Ramkhamhaeng University for her kind suggestions and many useful remarks.

My sincere thanks to the development and promotion of science and technology talents project (DPST) scholarship for their financial support of my entire Ph.D. study.

In addition, I would like to thank my fellow labmates: Dr. Pornpat Samang, Miss Sucheera Modsiri, Miss Prapinporn Pongmaneerata, Miss. Duangkamon Kaewwichit, Miss. Supranee Watpathomsub, Miss Sumana Sriputtirat and all those others that have not been mentioned above. They have always been hugely supportive and encouraging me with their best wishes.

Finally, my heartfelt thanks to my family for their moral principal, love, care and supporting me spiritually throughout my life.

CONTENTS

	Page
THAI ABSTRACT.....	iv
ENGLISH ABSTRACT.....	v
ACKNOWLEDGEMENTS	vi
CONTENTS.....	vii
LIST OF FIGURES.....	xi
LIST OF SCHEMES.....	xv
LIST OF ABBREVIATIONS	xvi
CHAPTER I INTRODUCTION	20
1.1 Objective of Research.....	21
1.2 Scope of Research.....	21
CHAPTER II THEORY AND LITERATURE REVIEWS	23
2.1 Free radical.....	23
2.1.1 The Oxidation of Protein.....	23
2.1.2 Oxidation of membrane lipids	24
2.1.3 Oxidation of DNA.....	25
2.2 Antioxidant	25
2.3 Glutathione (GSH)	26
2.4 Literature review on glutathione derivatives	28
2.5 Lipoic acid (LA)	29
2.6 Literature review on LA derivatives.....	32
2.7 Porphyrins.....	33
2.8 Structural Modifications of Porphyrins.....	35

	Page
2.9 Role of porphyrin derivatives as an antioxidant agent	36
2.10 Literature review on porphyrin derivatives.....	36
2.11 Detection of Biological Activities.....	39
2.11.1 Cytotoxicity test.....	39
2.11.2 ROS generation assay	40
2.11.3 Mitochondria targeting evaluation	42
CHAPTER III EXPERIMENT	44
3.1 Chemicals.....	44
3.2 Instrumentation	46
3.3 Chromatographic System	46
3.4 Synthesis of Porphyrin derivatives and Characterizations.....	47
3.4.1 Synthesis of 5-(4-hydroxyphenyl)-10,15,20-tris(4-pyridyl)porphyrin (P1)....	47
3.4.2 Synthesis of 5-(4-(4-chlorobutoxy)phenyl)-10,15,20-tris(4-pyridyl)porphyrin (P2).....	48
3.4.3 Synthesis of P-Glu1	49
3.4.4 Synthesis of P-Glu2	50
3.4.5 Synthesis of 5,10,15,20-Tetrakis(4-pyridyl)porphyrin (P3).....	51
3.4.6 Synthesis of 5,10,15,20-Tetrakis(4-N-(4-chlorobutyl)-pyridyl)porphyrin (P4).....	52
3.4.7 Synthesis of P-Glu3	53
3.4.8 Synthesis of tert-Butyl-N-(2-bromoethyl)carbamate (1).....	54
3.4.9 Synthesis of 5,10,15,20-tetrakis(4-N-(2-aminoethyl)-pyridyl)porphyrin bromide (P5).....	55
3.4.10 Synthesis of Lipoic acid anhydride.....	56

	Page
3.4.11 Synthesis of 5, 10, 15, 20-tetrakis(4-N-(N-Lipoyl-2-aminoethyl)pyridyl)porphyrin bromide (P-4Lp).....	57
3.4.12 Synthesis of Mn(II)-5,10,15,20-tetrakis(4-N-(N-Lipoyl-2-aminoethyl)pyridyl)porphyrin bromide (Mn-P-4Lp)	58
3.4.13 Synthesis of 5,10,15,20-tetrakis(4-N-methyl-pyridyl)porphyrin iodide (TMPyP).....	59
3.5 Biological studies of Porphyrin derivatives.....	60
3.5.1 Cell culture	60
3.5.2 Cytotoxicity test (cell viability assay).....	60
3.5.3 Antioxidant Activity (ROS generation assay).....	60
3.5.4 Mitochondria targeting evaluation.....	61
3.5.5 Statistical analysis.....	61
CHAPTER IV RESULTS AND DISCUSSION.....	62
4.1 Synthesis of Porphyrin derivatives and Characterizations.....	63
4.1.1 Synthesis of glutathione-porphyrin derivatives P-Glu1 and P-Glu2.....	63
4.1.2 Synthesis of glutathione-porphyrin derivative P-Glu3	65
4.1.3 Synthesis of lipoic acid-porphyrin derivatives P-4Lp and Mn-P-4Lp.....	68
4.2 Biological studies of Porphyrin derivatives.....	74
4.2.1 Cytotoxicity	74
4.2.2 Antioxidant Activity	81
4.2.2.1 ROS generation in the HDFa cells.....	82
4.2.2.2 ROS generation in the HaCaT cells.....	89
4.2.3 Mitochondria targeting evaluation.....	97
CHAPTER V CONCLUSION.....	99

	Page
REFERENCES.....	100
APPENDIX	109
VITA	131



LIST OF FIGURES

	Page
Figure 1.1: The structure of the target porphyrinic derivatives	22
Figure 2.1: Peptide bond cleavage by the (a) diamide and (b) alpha-amidation pathways.....	24
Figure 2.2: Mechanism of lipid peroxidation.....	25
Figure 2.3: The chemical structure of glutathione	26
Figure 2.4: The reversible process of GSH and GSSG.....	27
Figure 2.5: Antioxidant process of glutathione	27
Figure 2.6: Nucleophilic substitution of a thiol group in glutathione	28
Figure 2.7: Esterification of a carboxyl group of glutathione	28
Figure 2.8: Acylation and selective deacylation of glutathione	29
Figure 2.9: The chemical structure of LA	30
Figure 2.10: The chemical structure of R and S lipoic acid.....	30
Figure 2.11: The reversible process of oxidized and reduced forms of LA	30
Figure 2.12: Dynamic roles of LA in regeneration of glutathione	31
Figure 2.13: The chemical structure of indole-lipoic acid derivatives	32
Figure 2.14: The structure of coumarin–lipoic acid conjugates.....	32
Figure 2.15: The chemical structure of the hybrid compound between lipoic acid and derivative of chroman moiety of vitamin E	33
Figure 2.16: The structure of porphyrin (porphine).....	34
Figure 2.17: Typical UV-Vis absorption spectrum of the porphyrin.....	34
Figure 2.18: Structure of metalloporphine	35
Figure 2.19: The structure of natural metalloporphyrins.....	35

Figure 2.20: Structures of meso- and beta-substituted porphyrins.....	36
Figure 2.21: The synthesis pathway of meso-substituted porphyrin by Adler and Longo method.....	37
Figure 2.22: the molecular Structures of TMPyP	37
Figure 2.23: the molecular Structures of P1	38
Figure 2.24: (A) the molecular structure of Mn-porphyrin-oligopeptide compound and (B) Scavenging ability of manganese superoxide dismutase.....	39
Figure 2.25: Conversion of resazurin to resorufin by reducing environment within viable cell.....	40
Figure 2.26: Formation of fluorescent Compound DCF by ROS in cell.....	42
Figure 2.27: (A) The structure of JC-1 dye, (B) Estimated formation of JC-1 J-aggregate and (C) The color of JC-1 dye as a green-fluorescent monomer at cytoplasm and as a red-fluorescent J-aggregate within the mitochondria in cultured human pre-adipocytes cells.....	43
Figure 4.1: Structure of glutathione-/lipoic acid-porphyrin derivatives.....	62
Figure 4.2: ¹ H-NMR spectrum of compound P3	66
Figure 4.3: ¹ H-NMR spectrum of compound P3 and P4	67
Figure 4.4: ¹ H-NMR spectrum of compound P3 and P5	70
Figure 4.5: ¹ H-NMR spectrum of compound P-4Lp	71
Figure 4.6: (A) Normalized UV-Vis absorption spectra of Mn-P-4Lp and P-4Lp , (B) emission spectra of Mn-P-4Lp and P-4Lp	72
Figure 4.7: ¹ H-NMR spectrum of TMPyP	73
Figure 4.8: Cell viability upon the treatment of HDFa cell with (A) LA , (B) TMPyP , (C) P-4Lp , (D) Mn-P-4Lp at 25, 50, 100, 150 mg/L. (“***” indicates p < 0.001, “*” indicates p < 0.05, significant differences between control and each treatment group).....	75

Figure 4.9: Cell viability upon the treatment of HaCaT cell with (A) LA , (B) TMPyP , (C) P-4Lp , (D) Mn-P-4Lp at 25, 50, 100, 150 mg/L. (“***” indicates $p < 0.001$, “*” indicates $p < 0.05$, significant differences between control and each treatment group).....	78
Figure 4.10: Formation of fluorescent Compound DCF by H_2O_2 in cell.	81
Figure 4.11: ROS generation observed in the HDFa cells upon the treatment of DMEM and LA at the concentration of 25 and 50 mg/L for 24 h then HDFa cells was treated with H_2O_2 for 0, 10, 20, 30, 40, 50 and 60 min.....	82
Figure 4.12: ROS generation observed in the HDFa cells upon the treatment of DMEM and TMPyP at the concentration of 25 and 50 mg/L for 24 h then HDFa cells was treated with H_2O_2 for 0, 10, 20, 30, 40, 50 and 60 min.....	83
Figure 4.13: ROS generation observed in the HDFa cells upon the treatment of DMEM and P-4Lp at the concentration of 25 and 50 mg/L for 24 h then HDFa cells was treated with H_2O_2 for 0, 10, 20, 30, 40, 50 and 60 min.....	83
Figure 4.14: ROS generation observed in the HDFa cells upon the treatment of DMEM and Mn-P-4Lp at the concentration of 25 and 50 mg/L for 24 h then HDFa cells was treated with H_2O_2 for 0, 10, 20, 30, 40, 50 and 60 min (“***” indicates $p < 0.001$, “**” indicates $p < 0.01$ and “*” indicates $p < 0.05$).....	84
Figure 4.15: The ROS generation observed in the HDFa cells upon the treatment with LA and P-Lp at the concentration of (A) 25 mg/L and (B) 50 mg/L for 24 h, followed by the treatment with H_2O_2 for 0, 10, 20, 30, 40, 50 and 60 min.	85
Figure 4.16: The ROS generation observed in the HDFa cells upon the treatment with TMPyP and P-Lp at the concentration of (A) 25 mg/L and (B) 50 mg/L for 24 h, followed by the treatment with H_2O_2 for 0, 10, 20, 30, 40, 50 and 60 min.....	86
Figure 4.17: ROS generation observed in the HDFa cells upon the treatment of P-4Lp and Mn-P-4Lp at the concentration of 25 mg/L (A) and 50 mg/L (B) for 24 h then HDFa cells was treated with H_2O_2 for 0, 10, 20, 30, 40, 50 and 60 min (“***” indicates $p < 0.01$ and “*” indicates $p < 0.05$).....	87

- Figure 4.18:** ROS generation observed in the HaCaT cells upon the treatment of DMEM and **LA** at the concentration of 25 and 50 mg/L for 24 h then HaCaT cells was treated with H₂O₂ for 0, 10, 20, 30, 40, 50 and 60 min.....89
- Figure 4.19:** ROS generation observed in the HaCaT cells upon the treatment of DMEM and **TMPyP** at the concentration of 25 and 50 mg/L for 24 h then HaCaT cells was treated with H₂O₂ for 0, 10, 20, 30, 40, 50 and 60 min.....90
- Figure 4.20:** ROS generation observed in the HaCaT cells upon the treatment of DMEM and **P-4Lp** at the concentration of 25 and 50 mg/L for 24 h then HaCaT cells was treated with H₂O₂ for 0, 10, 20, 30, 40, 50 and 60 min.....91
- Figure 4.21:** ROS generation observed in the HaCaT cells upon the treatment of DMEM and **Mn-P-4Lp** at the concentration of 25 and 50 mg/L for 24 h then HaCaT cells was treated with H₂O₂ for 0, 10, 20, 30, 40, 50 and 60 min (“**” indicates p < 0.01 and “*” indicates p < 0.05).92
- Figure 4.22:** The ROS generation observed in the HaCaT cells upon the treatment with **LA** and **P-Lp** at the concentration of (A) 25 mg/L and (B) 50 mg/L for 24 h, followed by the treatment with H₂O₂ for 0, 10, 20, 30, 40, 50 and 60 min.93
- Figure 4.23:** ROS generation observed in the HaCaT cells upon the treatment of **TMPyP** and **P-4Lp** at the concentration of 25 mg/L (A) and 50 mg/L (B) for 24 h then HaCaT cells was treated with H₂O₂ for 0, 10, 20, 30, 40, 50 and 60 min (“*” indicates p < 0.05).94
- Figure 4.24:** ROS generation observed in the HaCaT cells upon the treatment of **P-4Lp** and **Mn-P-4Lp** at the concentration of 25 mg/L (A) and 50 mg/L (B) for 24 h then HaCaT cells was treated with H₂O₂ for 0, 10, 20, 30, 40, 50 and 60 min (“***” indicates p < 0.001, “**” indicates p < 0.01 and “*” indicates p < 0.05).95
- Figure 4.25:** Images of the HaCaT cells treated by (A) **DMEM**, (B) **LA**, (C) **P-4Lp**, (D) **Mn-P-4Lp**.97

LIST OF SCHEMES

	Page
Scheme 3.1: The synthesis of P1	47
Scheme 3.2: The synthesis of P2	48
Scheme 3.3: The synthesis of P-Glu1	49
Scheme 3.4: The synthesis of P-Glu2	50
Scheme 3.5: The synthesis of P3	51
Scheme 3.6: The synthesis of P4	52
Scheme 3.7: The synthesis of P-Glu3	53
Scheme 3.8: The synthesis of compound 1	54
Scheme 3.9: The synthesis of P5	55
Scheme 3.10: The synthesis of Lipoic acid anhydride.....	56
Scheme 3.11: The synthesis of P-4Lp	57
Scheme 3.12: The synthesis of Mn-P-4Lp	58
Scheme 3.13: The synthesis of TMPyP	59
Scheme 4.1: The synthetic route of P-Glu1 and P-Glu2	63
Scheme 4.2: The synthetic route of P-Glu3	65
Scheme 4.3: The synthetic route of lipoyl porphyrin derivatives.....	68

LIST OF ABBREVIATIONS

°C	: degree Celcius
calcd	: calculated
CDCl ₃	: deuterated chloroform
CO ₂	: carbondioxide
¹³ C-NMR	: carbon nuclear magnetic resonance spectroscopy
DMF	: <i>N,N'</i> -dimethylformamide
DMSO-d ₆	: deuterated dimethyl sulfoxide
DMSO	: dimethylsulfoxide
DMEM	: Dulbecco's Modified Eagle Medium
DNA	: Deoxyribonucleic acid
D ₂ O	: Deuterium oxide
d	: doublet (NMR)
ESI-HR-MS	: electrospray ionization-high resolution mass spectrometry
EtOH	: Ethanol
Et ₂ O	: Diethylether
equiv	: equivalent(s)
g	: gram(s)
GSH	: glutathione

HDFa	: human dermal fibroblast, adult
HaCaT	: Human keratinocyte
h	: hour(s)
$^1\text{H-NMR}$: proton nuclear magnetic resonance spectroscopy
Hz	: Hertz
H_2O_2	: hydrogen peroxide
IC_{50}	: the half maximal inhibitory concentration
J	: coupling constant
m/z	: mass per charge ratio
MALDI-TOF-MS	: matrix-assisted laser desorption ionization-time of flight-mass spectrometry
MeOH	: methanol
CH_2Cl_2	: methylene chloride
MHz	: megahertz
Min	: minute(s)
ϵ	: molar absorptivity
m	: multiplet (NMR)
mmol	: millimole(s)
mg	: milligram(s)

mL	: milliliter(s)
nm	: nanometer(s)
N ₂	: nitrogen
O ₂	: oxygen
obsd	: observed
ppm	: part per million
rt	: room temperature
RNS	: reactive nitrogen species
ROS	: reactive oxygen species
s	: singlet (NMR)
SOD	: superoxide dismutase
t	: triplet (NMR)
TEA	: triethylamine
THF	: tetrahydrofuran
TLC	: thin layer chromatography
UV-Vis	: ultraviolet and visible spectroscopy
λ	: wavelength
λ_{ex}	: excitation wavelength
λ_{abs}	: absorption wavelength

λ_{em} : emission wavelength

μL : microliter (s)

μM : micromolar (s)

δ : chemical shift

% yield : percentage yield



CHAPTER I

INTRODUCTION

During the last few decades, oxidative stress caused by free radicals has become one of the most significant health problem worldwide. Those radicals is claimed to be a primary cause of many chronic diseases¹. Normally, free radicals, also referred to reactive oxygen species (ROS) and reactive nitrogen species (RNS), live in balance with antioxidants in the body. The problem is occurs when this balance is disturbed and free radicals level in the body is higher than that of antioxidant due to poor nutrition or health problems, resulting in cell damage, DNA mutation, and deficiency immune system².

In order to prevent damage from those radicals, many antioxidants are synthesized such as butylated hydroxyanisole (BHA), butylated hydroxytoluene (BHT), propyl gallate (PG), and *tert*-butylhydroquinone (TBHQ). However, some of them may involve in liver damage and carcinogenesis³. Thus, it is important to develop biocompatible antioxidants so that they can protect the human body from free radicals without being any cause of chronic diseases.

Nowadays, there have been numerous research studies on biomedical applications of porphyrins due to their low toxicity to human cells, high thermal and chemical stability. The structural modification of the porphyrins can be easily achieved by coordination of various metal ions at the center of the macrocycles⁴ or insertion of substituents at the meso and beta positions of the porphyrin rings to adjust the biological activity⁵. Thus, several porphyrin derivatives have been prepared and applied as antioxidant compounds⁶.

One of the interesting compounds which can be modified on porphyrin to enhance antioxidant activity is Lipoic acid (LA). LA is a naturally occurring compound synthesized by plant and animal, including mitochondria in humans⁷. Generally, LA

was found to be highly reactive against variety of radicals *in vitro*. Furthermore, it has been suggested to reactivate other antioxidants such as glutathione and vitamin C⁸.

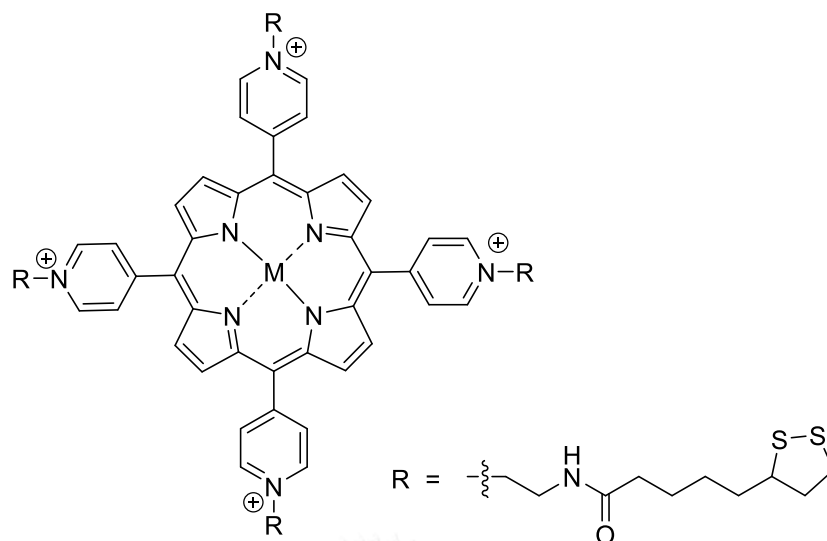
In this work, metal-free and metal lipoyl porphyrin compounds were synthesized, characterized and their potential use were investigated as antioxidative agents. The efficiency in reduction of radical of all target molecules were compared.

1.1 Objective of Research

The objective of this research is to synthesize free-base and manganese lipoyl-containing porphyrin derivatives. The cytotoxicity and antioxidant activity are studied by mean of cell viability assay and ROS generation assay, respectively.

1.2 Scope of Research

The scope of this research covers the synthesis of porphyrin derivatives bearing the lipoyl *meso*-substituents and manganese at center as shown in **Figure 1.1**. The free-base porphyrin derivative also investigated to determine the antioxidant activity and to study the effect of manganese at central on the antioxidant efficiency. All compounds were fully characterized by spectroscopic techniques, *i. e.*, mass spectrometry, and ¹H-NMR and ¹³C-NMR spectroscopy. Photophysical properties were investigated by UV-Vis spectrophotometry and fluorescent spectrophotometry. The cytotoxicity and antioxidant activity were determined by cell viability assay and ROS generation assay, respectively.



$M = H, H$ (**P-4Lp**) and Mn (**Mn-P-4LP**)

Figure 1.1: The structure of the target porphyrinic derivatives

CHAPTER II

THEORY AND LITERATURE REVIEWS

2.1 Free radical

Free radical can be defined as any molecular species containing an unpaired electron in their orbital of an atom or molecule. Many radicals are unstable and highly reactive. They always donate or accept an electron from other molecules resulting in a new free radical⁹. Free radicals formation occurs generally in a cell as a consequence of cell activities especially in mitochondria¹⁰. In addition, free radicals can also be generated by external sources such as UV light, radioactive compound, dust, pollution and an infection from bacteria or virus¹¹. A balance between free radical and antioxidant in human cell is necessary. If there are more radicals than the human body's ability to destroy them, the oxidative stress will occur. Free radicals can damage all kinds of molecules in the body. Among them, cell membranes, lipids, nucleic acids, and proteins are the major targets which associated with changes in their structures and functions. This can lead to many diseases for examples, all types of cancer, aging, diabetes mellitus, Parkinson's, cardiovascular diseases, rheumatoid arthritis, and Alzheimer's disease. Therefore, prevention of oxidative stress-caused radical has benefits for inhibition of those diseases¹².

2.1.1 The Oxidation of Protein

Oxidative forms of proteins are occurred when a hydroxyl radical abstracts alpha hydrogen atom of an amino acid residue to form a carbon-centered radical. The carbon-centered radical then reacts rapidly with O₂ to form an alkylperoxyl radical intermediate which is converted to a hydroxyl protein derivative. Finally, cleavage of the peptide bond by both the diamide and alpha-amidation pathways was found as shown in **Figure 2.1**¹³. In addition, sulfur-containing amino acid residues such as

methionine and cysteine are very sensitive to the oxidation¹⁴. This transformation of proteins may affect the activity of enzymes, receptors, and membrane transport.

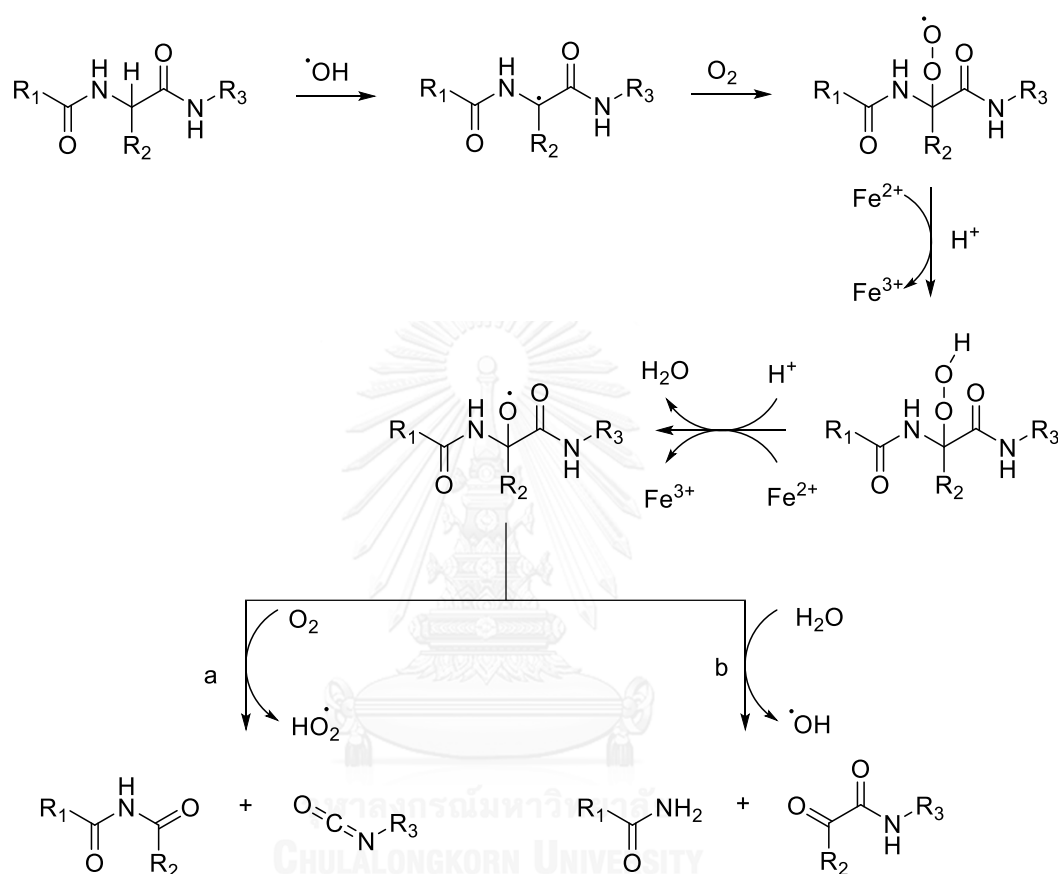


Figure 2.1: Peptide bond cleavage by the (a) diamide and (b) alpha-amidation pathways.

2.1.2 Oxidation of membrane lipids

Lipid peroxidation occurs when free radical takes one electron from a polyunsaturated fatty acid on the cell membrane resulting in a free radical on lipid membrane. This resulting radical can react with O_2 affording a peroxy-fatty acid radical as shown in **Figure 2.2**. In addition, radical chain reaction with another fatty acid can lead to cell apoptosis¹⁵.

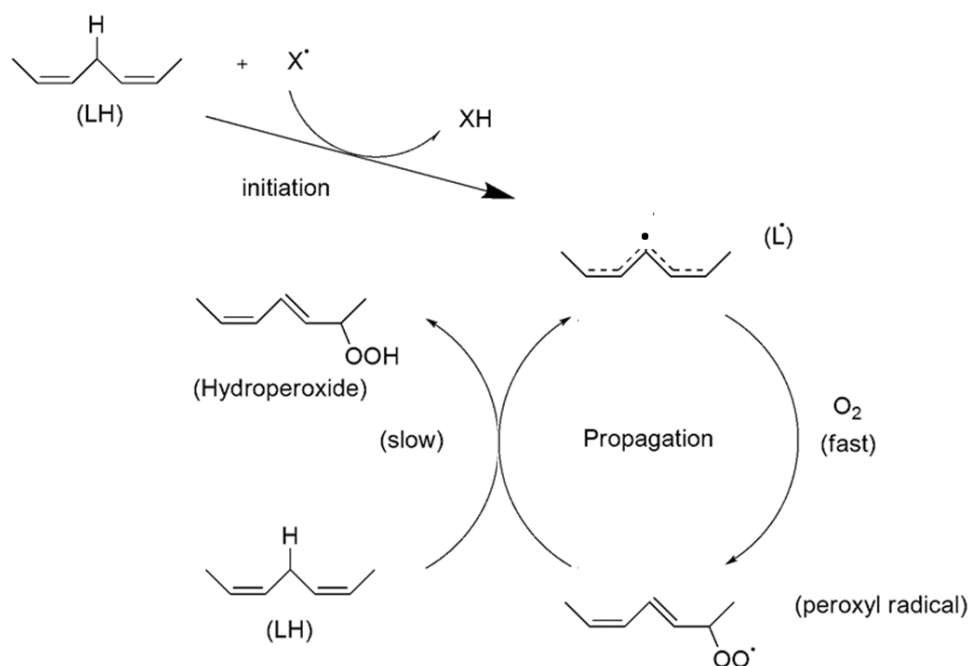


Figure 2.2: Mechanism of lipid peroxidation.

2.1.3 Oxidation of DNA

The oxidative damage on DNA normally takes place at guanine which is the base in DNA due to their high oxidation potential. Nowadays, there are many types of DNA lesions occur in the body's cells¹⁶, resulting in mutations of DNA by breaking in DNA strands, faulty links and base gaps in sequences. This type of damage may be an important effect in aging and numerous diseases such as cancer and Alzheimer's disease¹⁷.

2.2 Antioxidant

Antioxidant is enzyme or substance that greatly inhibits oxidation of other molecules. Generally, antioxidant compounds can react with free radicals and make them inactive resulting in less radical chain reaction. Therefore, antioxidant inhibits the risk for many diseases¹⁸. Some of antioxidants are exist in the human body such as superoxide dismutase (SOD), glutathione reductase (GR), glutathione, lipoic acid. Others

can be found in dietary such as Carotenoids, vitamin E and vitamin C. These compounds exhibit potential antioxidant activity which can protect tissues and cells from oxidative damage¹⁹.

2.3 Glutathione (GSH)

Glutathione (GSH) is a tripeptide compound consisting of three amino acids which are cysteine, glycine and glutamate as shown in **Figure 2.3**. Glutathione can be found in plants, animals, fungi, and some bacteria. In human body, glutathione is an essential compound in somatic defense system. Glutathione plays an importance role in enhancing immune system, increasing ability to detoxify, repairing damaged DNA and being an antioxidant agent²⁰. Nowadays, Glutathione is used as drugs to treat or reduce the symptoms of male infertility, Alzheimer's disease, heart disease, peripheral neuropathies and many kinds of cancers²¹.

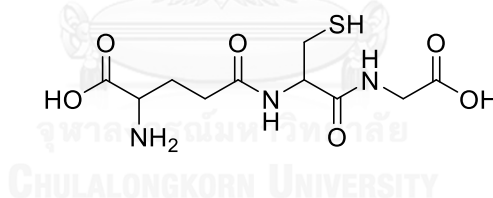


Figure 2.3: The chemical structure of glutathione

Two kinds of glutathione exist in the body. Most of glutathione found in the body is reduced form (GSH) and less than 10 percent is oxidized form (GSSG). The reversible process of GSH and GSSG are shown in **Figure 2.4**. The ratio of GSSG to GSH is usually considered as indicator for oxidative stress²². During oxidative stress, the increase in GSSG to GSH ratio is observed.

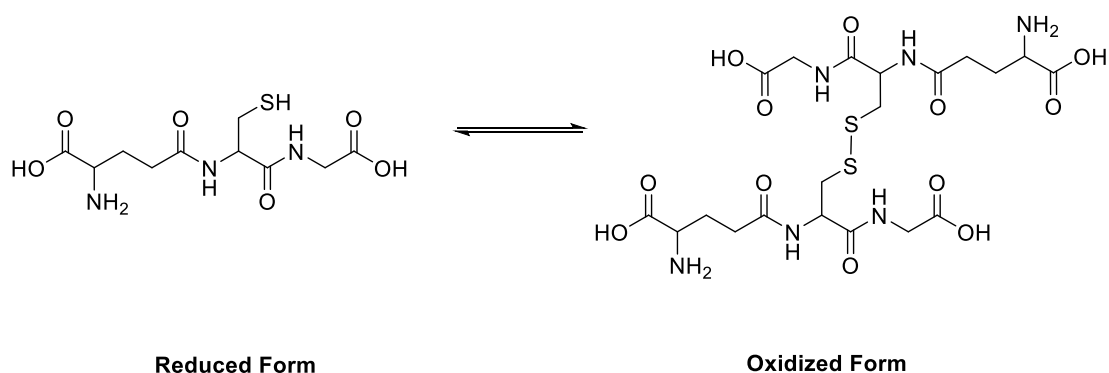


Figure 2.4: The reversible process of GSH and GSSG

In antioxidant defense system, GSH acts in association with glutathione peroxidase to catalyze the conversion of H_2O_2 to water²³. This conversion turn the GSH into oxidized form. Then, glutathione is reduced back to its reduced form by glutathione reductase and nicotinamide adenine dinucleotide phosphate (NADPH) as shown in **Figure 2.5**.

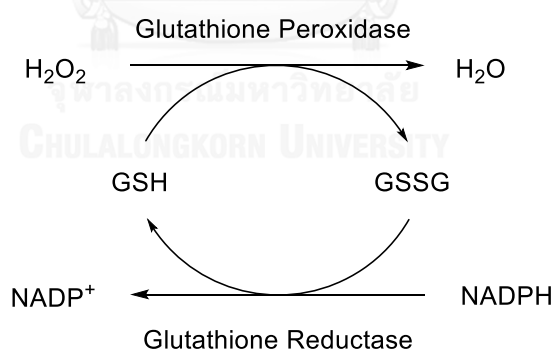


Figure 2.5: Antioxidant process of glutathione

2.4 Literature review on glutathione derivatives

To improve the biological properties of glutathione, the structural modification of the glutathione can be achieved by the insertion of substituents at the thiol, amino or carboxyl groups of glutathione. In 2005, Procopio and co-workers²⁴ successfully synthesized the glutathione derivative with alkyl chains at thiol group via nucleophilic substitution of alkyl halide and phenyl epoxide in the heterogeneous solvents as shown in **Figure 2.6**.

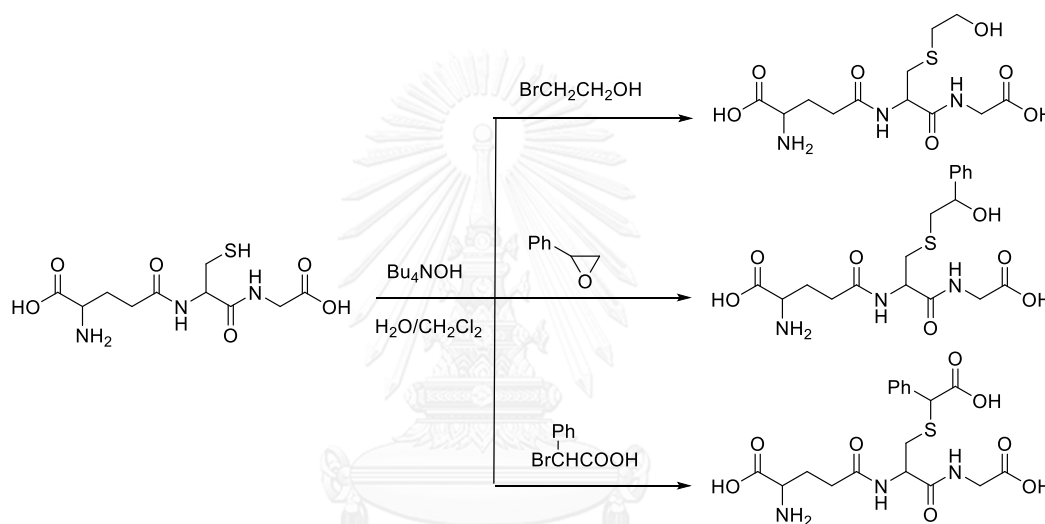


Figure 2.6: Nucleophilic substitution of a thiol group in glutathione

In 2005, Falck and co-workers²⁵ modified the structure of glutathione by the esterification of methanol at the carboxyl groups of glutathione. This reaction was achieved in low temperature using hydrochloric acid as acid catalyst.

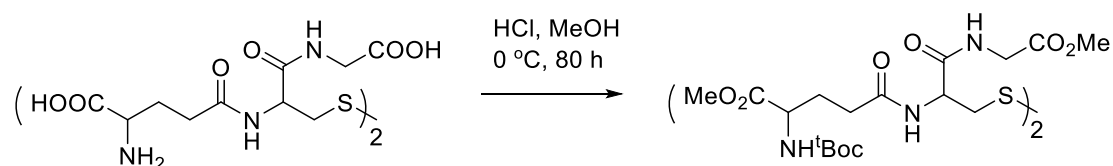


Figure 2.7: Esterification of a carboxyl group of glutathione

In 2005, Katritzky and co-workers²⁶ designed and synthesized the glutathione modified with 4-nitrobenzoyl at amino group of glutathione. The reaction started by adding two 4-nitrobenzoyl at both carboxyl and amino group of glutathione. Then the selective deacylation of the 4-nitrobenzoyl groups from these double acylated glutathione derivatives was archived at carboxyl group of glutathione resulting in N-acyl glutathiones as shown in **Figure 2.8**. This reaction is mild and gave high yield. These mild reaction condition exhibited high yields of the corresponding glutathione.

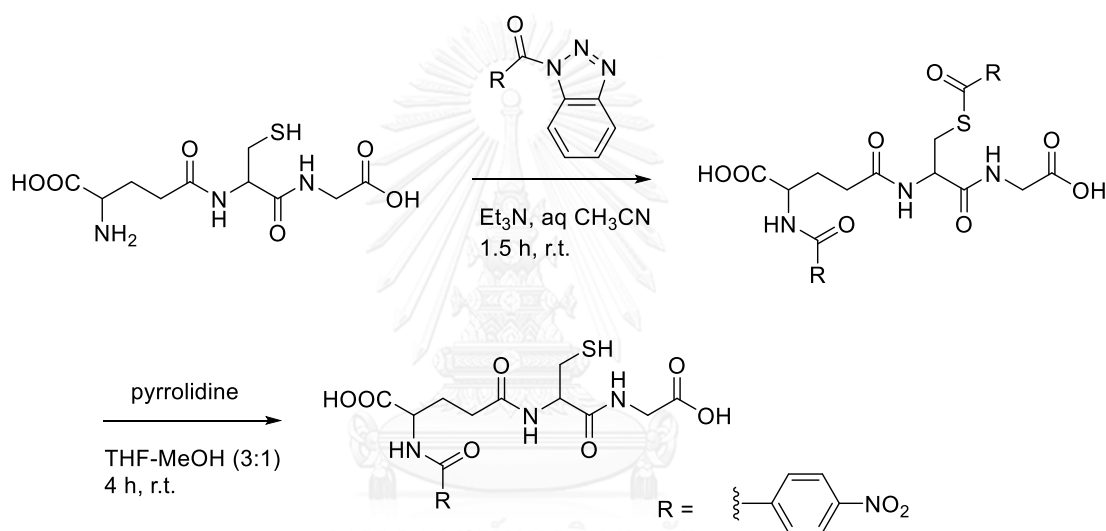


Figure 2.8: Acylation and selective deacylation of glutathione

2.5 Lipoic acid (LA)

LA is a sulfur-containing compound derived from octanoic acid. It is composed of two sulfur atoms at C6 and C8 linked by a disulfide bond in dithiolane ring and it also contains a terminal carboxylic acid at hydrocarbon chain that connected with dithiolane ring²⁷. The chemical structure of LA is shown in the **Figure 2.9**.

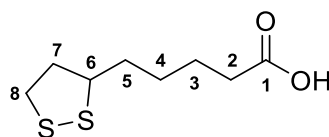


Figure 2.9: The chemical structure of LA

Because the C6 carbon is chiral, LA exists as two enantiomers which are R-(+)-lipoic acid and S-(-)-lipoic acid as shown in **Figure 2.10**. Only R-(+)-lipoic acid is naturally occurring²⁸.

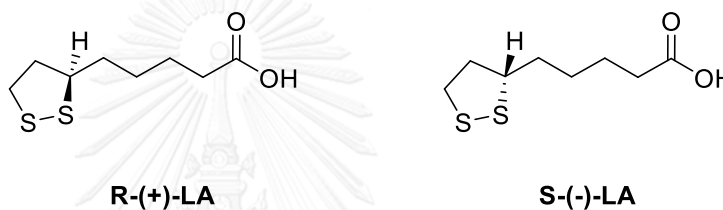


Figure 2.10: The chemical structure of R and S lipoic acid

In cells, LA exists in two forms which are oxidized form of lipoic acid (LA) and reduced form of dihydrolipoic acid (DHLA). This reversible process is working as an intramolecular redox system²⁹ as shown in **Figure 2.11**.

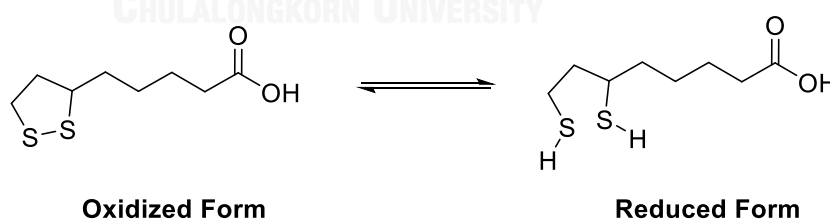


Figure 2.11: The reversible process of oxidized and reduced forms of LA

Normally, LA is an antioxidant which is synthesized by the body. Unlike the other antioxidants which work only in water, such as vitamin C, Glutathione (GSH), or work only in fatty tissues, such as vitamin E, LA is soluble both in water and lipid thus

it can react with oxidants in the aqueous solution in cell and the blood plasma and also protect cell membranes from lipid peroxidation.

Recently, LA has been suggested as an essential mitochondrial co-factor. Moreover, LA was found to have the capacity to regenerate the other endogenous antioxidants vitamin E, vitamin C and glutathione³⁰. The thiolane ring of LA can be reduced to dihydrolipoic acid (DHLA) at both extracellular and intracellular *via* NADH and NADPH pathways. Then the DHLA is released into the extracellular and rapidly converted cysteine to cysteine. After that, cysteine passed through the cell and accelerated the GSH production in the cells as shown in **Figure 2.12**.

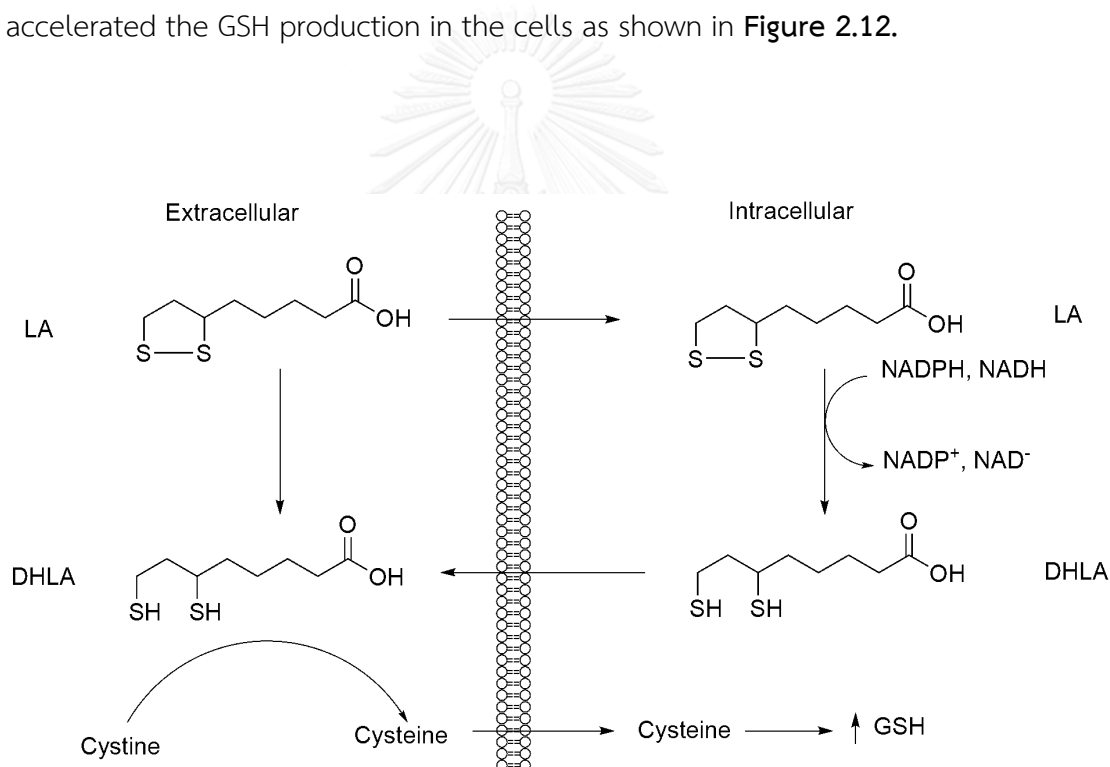


Figure 2.12: Dynamic roles of LA in regeneration of glutathione

2.6 Literature review on LA derivatives

In 2005, A. S. Gurkan and co-workers³¹ designed and synthesized novel indole-lipoic acid derivatives (**Figure 2.13**). These compounds show good antioxidant activities on rat liver microsomal, especially those containing amide linker at position 5 of indole ring was proved to be highly effective in inhibiting lipid peroxidation as compared to LA.

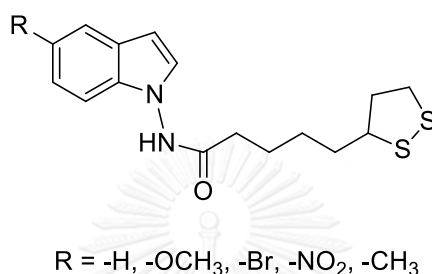


Figure 2.13: The chemical structure of indole-lipoic acid derivatives

In 2009, G. Melagraki and co-workers³² successfully synthesized 4-hydroxycoumarin-3-carboxamides bearing with lipoic acid (**Figure 2.14**). Normally, the 4-hydroxycoumarin moiety which is widely spread among coumarin natural products, has been used as molecular template for the synthesis of important biological activity compounds. After attachment with lipoic acid, those new compounds can exhibit good *in vitro* antioxidant and *in vivo* anti-inflammatory activities in rat paw.

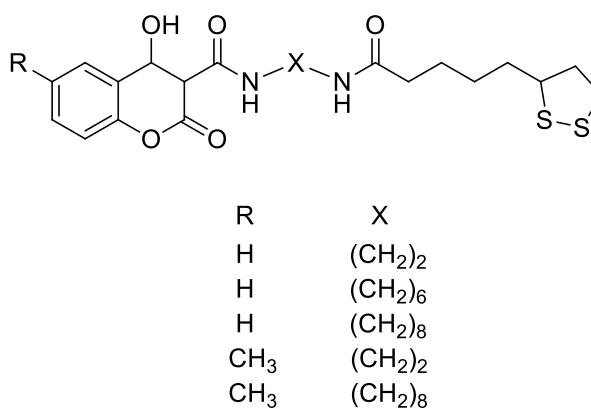


Figure 2.14: The structure of coumarin-lipoic acid conjugates.

In 2004, M. Koufaki and co-workers³³ investigated the effect of a novel hybrid compound between lipoic acid and derivative of chroman moiety of vitamin E through an amide bond on lipid hydroperoxide induced cell injuries. The result showed that this compound exhibited strong inhibition of the microsomal lipid peroxidation. Moreover, this compound also protects phospholipid components of the myocardium together with maintaining selective permeability of cell membranes. The chemical structure of this compound was shown in **Figure 2.15**.

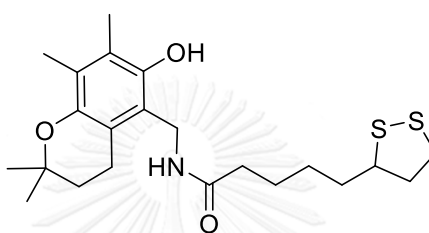


Figure 2.15: The chemical structure of the hybrid compound between lipoic acid and derivative of chroman moiety of vitamin E

According to the literature reviews, most of LA are modified *via* amide linkage at terminal carboxylic acid. LA can combine with other molecules without losing antioxidant properties. On the other hand, the combination of LA and other antioxidants biomolecules is more effective in improving antioxidant properties. Therefore, this research focuses on synthesis of new antioxidant agent bearing LA.

2.7 Porphyrins

Porphyrins are macrocyclic compounds consisting of 4 pyrrole rings linked together *via* methane bridges to give a highly conjugated macrocycle. Porphyrin without any substituent is called porphine. The structure of porphine is shown in **Figure 2.16**³⁴.

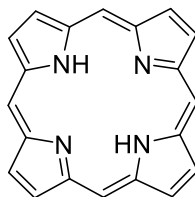


Figure 2.16: The structure of porphyrin (porphine)

Normally, porphyrin molecule has highly thermal and chemical stability. There are 22 π -electrons inside the porphyrin macrocycle, but only 18 electrons are found to delocalize in their macrocycle³⁵. Those electrons are consistent with Hückel's $[4n+2]$ rule for aromaticity, where $n = 4$. In addition, porphyrin and their derivatives exhibit strong absorption in the visible region. The highest absorption band, known as the Soret or B band appears around 400 nm with molar extinction coefficient about $10^5 \text{ Mol}^{-1}\cdot\text{L}$. The other small 4 bands or Q-band appear between 450–700 nm as shown in **Figure 2.17**³⁶.

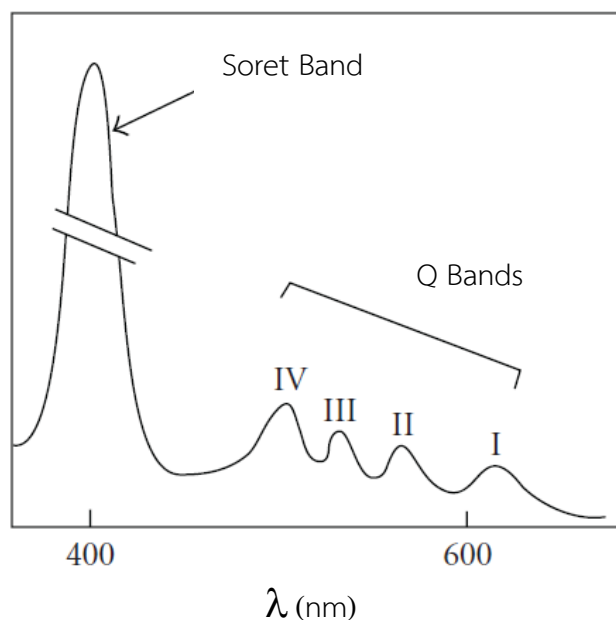
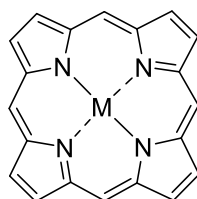


Figure 2.17: Typical UV-Vis absorption spectrum of the porphyrin

2.8 Structural Modifications of Porphyrins

To improve the physical or chemical properties of porphyrin, the structural modification of the porphyrins can be achieved by the coordination of various metal ions at the center of macrocycle³⁷ as shown in **Figure 2.18**.



M = Metal (i.e. Zn, Mn, Fe)

Figure 2.18: Structure of metalloporphine

Those porphyrins with metal in the center are called metalloporphyrins. Several metalloporphyrins play significant role in biological systems (**Figure 2.19**). For example, the complex of porphyrin derivatives with magnesium are the main part in chlorophyll using to convert light energy into chemical energy in the form of adenosine triphosphate (ATP)³⁸. While Fe-protoporphyrin IX complex found in heme B which are responsible for oxygen transport in human body³⁹.

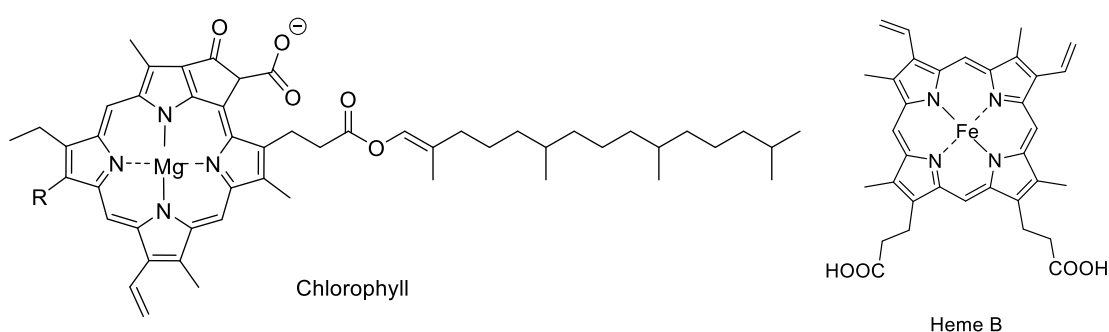


Figure 2.19: The structure of natural metalloporphyrins

Moreover, the insertion of substituents at the meso and beta positions of the porphyrin ring, as shown in **Figure 2.20**, can also adjust the properties of porphyrin⁵.

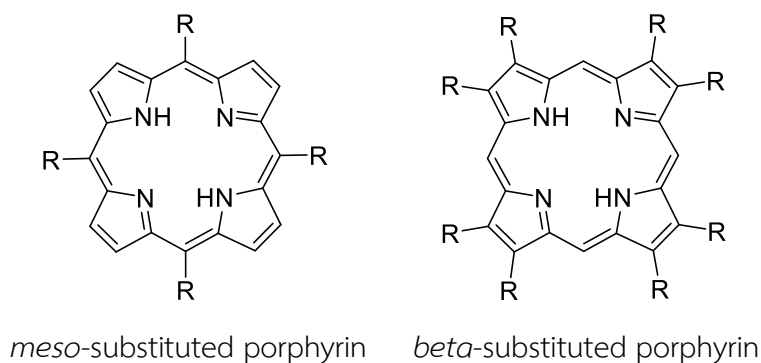


Figure 2.20: Structures of meso- and beta-substituted porphyrins

2.9 Role of porphyrin derivatives as an antioxidant agent

Nowadays, numerous of porphyrin compounds are of great interest as an antioxidant for biomedical applications due to their low toxicity, chemical stability, rapid body clearance and easy to adjust the biological activity⁴⁰. In addition, many previous papers demonstrated that the cationic porphyrin has ability to localize and accumulate in mitochondria which is the main source that radical is generated in a cell. As a result, oxidant compounds are effectively destroyed by the antioxidant activity of those porphyrin derivatives⁴¹.

2.10 Literature review on porphyrin derivatives

In 1967, Adler and Longo⁴² developed a method for synthesis of meso substituted porphyrin by a condensation of benzaldehyde and pyrrole in refluxing propionic acid for 30 mins. This method have allowed a wider selection of substituted benzaldehydes to be converted to the corresponding porphyrins in yields of up to 20%. The reaction can be used in a large-scale synthesis. The synthesis pathway was shown in **Figure 2.21**.

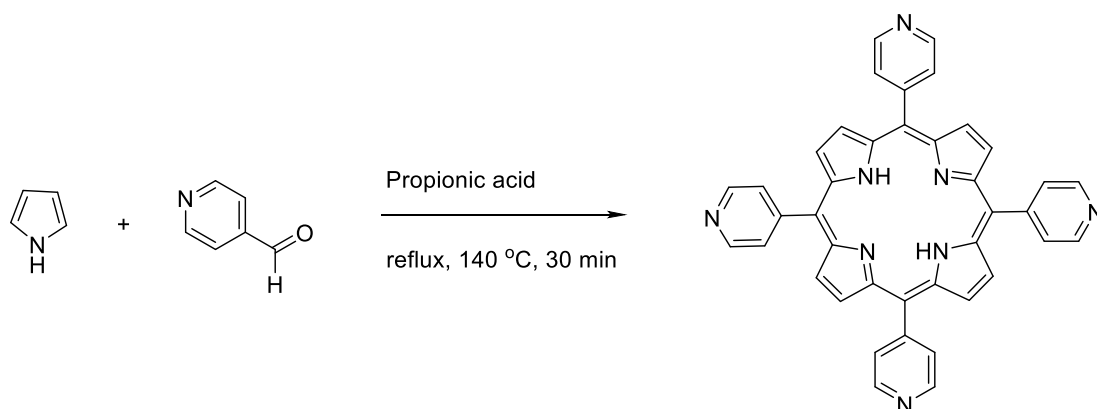


Figure 2.21: The synthesis pathway of meso-substituted porphyrin by Adler and Longo method

For biological applications of porphyrins, water solubility is an important characteristic in handling the porphyrins in aqueous solution. In 2003, A. Szurko and co-workers⁴³ synthesized the 5,10,15,20-tetra(N-methyl-4-pyridyl)porphyrin iodide (TMPyP). This pyridinium ring on porphyrin can enhance the solubility in water. The structure of TMPyP was shown in **Figure 2.22**.

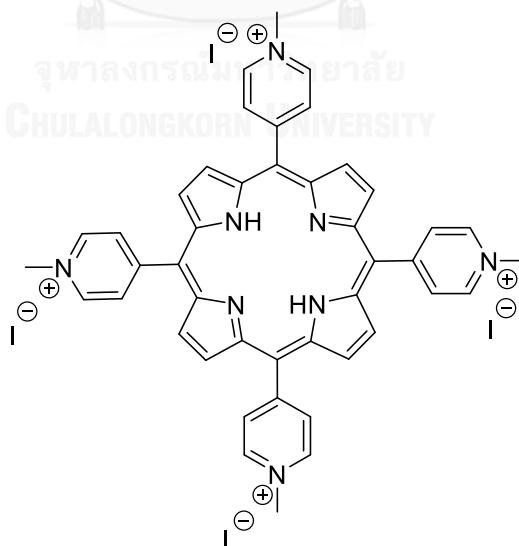


Figure 2.22: the molecular Structures of TMPyP

In 2009, Cernay and co-workers⁴⁴ synthesized the cationic porphyrin with alkyl chains at meso-position (P1). Fluorescence microscopy was used to support a specific binding to mitochondria of living HeLa cells. The results revealed that hydrophobicity and cationic charges of the porphyrin are the main factors for transporting this porphyrin to the mitochondria. The structure of P1 was shown in **Figure 2.23**.

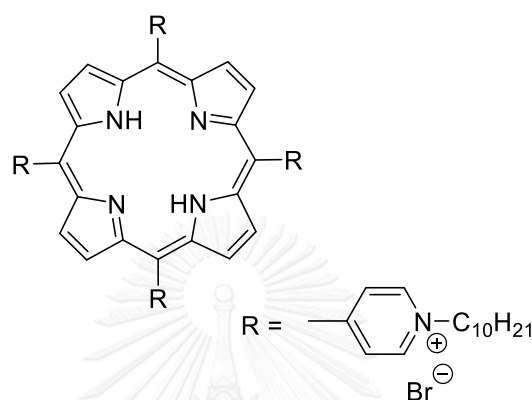


Figure 2.23: the molecular Structures of P1

In 2006, S. Asayama and co-workers^{6a} designed and synthesized the Mn-porphyrin modified with a mitochondrial signal peptide for a new class of antioxidant (**Figure 2.24A**). The resulting Mn-porphyrin-oligopeptide conjugate exhibited significant antioxidant activity *via* Mn-oxidation-reduction-cycle in the center of porphyrin ring (**Figure 2.24B**). In the first half reaction, Mn(III) was reduced by superoxide, affording oxygen (O₂) and a Mn(II). The Mn(II) was then returned to its former oxidation state Mn(III) by reducing a second superoxide molecule, affording hydrogen peroxide. The result suggested that the Mn-porphyrin could protect mitochondria from oxidative damage.

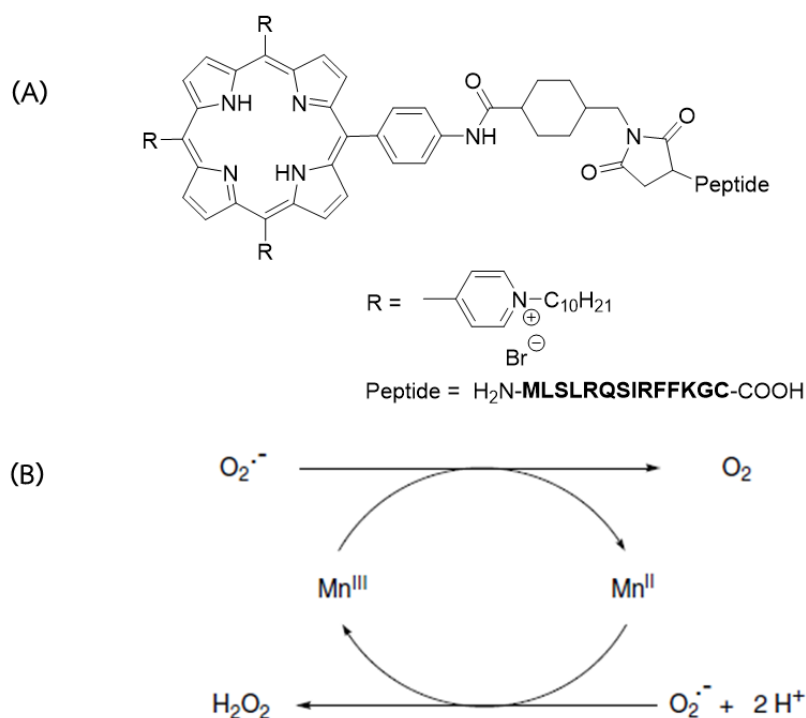


Figure 2.24: (A) the molecular structure of Mn-porphyrin-oligopeptide compound and (B) Scavenging ability of manganese superoxide dismutase

2.11 Detection of Biological Activities

2.11.1 Cytotoxicity test

The cytotoxicity test is one of the fundamental biological evaluation and screening tests by observing the cell growth, reproduction and morphological effects. With the continuous development of cytotoxicity tests, many assays have gradually been developed, such as detection of cell damage by morphological changes, determination of cell damage, measuring cell growth and metabolic properties. Among of them, the cell viability assays is an outstanding methods that achieves faster results, inexpensive and requires smaller sample volumes⁴⁵.

Cell viability assays generally measure an importance enzymes or substrates in the cell such as protease, ATP content or assessment of cell membrane integrity. These assays usually require a specific reagent which can be converted to a color or fluorescent product in an alive or viable cells. Conversely, the dead cells cannot convert this reagent to color or fluorescent product. This difference provides the basis for many of the commonly used cell viability assays. While many cell viability methods have been used for decades, there have been recent developments which offer increased sensitivity, throughput, and specificity. The new redox-based assay is detecting the reducing environment within alive or viable cell⁴⁶. By using Prestobluereagent (resazurin dye), the reducing environment convert the weakly fluorescent resazurin to highly red fluorescence resorufin as shown in **Figure 2.25**.

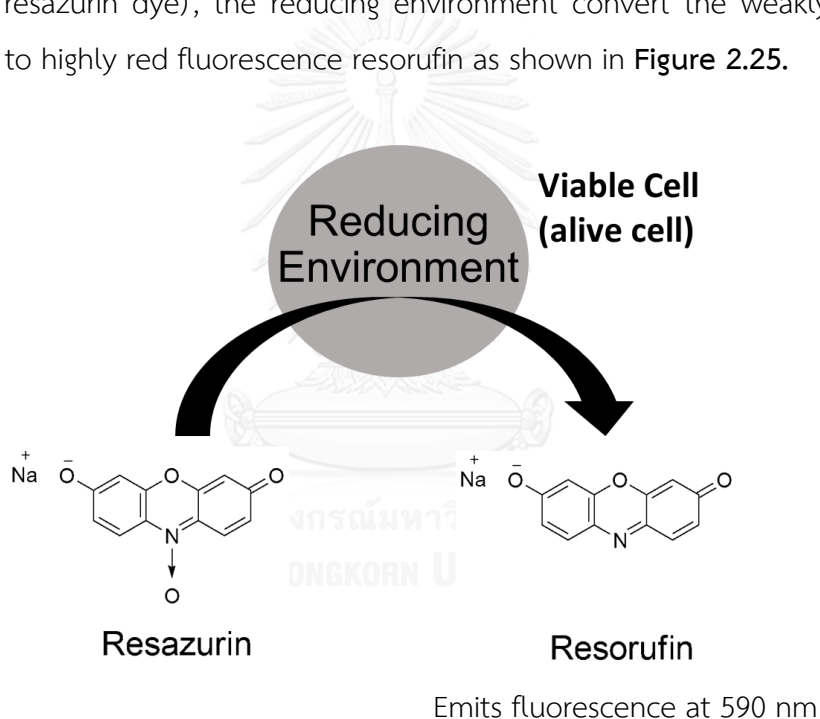


Figure 2.25: Conversion of resazurin to resorufin by reducing environment within viable cell.

2.11.2 ROS generation assay

ROS are generally produced during metabolic processes. These reactive molecules are formed by many different mechanisms and can be detected by various techniques. The detection of ROS depend on the analytic target. At the cellular level, ROS can be assessed from cell or tissue culture. While at the whole-body level, the

effects of oxidative stress are measured from blood product (e.g. serum or plasma) or from urine samples. Initially, the detection of ROS was based on the measurement of glutathione levels by absorption spectroscopy to assess oxidative stress at the tissue or whole-body level⁴⁷. Moreover, lipid peroxidation is also one of the most widely used as indicators of ROS formation. The measurement of lipid peroxidation is based on detection of reactive compounds generated from the decomposition of lipid peroxidation such as malondialdehyde⁴⁸. However, this method has low specificity for those decomposition of lipid peroxidation⁴⁹. Nowadays, the cell permeable fluorescent probes, 2'-7'-dichlorodihydrofluorescein diacetate (H₂DCFDA) is one of the most popular used for ROS detection due to its easy to use, high sensitivity, inexpensive and can be used to follow changes in ROS over time⁵⁰. After diffusion in to the cell, H₂DCFDA is deacetylated by cellular esterases to a non-fluorescent 2',7'-dichlorodihydrofluorescein (H₂DCF). Then, the H₂DCF is further oxidized by ROS resulting in highly fluorescent 2', 7'-dichlorofluorescein (DCF) as shown in **Figure 2.26**. This oxidation can be detected by monitoring the increase in fluorescence which is maximally excited at 495 nm and emits at 520 nm.



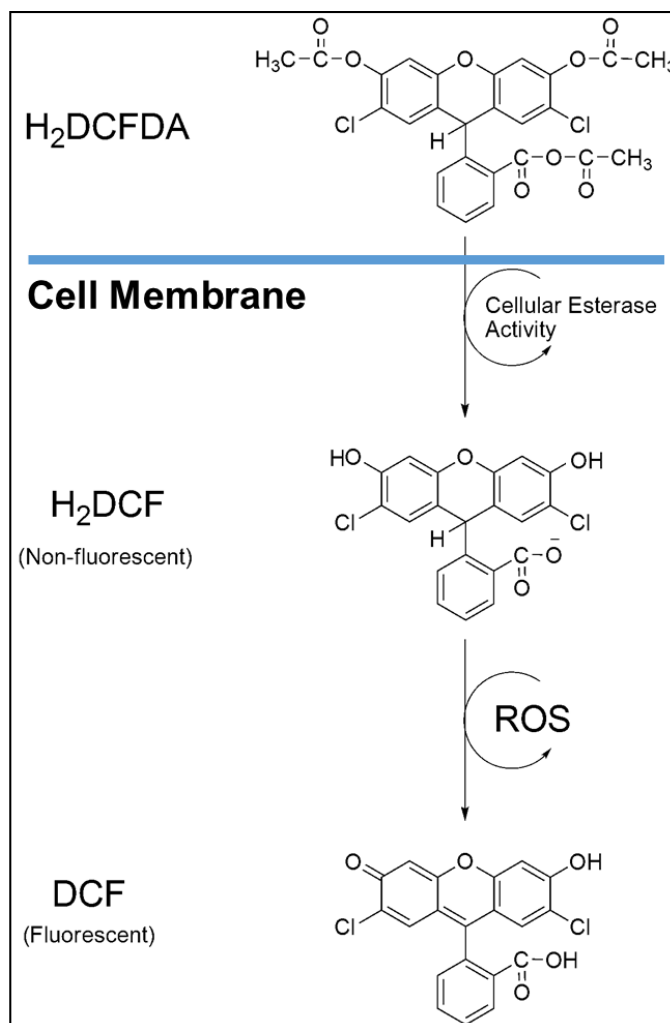


Figure 2.26: Formation of fluorescent Compound DCF by ROS in cell.

2.11.3 Mitochondria targeting evaluation

During the past decades, mitochondria targeting compounds has been extensively studied by several research groups because the mitochondria are the major producers of intracellular ROS and also play an important role in controlling life and death of a cell⁵¹. Consequently, the mitochondria are attractive sites for effective elimination of ROS⁵². Normally, mitochondrial membrane potential has been used as an indicator for detecting the mitochondria targeting ability. Permeability of various compounds into the mitochondria can result in either increasing or decreasing of mitochondrial membrane potential⁵³. Those changes can be observed from many

kinds of fluorescent probes. 5,5',6,6' - tetrachloro- 1,1',3,3' tetraethylbenzimidazolylcarbocyanine iodide (JC-1 dye) is one of the fluorescent probe which is widely used to detect the changes of mitochondrial membrane potential by high-resolution imaging⁵⁴. JC-1 dye is a novel cationic carbocyanine dye that can accumulate in mitochondria. The loss of mitochondrial membrane potential make JC-1 dye less accumulate within the mitochondria. In these case, JC-1 dye remains in the cytoplasm in a green fluorescent monomeric form. Conversely, a subsequent increasing of mitochondrial membrane potential will result in more JC-1 dye entering into mitochondria, causing further J-aggregates and thus increasing in red fluorescent signal as shown in **Figure 2.27**.

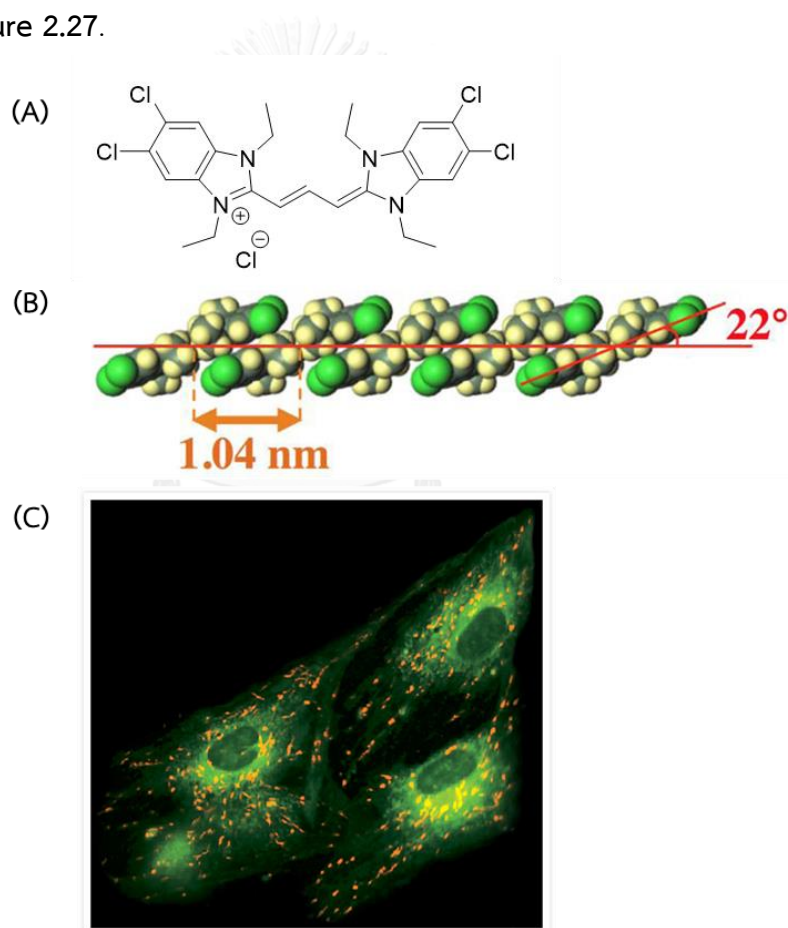


Figure 2.27: (A) The structure of JC-1 dye, (B) Estimated formation of JC-1 J-aggregate and (C) The color of JC-1 dye as a green-fluorescent monomer at cytoplasm and as a red-fluorescent J-aggregate within the mitochondria in cultured human pre-adipocytes cells.

CHAPTER III

EXPERIMENT

3.1 Chemicals

All chemicals are purchased from commercial sources and used as received without further purification.

1. 4-Pyridine carboxzaldehyde :Sigma-Aldrich
2. Pyrrole :Sigma-Aldrich
3. Propionic acid :Merck
4. Sodium hydroxide (NaOH) :Merck
5. *Di-tert-butyl* dicarbonate (Boc₂O) :Merck
6. 4-Dimethylaminopyridine (DMAP) :Merck
7. 2-Bromoethylamine hydrobromide :Merck
8. Lipoic acid :Sigma-Aldrich
9. *N,N'*-Dicyclohexylcarbodiimide (DCC) :Sigma-Aldrich
10. Dimethylformamide (DMF) :Lab-scan
11. Manganese(II) chloride tetradhydrate
(MnCl₂·4H₂O) :Fluka
12. Methylene chloride (CH₂Cl₂) :Lab-scan
13. Methanol (MeOH) :Merck
14. Ethanol (EtOH) :Merck
15. Triethylamine (Et₃N) :Lab-scan
16. Diethylether (Et₂O) :Merck
17. Acetone :Lab-scan
18. Sodium sulfate (Na₂SO₄) :Merck

19. Silica gel :Merck
20. Deuterated chloroform (CDCl_3) :Merck
21. Deuterated dimethyl sulfoxide
($\text{DMSO-}d_6$) :Merck
22. Deuterium oxide (D_2O) :Merck



3.2 Instrumentation

All ^1H -NMR spectra were determined on a Varian Mercury NMR spectrometer, which operated at 400 MHz for ^1H nuclei and ^{13}C NMR spectra were determined on a Bruker NMR spectrometer, which operated at 100 MHz for ^{13}C nuclei. All chemical shifts (δ) were reported in parts per million (ppm) relative to the residual CHCl_3 , D_2O , DMSO-d_6 peak at 7.26, 4.79, 2.50 ppm respectively for ^1H -NMR. The following abbreviations are used for multiplicity: s=singlet, d=doublet, t=triplet, q=quartet, br=broad singlet and m=multiplet. Coupling constants (J) are reported in Hertz (Hz).

Mass spectra were recorded on a Microflex MALDI-TOF mass spectrometer (Bruker Daltonics) using α -cyano-4-hydroxycinnamic acid (CCA) as a matrix.

Absorption spectra were measured at room temperature by Cary 60 UV-vis spectrophotometer. Emission spectra were recorded by Varian Cary Eclipse spectrofluorometer. The maximum absorption wavelength was used as the excitation wavelength of each porphyrins. Absorption and emission were measured at room temperature.

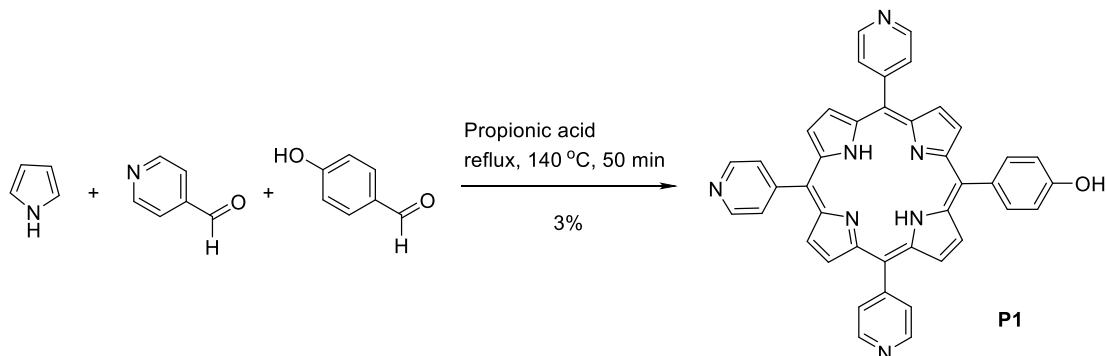
3.3 Chromatographic System

Analytical thin layer chromatography (TLC) was carried out on Merck Kieselgel 60, F254, 1 mm aluminium-backed silica plates (Merck KgaA, Darmstadt, Germany). The chromatograms were visualized under 254 nm ultraviolet (UV) light.

Column chromatography was performed on glass column using Merck silica gel 60 (60-230 mesh). The size of the chromatographic column used depended on the amount (weight) of the sample. The column was eluted with some suitable solvents which best separated the sample and each fraction was monitored by Thin-Layer Chromatography (TLC).

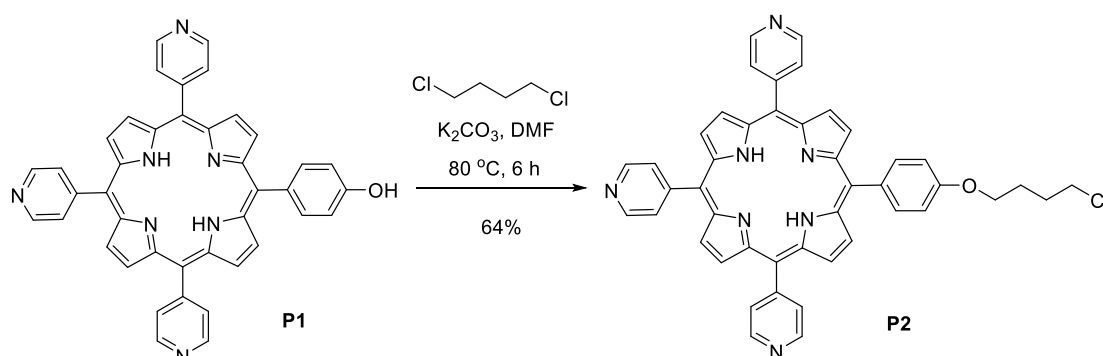
3.4 Synthesis of Porphyrin derivatives and Characterizations

3.4.1 Synthesis of 5-(4-hydroxyphenyl)-10,15,20-tris(4-pyridyl)porphyrin (**P1**)



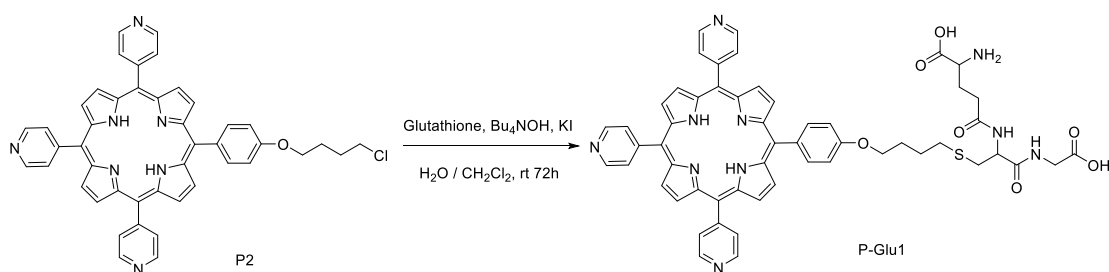
Scheme 3.1: The synthesis of **P1**

The compound **P1** was synthesized according to a previous report with a slightly change in purification step⁵⁵. Mixture of 4-pyridylcarboxaldehyde (3.80 ml, 40.3 mmol), 4-hydroxybenzaldehyde (1.225 g, 10.03 mmol) and freshly distilled pyrrole (2.80 ml, 40.4 mmol) were refluxed in 200 ml of propionic acid for 50 min. The mixture was cooled down to room temperature, diluted with distilled water (500 ml) and then neutralized with 1 M aqueous solution of NaOH until pH was 6. The solution was filtered and washed several times with water and methanol. The filtrate was dissolved in 4% MeOH in CH₂Cl₂. The crude product was purified by flash column chromatography using 10% EtOH in CH₂Cl₂ as an eluent to yield **P1** as purple solid (180 mg, 3%). MALDI-TOF-MS *m/z* obsd 633.503, calcd mass 633.715 ([M]⁺, M = C₄₁H₂₇N₇O) (**Figure A1**).

3.4.2 Synthesis of 5-(4-(4-chlorobutoxy)phenyl)-10,15,20-tris(4-pyridyl)porphyrin (**P2**)Scheme 3.2: The synthesis of **P2**

Mixture of compound **P1** (52 mg, 0.084 mmol), 1,4-dichlorobutane (320 mg, 2.52 mmol) and potassium carbonate (K_2CO_3 , 15 mg, 0.11 mmol) were heated in 20 ml of DMF at $80\text{ }^\circ\text{C}$ for 6 h. The solution was allowed to stand for 1h at room temperature. This solution was added with dichloromethane and subsequently extracted several times with brine. The organic phase was dried over Na_2SO_4 , filtered off and concentrated in vacuo. The crude product was purified by flash column chromatography using 5% EtOH in CH_2Cl_2 as an eluent to yield **P2** as purple solid (39 mg, 64%). MALDI-TOF-MS m/z obsd 723.540, calcd mass 723.251 ($[M]^+$, $M = C_{45}H_{34}ClN_7O$) (Figure A2).

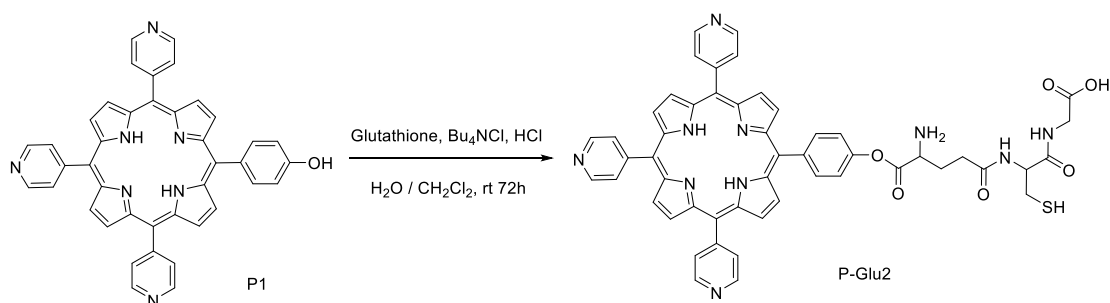
3.4.3 Synthesis of P-Glu1



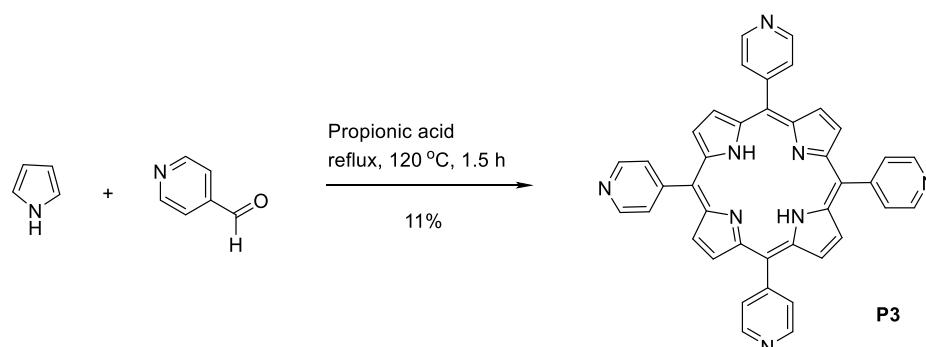
Scheme 3.3: The synthesis of P-Glu1

The solution of **P2** (29 mg, 0.040 mmol) and Bu₄NOH (1.008g, 3.885 mmol) in 3 mL of dichloromethane was added with a solution of glutathione (217 mg, 0.706 mmol) and KI (6 mg, 0.04 mmol) in a 7 mL of water. The reaction mixture was stirred for 72 h at room temperature. Then the organic phase was extracted with brine and dried over Na₂SO₄, filtered off and concentrated in vacuo to obtain the purple solid (the desired product was not found).

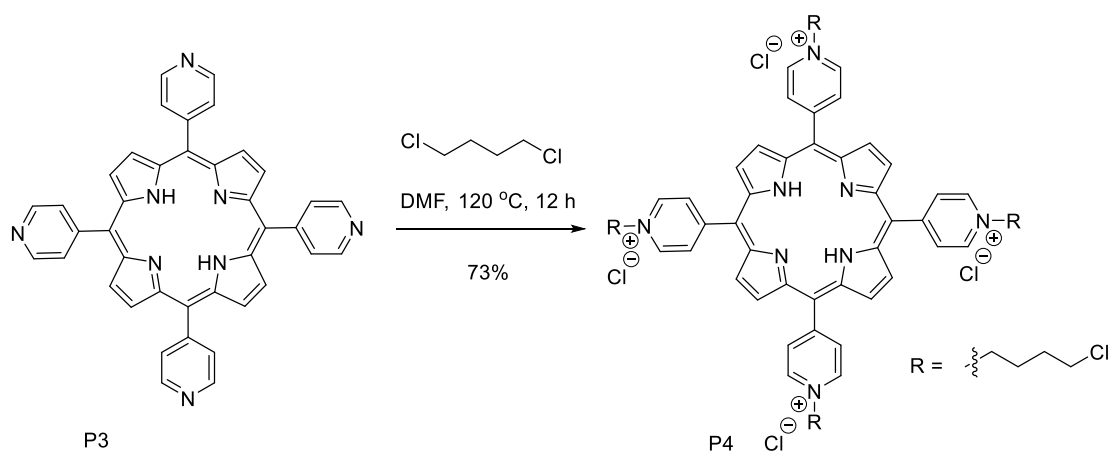
3.4.4 Synthesis of P-Glu2

**Scheme 3.4:** The synthesis of P-Glu2

The solution of **P1** (31 mg, 0.049 mmol) and Bu₄NCl (0.982g, 3.53 mmol) in 3 mL of dichloromethane was added with a solution of glutathione (197 mg, 0.641 mmol) in a 7 mL of 1 mol/L hydrochloric acid. The reaction mixture was stirred for 72 h at room temperature. Then the organic phase was extracted with brine and dried over Na₂SO₄, filtered off and concentrated in vacuo to obtain the purple solid (the desired product was not found).

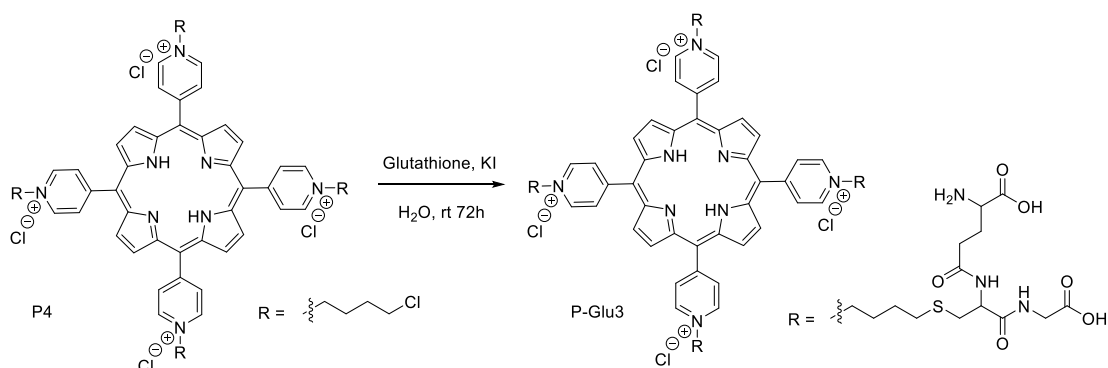
3.4.5 Synthesis of 5,10,15,20-Tetrakis(4-pyridyl)porphyrin (**P3**)Scheme 3.5: The synthesis of **P3**

The compound **P3** was synthesized according to a previous report with a slightly change in purification step⁵⁶. Mixture of 4-pyridylcarboxaldehyde (3.80 ml, 40.34 mmol) and freshly distilled pyrrole (2.80 ml, 40.36 mmol) were refluxed in 150 ml of propionic acid for 1.5 h. The mixture was cooled down to room temperature, diluted with distilled water (500 ml) and then neutralized with 1 M aqueous solution of NaOH until pH was 7. The solution was filtered and washed several times with water and methanol. The filtrate was dissolved in 4% MeOH in CH₂Cl₂. The crude product was purified by flash column chromatography using 8% EtOH in CH₂Cl₂ as an eluent to yield **P3** as purple solid (661 mg, 11%). ¹H-NMR (CDCl₃/MeOD) δ : 8.18 (d, *J* = 4.0 Hz, 8H), 8.94-8.68 (br, 8H), 8.97 (d, *J* = 4.0 Hz, 8H) (**Figure A3**); MALDI-TOF-MS *m/z* obsd 620.027 [(M+H)⁺], calcd mass 618.704 ([M]⁺, M = C₄₀H₂₆N₈) (**Figure A4**); λ_{abs} 417, 513, 547, 587, 642 nm (**Figure A5**); λ_{em} (λ_{ex} = 417) 647, 712 nm (**Figure A6**).

3.4.6 Synthesis of 5,10,15,20-Tetrakis(4-N-(4-chlorobutyl)-pyridyl)porphyrin (**P4**)Scheme 3.6: The synthesis of **P4**

A mixture of **P3** (32 mg, 0.052 mmol), 1,4-dichlorobutane (297 mg, 2.34 mmol) was stirred in DMF at 120 °C for 12 h. After cooling the mixture to room temperature, crude product was precipitated in acetone. Subsequently, crude product was washed with dichloromethane and acetone in an ultrasonic bath, affording green-brown solid (43 mg, 73%). $^1\text{H-NMR}$ (DMSO) δ : -3.09 (s, 2H), 2.11 (m, 8H), 2.44 (m, 8H), 3.91 (t, $J = 6.0$ Hz, 8H), 5.07 (t, $J = 6.0$ Hz, 8H), 9.06 (d, $J = 4.0$ Hz, 8H), 9.27 (s, 8H), 9.68 (d, $J = 4.0$ Hz, 8H) (**Figure A7**); HR-ESI-MS obsd 981.3102; calcd mass 982.3517 ($[\text{M}]^+$, $\text{M} = \text{C}_{56}\text{H}_{58}\text{Cl}_4\text{N}_8$) (**Figure A8**).

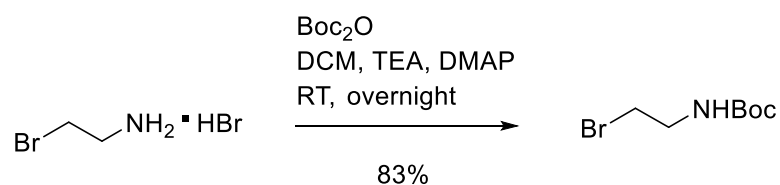
3.4.7 Synthesis of P-Glu3



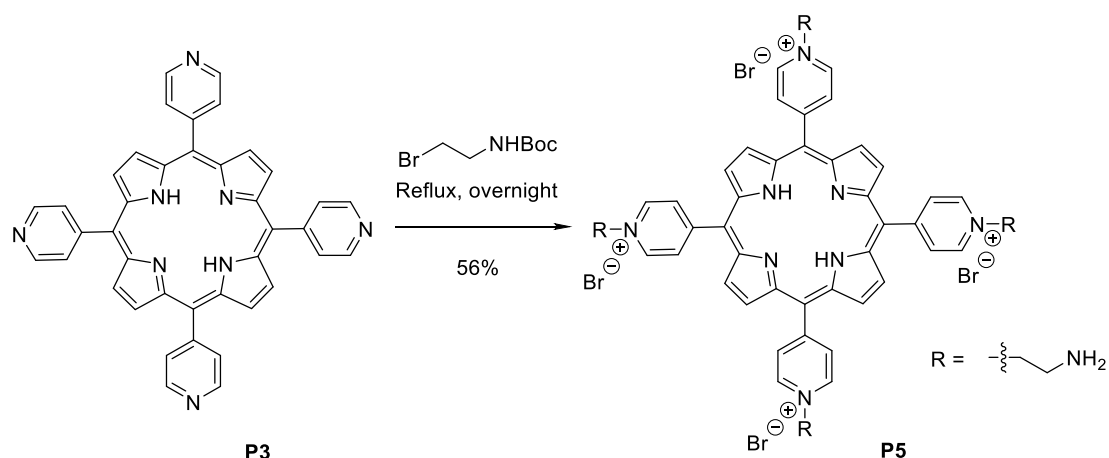
Scheme 3.7: The synthesis of P-Glu3

A mixture of **P4** (43 mg, 0.038 mmol), glutathione (207 mg, 0.674 mmol) and KI (6 mg, 0.04 mmol) in a 10 mL of water was stirred for 72 h at room temperature. After that, acetone was added to precipitate crude product. The crude product was purified by reverse phase column chromatography using 20% H₂O in MeOH as an eluent to obtain dark green solid (the desired product was not found).

3.4.8 Synthesis of tert-Butyl-N-(2-bromoethyl)carbamate (1)

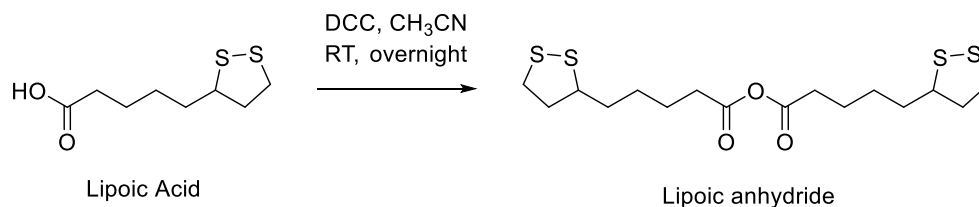
**Scheme 3.8:** The synthesis of compound 1

This compound was prepared according to a literature procedure with some modification⁵⁷. The suspension of 2-Bromoethylamine hydrobromide (8.077 g, 39.42 mmol) in 60 mL of dichloromethane was added dropwise with a solution of di-*tert*-butyl dicarbonate (Boc₂O) (9.465 g, 43.37 mmol) in a 30 mL of dichloromethane and 6 mL of triethylamine. The reaction mixture was stirred for 18 h at room temperature. Then, 4-Dimethylaminopyridine (DMAP) (2.655 g, 21.73 mmol) was added. The solution was allowed to stand for 1h at room temperature. This solution was subsequently extracted with sat'd NH₄Cl and brine. The organic phase was dried over Na₂SO₄, filtered off and concentrated in vacuo to afford a yellow oil (7.356 g, 83%). ¹H-NMR (CDCl₃) δ: 1.44 (s, 9H), 3.45 (t, *J* = 4.0 Hz, 2H), 3.52 (m, 2H), 4.97 (br, 1H) (**Figure A9**).

3.4.9 Synthesis of 5,10,15,20-tetrakis(4-N-(2-aminoethyl)-pyridyl)porphyrin bromide (**P5**)Scheme 3.9: The synthesis of **P5**

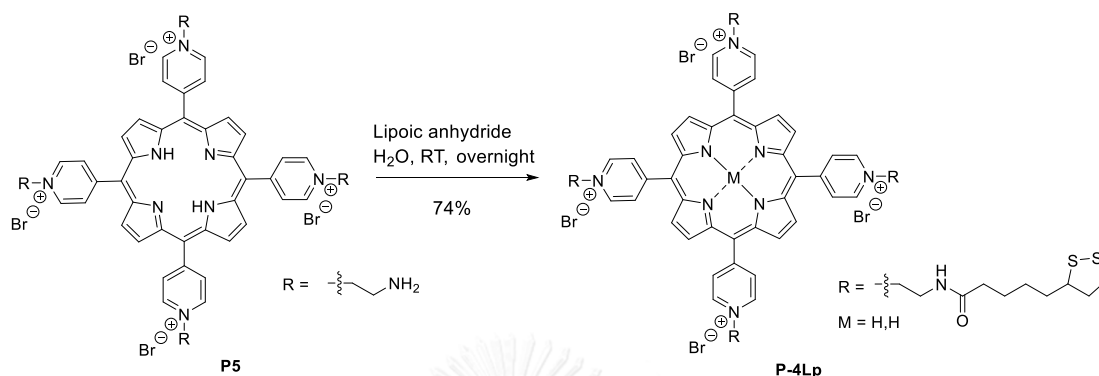
A mixture of **P3** (0.020 g, 0.032 mmol) and compound **1** (2.008 g, 8.960 mmol) was stirred at 120 °C for 12 h. After cooling the mixture to room temperature, a brown solid was washed with DMF, ethanol and then acetone in an ultrasonic bath. Subsequently, crude product was precipitated in 6% H₂O in acetone, affording purple-brown solid (0.020 g, 56%). ¹H-NMR (D₂O) δ : 4.10 (t, *J* = 8.0 Hz, 8H), 5.43 (t, *J* = 8.0 Hz, 8H), 9.14 (d, *J* = 4.0 Hz, 8H), 8.95–9.44 (br, 8H), 9.53 (d, *J* = 4.0 Hz, 8H) (**Figure A10**); ¹³C-NMR (D₂O) δ : 39.6, 58.5, 115.8, 134.1, 143.8, 159.1 (**Figure A11**); MALDI-TOF-MS obsd 794.782; calcd mass 795.010 ([M]⁺, M = C₄₈H₅₀N₁₂) (**Figure A12**); λ_{abs} (H₂O) 426, 521, 556, 586, 641 nm (**Figure A13**); λ_{em} (H₂O, λ_{ex} = 426 nm) 711 nm (**Figure A14**).

3.4.10 Synthesis of Lipoic acid anhydride

**Scheme 3.10:** The synthesis of Lipoic acid anhydride

This synthesis was performed, following a previous report with a modification as the use of dichloromethane was replaced by acetonitrile⁵⁸. A mixture of lipoic acid (200 mg, 0.969 mmol) and dicyclohexylcarbodiimide (DCC, 120 mg, 0.582 mmol) was stirred in 8 mL of acetonitrile for 18 h at room temperature. The mixture was filtered to remove the byproduct, dicyclohexylurea. The yellow solution was used without further purification in the synthesis of 5, 10, 15, 20-tetrakis(4-*N*-(*N*-Lipoyl-2-aminoethyl)pyridyl)porphyrin.

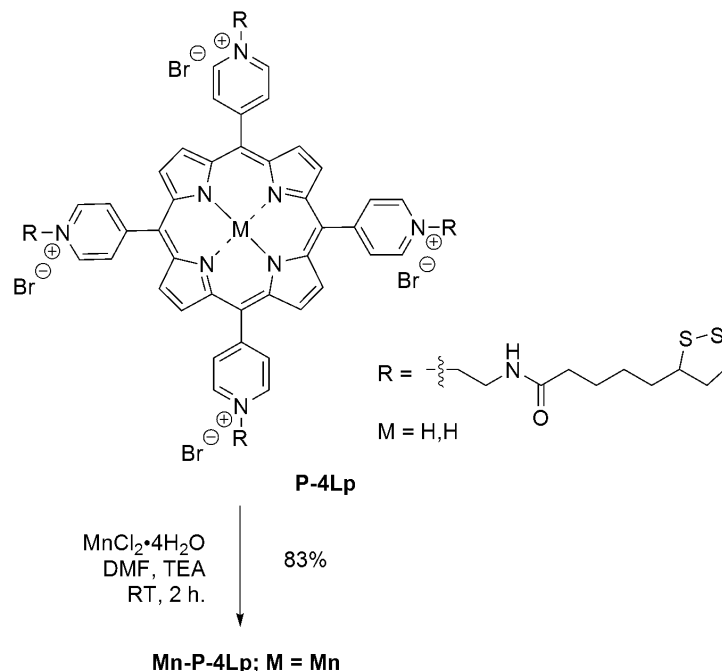
3.4.11 Synthesis of 5, 10, 15, 20-tetrakis(4-N-(N-Lipoyl-2-aminoethyl)pyridyl)porphyrin bromide (**P-4Lp**)



Scheme 3.11: The synthesis of **P-4Lp**

A solution of **P5** (20 mg, 0.018 mmol) in water (2 mL) was added to a solution of lipoic acid anhydride at room temperature under N_2 atmosphere. After 18 h, the resulting mixture was filtered to remove solid byproduct. The solution was poured into acetone to precipitate. The solid was washed several times with acetone to afford purple-brown solid (25 mg, 74%). $^1\text{H-NMR}$ (DMSO) δ : -3.09 (s, 2H), 1.21–1.47 (m, 16H), 1.48–1.67 (m, 16H), 1.99–2.11 (m, 4H), 2.22 (t, $J = 7.2$ Hz, 8H), 2.65–2.75 (m, 4H), 2.79–2.90 (m, 4H), 3.94 (br, 8H), 5.02 (br, 8H), 8.49 (t, $J = 8.0$ Hz, 4H), 9.00 (d, $J = 4.0$ Hz, 8H), 9.21 (s, 8H), 9.54 (d, $J = 4.0$ Hz, 8H) (**Figure A15**); $^{13}\text{C-NMR}$ (DMSO) δ : 24.9, 28.4, 34.0, 35.1, 37.8, 39.7, 55.8, 61.3, 115.8, 132.1, 143.9, 156.4, 173.5 (**Figure A17**); MALDI-TOF-MS obsd 1548.650; calcd mass 1548.222 ($[\text{M}]^+$, $\text{M} = \text{C}_{80}\text{H}_{98}\text{N}_{12}\text{O}_4\text{S}_8$) (**Figure A18**); λ_{abs} (H_2O) 430, 525, 560, 593, 649 nm (**Figure A19**); λ_{em} (H_2O , $\lambda_{\text{ex}} = 430$ nm) 658, 721 nm (**Figure A20**).

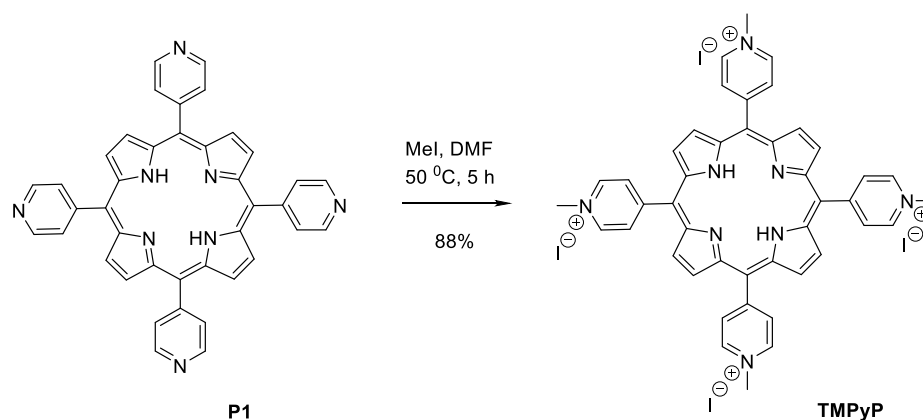
3.4.12 Synthesis of Mn(II)-5,10,15,20-tetrakis(4-N-(N-Lipoyl-2-aminoethyl)pyridyl)porphyrin bromide (Mn-P-4Lp)



Scheme 3.12: The synthesis of Mn-P-4Lp

Manganese(II) chloride tetrahydrate (38 mg, 0.19 mmol) was added to a solution of **P-4Lp** (10 mg, 0.0053 mmol) in DMF (2 mL) with one drop of triethylamine (TEA) at room temperature under N_2 atmosphere. The reaction was monitored by fluorescence spectroscopy until the emission band at 658 and 721 nm was completely disappeared (approximately 2h). Then, the mixture was precipitated by adding diethylether. The solid was washed with diethylether and ethanol to afford a dark-green solid (9 mg, 83%). MALDI-TOF-MS obsd 1601.134, 1789.296; calcd mass 1601.144 ($[\text{M}]^+$, $\text{M} = \text{C}_{80}\text{H}_{98}\text{MnN}_{12}\text{O}_4\text{S}_8$), 1789.3059 ($[\text{M}+\text{CCA}]^+$, $\text{M} = \text{C}_{90}\text{H}_{102}\text{MnN}_{13}\text{O}_7\text{S}_8$) (**Figure A210**); λ_{abs} (H_2O) 331, 378, 400, 464, 563 nm (**Figure A22**).

3.4.13 Synthesis of 5,10,15,20-tetrakis(4-N-methyl-pyridyl)porphyrin iodide (TMPyP)



Scheme 3.13: The synthesis of TMPyP

Following a previous report⁵⁹, a suspension of compound **P1** (0.505 g, 0.817 mmol) in DMF (5 mL) was mixed with excess of iodomethane (2.306 g, 16.24 mmol) and heated at 50 °C for 5 h. The resulting mixture was precipitated with diethyl ether. The solid was washed several times with diethyl ether and acetone to afford purple-brown solid (853 mg, 88%). ¹H-NMR (DMSO) δ : -3.11 (s, 2H), 4.73 (s, 12H), 9.00 (d, J = 4.0 Hz, 8H), 9.20 (s, 8H), 9.49 (d, J = 4.0 Hz, 8H) (**Figure A23**); MALDI-TOF-MS m/z obsd 679.158, calcd mass 678.842 ($M = C_{44}H_{38}N_8$) (**Figure A24**).

3.5 Biological studies of Porphyrin derivatives

3.5.1 Cell culture

Following a standard procedure⁶⁰, human dermal fibroblast, adult (HDFa) and Human keratinocyte (HaCaT) cell lines were cultured in DMEM (Gibco, USA) containing 10%(v/v) fetal bovine serum (FBS) (Gibco, USA) and 1% (v/v) antibiotic antimycotic (Gibco, USA) at 37 °C in 5% CO₂. Cells at early passages (below 30 passages) were used in cell experiments to avoid complications of replicative senescence. After HDFa and HaCaT cell lines reached 90% confluence, cells were sub-cultured using 0.25% trypsin/EDTA (Gibco, USA).

3.5.2 Cytotoxicity test (cell viability assay)

The cellular cytotoxicity was studied by cell viability assay using PrestoBlue™ as reagent (Invitrogen, USA)⁴⁶. HDFa and HaCaT cell lines were seeded into 96-well plates at density of 5x10³ cells/well in 100 µL of complete medium and incubated at 37 °C under 5% CO₂ atmosphere for 12 h. Cells were washed by phosphate buffered saline (PBS) twice and treated with various concentrations of Dulbecco's Modified Eagle Medium (DMEM), **LA**, **TMPyP**, **P-4Lp** and **Mn-P-4Lp** in 90 µL for 24 h. 10 µL of PrestoBlue™ reagent was added into cell and incubated for 30 min. Fluorescence was measured using a microplate reader with excitation at 560 and emission at 590 nm (Thermo, Varioskan flash, England). The percentage of cell viability was calculated by normalize the fluorescence intensity of analyte to fluorescence intensity of control group (DMEM).

3.5.3 Antioxidant Activity (ROS generation assay)

Antioxidant activity was studied by ROS generation assay using 2',7' – dichlorofluoreceine-diacetate (H₂DCF-DA) as reagent (Molecular probes™, USA)⁶¹. Briefly, HDFa and HaCaT cell lines were seeded into 96-black well plates at density of 5x10³ cells/well in 100 µL of complete medium and incubated at 37 °C under 5% CO₂ atmosphere for 12 h. Cells were washed by PBS twice. After that, 100 µL of various concentrations of DMEM, **LA**, **TMPyP**, **P-4Lp** and **Mn-P-4Lp** were added into cells for

pre-treatment and incubated for 24 h. After that, the solution was discarded and cells were added with H₂DCFDA then incubated for 30 min at 37 °C in dark place. Cells were washed by PBS twice and treated with 100 µL of 10% H₂O₂. Fluorescence was measured using a microplate reader with excitation at 485 nm and emission at 528 nm (Thermo, Varioskan flash, England) every 10 min until 1 h.

3.5.4 Mitochondria targeting evaluation

The evidence for mitochondria targeting was confirmed by cell imaging by LSM 800 confocal microscope. From previous paper⁶², HaCaT cells were seeded in 24 wells (Corning) plate at density 10⁵ cells per well, then cells were incubated at 37 °C under 5% CO₂ for 12 hours. Next, cells were treated with 50 mg/L of DMEM, **LA, P-4Lp** and **Mn-P-4Lp** and incubated at 37°C under 5% CO₂ for 6 hours. Protocol of JC-1 staining was applied from Chazotte B⁶³, briefly, Cells were washed by PBS. JC-1 dye and Hoechst 33342 (10 µg/ml) (MERK, Calbiochem) were loaded in each wells and incubated for 15 min, then cells were washed with PBS and imaged by LSM 800 confocal microscope (Carl Zeiss, Jena, Germany) using lens 40 x, with excitation at 488 and 561 nm and using emission filters of 505-550 nm for the green channel, and 575-630 nm for the red channel. The pictures were collected and analysed by ZEN software version 2.1.

3.5.5 Statistical analysis

Statistical analysis of the data was determined with a one-way randomized ANOVA design by GraphPad Prism 5.0 software. When the overall test of significance ($p < 0.05$, p -value is probability of the randomness in sampling) led to a rejection of the null hypothesis, post-hoc comparison (Tukey) were performed.

CHAPTER IV

RESULTS AND DISCUSSION

The concept of this work covers the synthesis of porphyrin derivatives bearing the glutathione-/lipoic acid-substituents with or without manganese at the center of porphyrin ring. The structures of these compounds are shown in **Figure 4.1**. The studies for their biological activities were performed in HDFa and HaCaT cell lines. The cytotoxicity was investigated by cell viability assay. The antioxidant activity was evaluated by ROS generation assay.

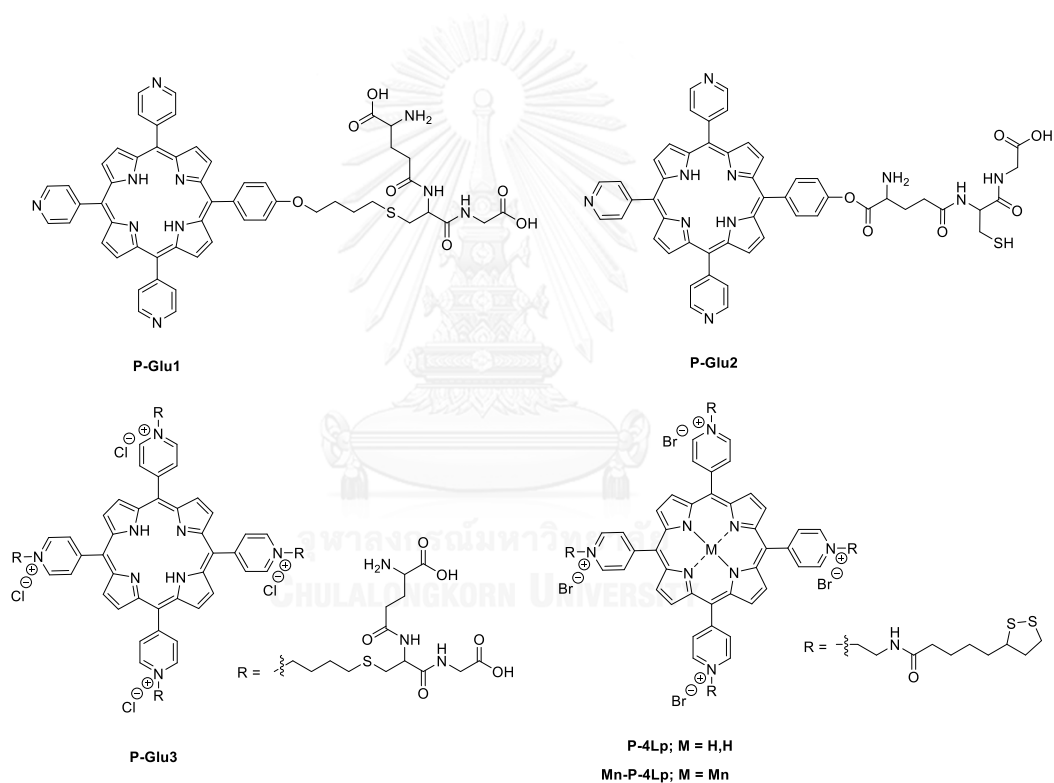
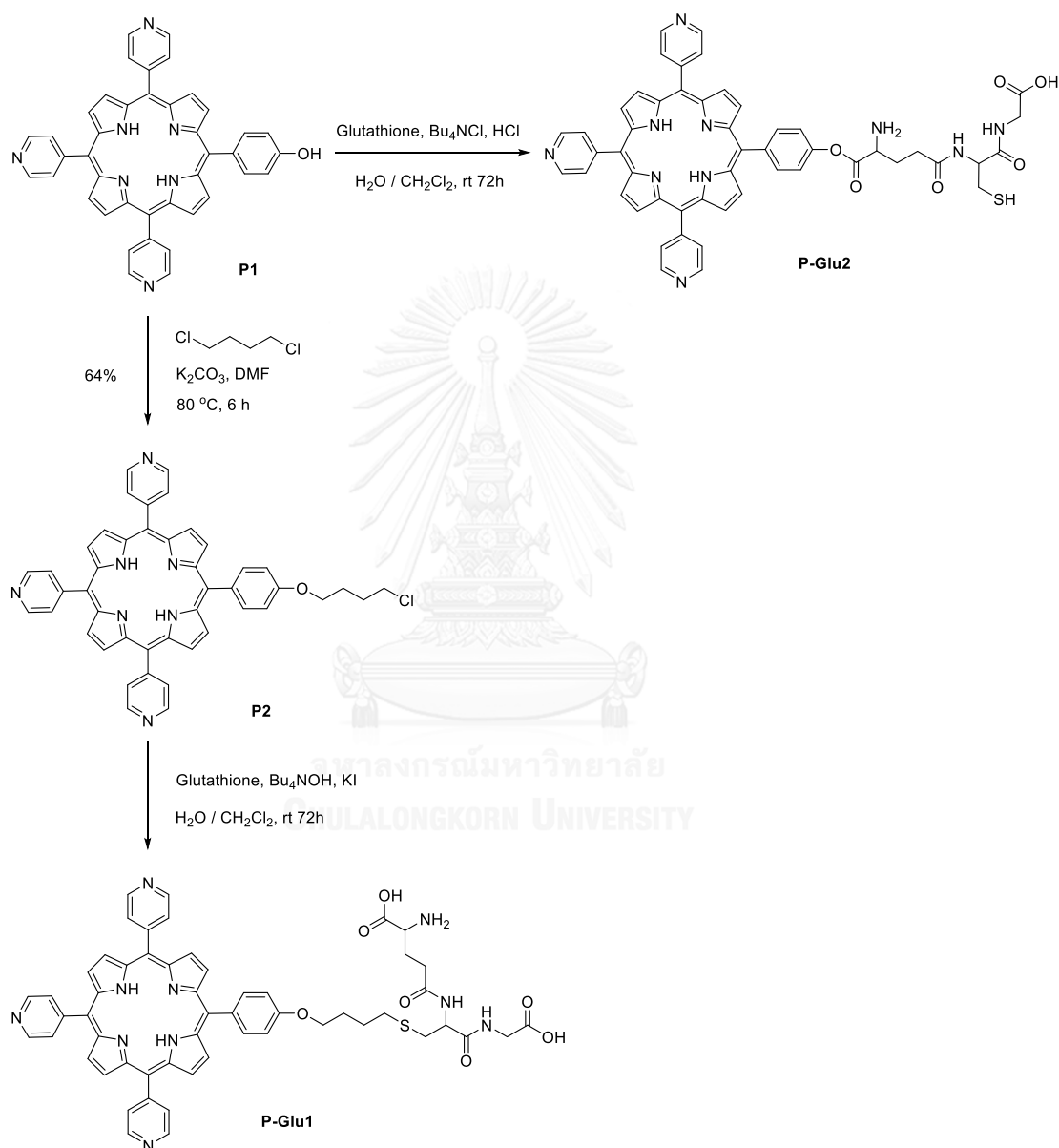


Figure 4.1: Structure of glutathione-/lipoic acid-porphyrin derivatives

4.1 Synthesis of Porphyrin derivatives and Characterizations

4.1.1 Synthesis of glutathione-porphyrin derivatives **P-Glu1** and **P-Glu2**

The synthetic route of **P-Glu1** and **P-Glu2** are described in **Scheme 4.1**.



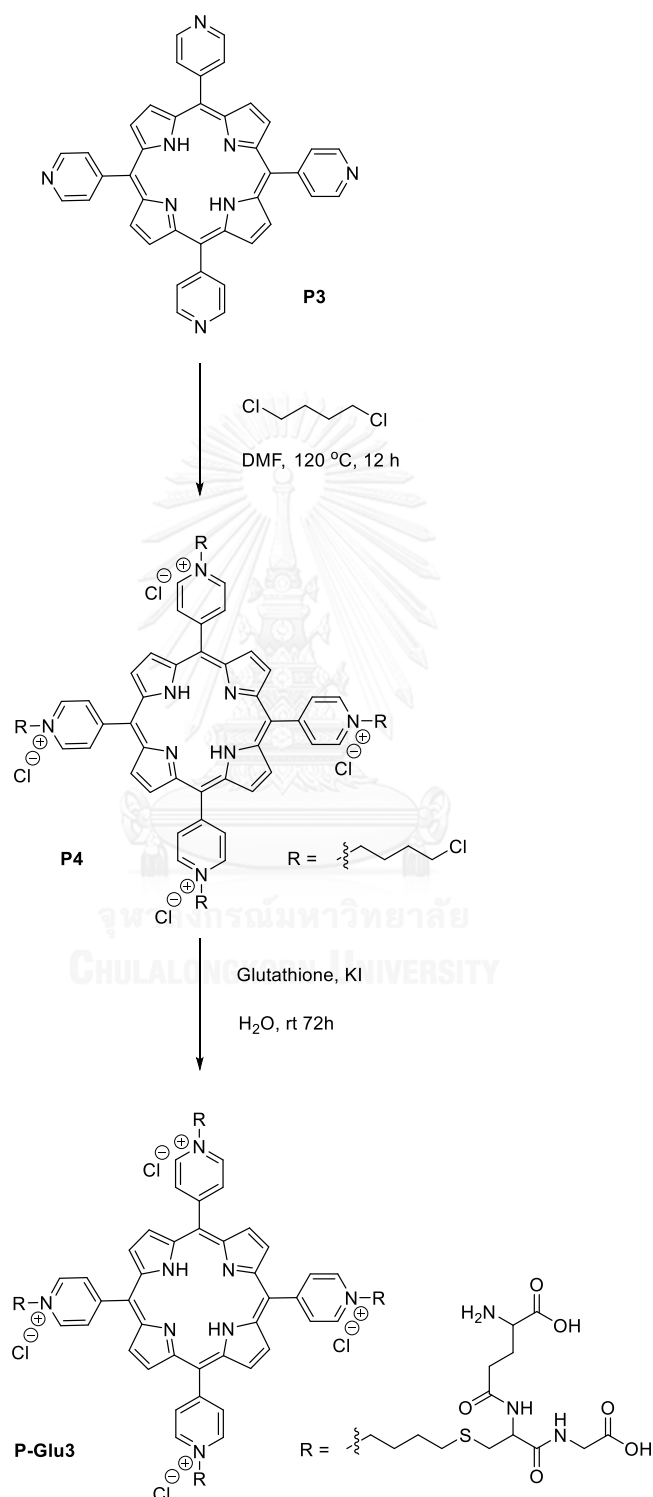
Scheme 4.1: The synthetic route of **P-Glu1** and **P-Glu2**

The synthesis of the target **P-Glu1** and **P-Glu2** started with a condensation of 4-hydroxybenzaldehyde, pyrrole and 4-pyridinecarboxaldehyde in propionic acid to give compound **P1** in 3% yield. The low yield of compound **P1** was attributed to the formation of other statistically possible porphyrinic byproducts and the polymerization of pyrrole upon heating. MALDI-TOF mass spectrum of compound **P1** exhibited its molecular ion peak at m/z 633.503 which was consistent with the previous report⁵⁵. Subsequently, compound **P1** was alkylated with an excess amount of 1,4-dichlorobutane in the presence of K_2CO_3 in DMF at 80 °C for 6 h, resulting in compound **P2** in 64% yield. Lower than this temperature resulted in slow reaction rate, while higher than this temperatures caused more additional alkylation at pyridyl ring of porphyrin. Formation of the compound **P2** was confirmed by the presence of a molecular ion peak in its MALDI-TOF mass spectrum at m/z 723.540 which was consistent with the calculated value (m/z 723.251). After that, glutathione was alkylated with compound **P2** in heterogeneous reaction to obtain **P-Glu1**. Solution of compound **P2** and Bu_4NOH in dichloromethane was added with a solution of glutathione and KI in water. Bu_4NOH is a phase transfer agent assisting the migration of the glutathione from aqueous phase into organic phase (dichloromethane, in this case) where reaction take place. The substitution of chloroalkanes in compound **P2** with KI led to the iodoalkane products which increase the reactivity toward glutathione. After several days, monitoring a reaction by TLC and MALDI-TOF mass spectrometry indicated that no desired product was observed. This is due to the fact that heterogeneous reaction occurs mostly at an interface of solution resulting in lower effectiveness of the reaction. In similar manner, the attempt to do the esterification of compound **P1** with glutathione in heterogeneous reaction to afford **P-Glu2** was also failed related to the reasons described above.

In order to enhance the effectiveness of the reaction, the water soluble porphyrin was used as shown in the next experiment.

4.1.2 Synthesis of glutathione-porphyrin derivative **P-Glu3**

The synthetic route of **P-Glu3** is described in **Scheme 4.2**.



Scheme 4.2: The synthetic route of **P-Glu3**

Compound **P3** was successfully synthesized from condensation of pyrrole and 4-pyridylcarboxaldehyde in propionic acid at 120 °C for 1.5 h affording compound **P3** in 11% yield by following the previously reported procedure⁵⁶. The competitive reaction in the porphyrin formation step, e.g. a polymerization of pyrrole and the formation of other possible N-confused isomers of porphyrin were detected. Therefore, the yield of **P3** was significantly suppressed. According to its ¹H-NMR spectrum, the compound **P3** show three signals for aromatic protons around δ 8 to 9 ppm. A singlet signal of two inner protons of **P3** was absented due to hydrogen–deuterium exchange. This hydrogen–deuterium exchange also makes pyrrole protons **c** broader than usual. In addition, Mass spectra of compound **P3** exhibited molecular ion peaks at m/z 620.027, which was consistent with the calculated value of m/z 618.704. This indicated successful formation of compound **P3**. ¹H-NMR spectrum of compound **P3** was shown in **Figure 4.2**.

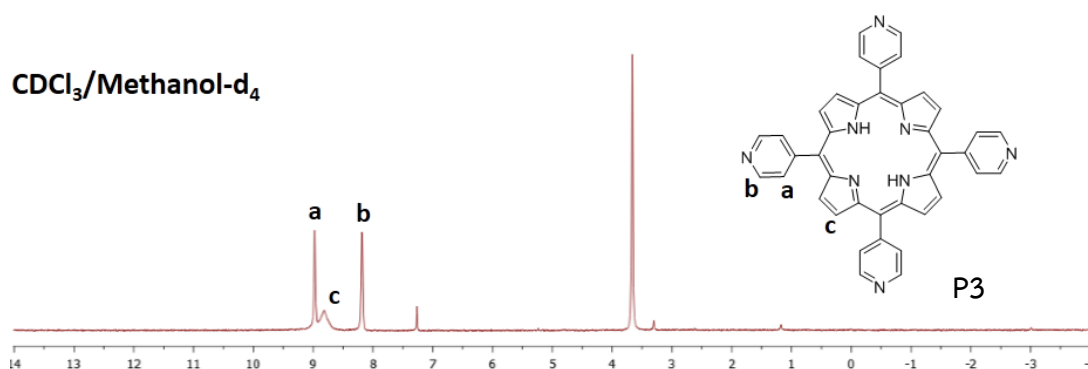


Figure 4.2: ¹H-NMR spectrum of compound **P3**

Compound **P3** was then alkylated with an excess amount of 1,4-dichlorobutane in DMF at 120 °C for 12 h, resulting in compound **P4** in 73% yield. Formation of the compound **P4** was confirmed by the presence of a molecular ion peak in its HR-ESI mass spectrum at m/z 981.310. Although compound **P4** has four positives charge on its molecule, this positive charges was subtracted by the counter anion, resulting in the zero total charge of compound **P4**. Thus, m/z value of compound **P4** was equivalent to its molecular weight. According to its ¹H-NMR

spectrum, compound **P4** exhibited a characteristic singlet signal of inner proton of porphyrin at δ -3.09 ppm. Multiplet protons signals of the pyrrole and pyridine rings slightly shifted from 8.18–8.97 ppm to 9.06–9.68 ppm, compared with compound **P3**, because of inductive effect from the pyridinium group. Moreover, the addition peak of alkyl-protons in **P4** appear around δ 2.11 to 5.07 ppm as shown in **Figure 4.3**.

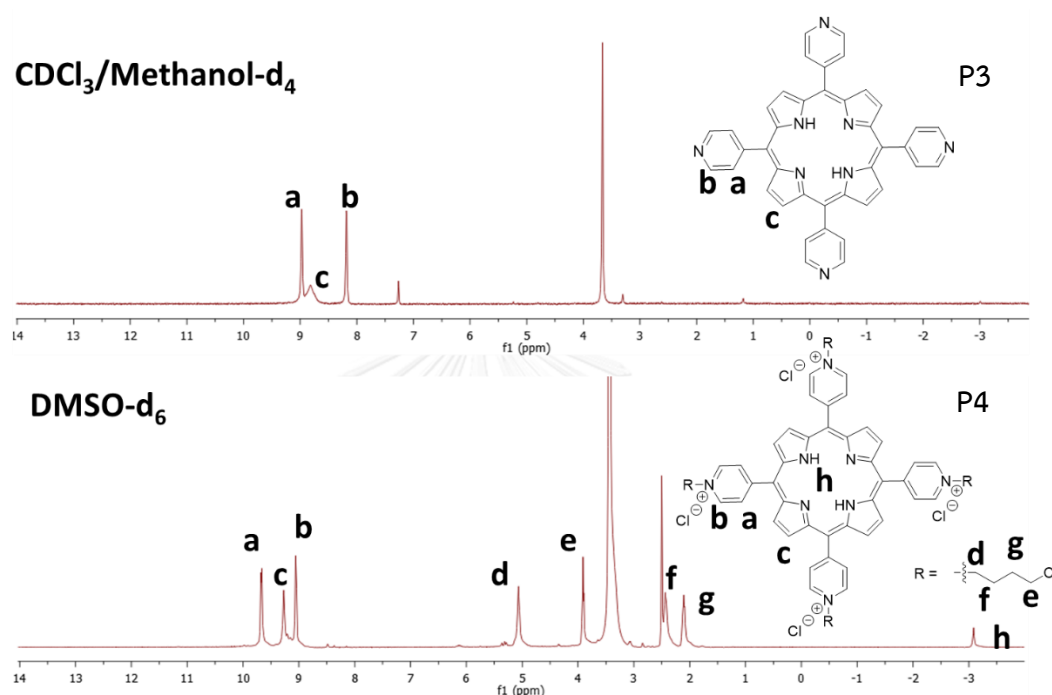
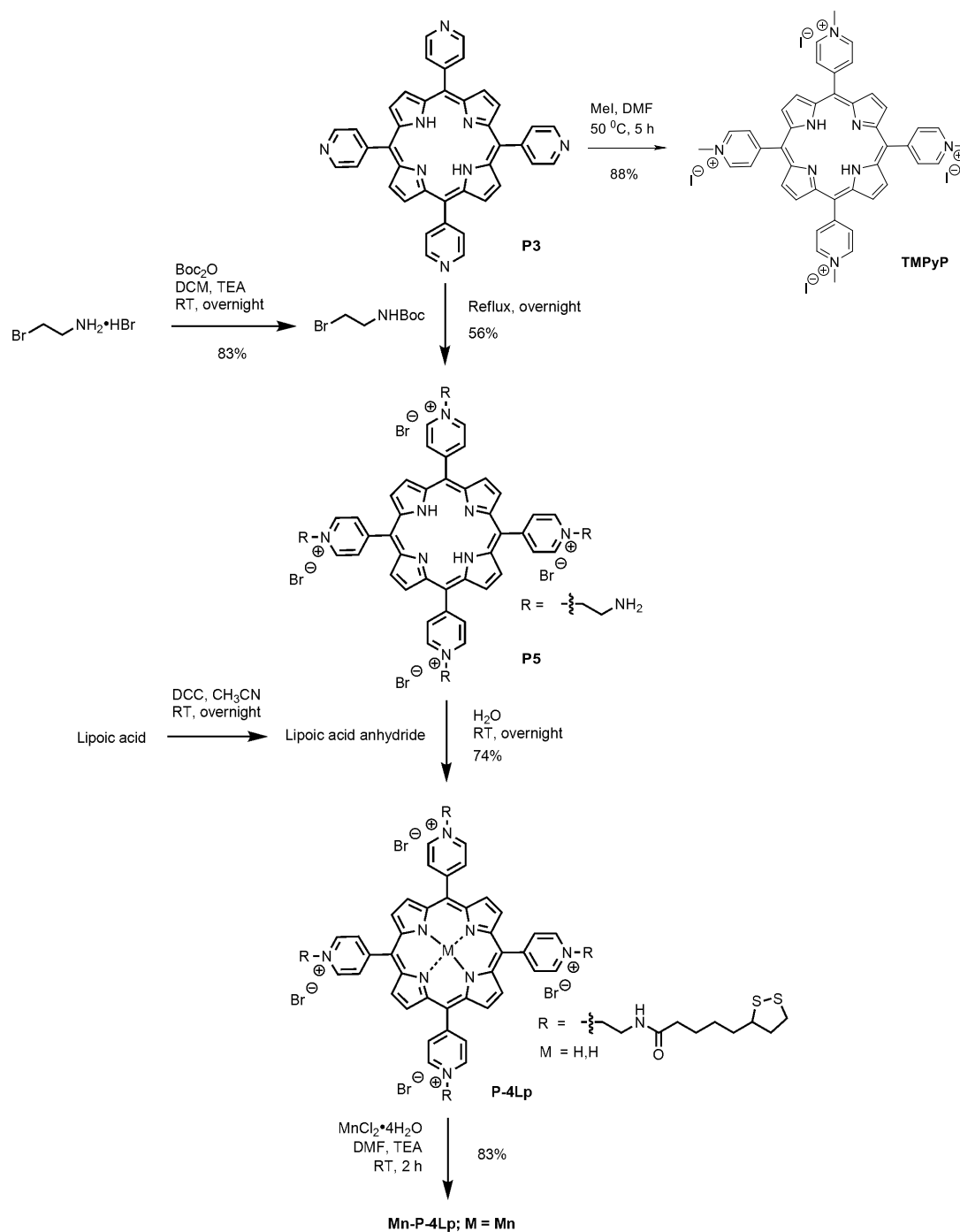


Figure 4.3: ¹H-NMR spectrum of compound **P3** and **P4**

After that, glutathione was alkylated with compound **P4** in water in the presence of KI. After several days, no desired product was observed when monitoring with MALDI-TOF mass spectrometry. The attempt to separate porphyrin from starting material glutathione (GSH) and byproduct glutathione dimer (GSSG), using reverse phase column chromatography with 20% H₂O in MeOH as an eluent, failed due to their similar in polarity. Thus, no evident was indicated that the desired product was really existed.

4.1.3 Synthesis of lipoic acid-porphyrin derivatives **P-4Lp** and **Mn-P-4Lp**

The synthetic route of **P-4Lp** and **Mn-P-4Lp** are described in **Scheme 4.3**.



Scheme 4.3: The synthetic route of lipoyl porphyrin derivatives

Firstly, 2-bromoethylamine hydrobromide was reacted with Boc_2O in the presence of triethylamine in order to reduce the activity of the amine group. The reaction mixture was stirred for 18 h at room temperature then the excess of Boc_2O was removed by adding 0.5 equivalent of DMAP. After several extractions with saturated NH_4Cl and brine, yellow oil of compound **1** was archived in 83% yield. The structure of compound **1** was verified by comparing the $^1\text{H-NMR}$ data with the literature report⁵⁷.

Alkylation of compound **P3** with compound **1** provided compound **P5** in 56% yield. The compound **P5** was obtained as a purple-brown solid after washing with DMF, ethanol and then acetone in an ultrasonic bath to remove excess of compound **1**. During the reaction, the decarboxylation of *tert*-butyl carbamate moiety was occurred due to high temperature presented, resulting in the direct formation of **P5**. Based on MALDI-TOF-MS, some byproducts from polymerization of the aminoethyl side chains were detected. Therefore, the yield of **P5** was significantly suppressed.

Compound **P5** was characterized by $^1\text{H-NMR}$. After attachment of ethylamine at pyridyl group in **P3**, the addition peak, comparing with **P3**, of alkyl-protons in **P5** appear at δ 4.10 and 5.43 ppm. Moreover the peak of aromatic protons **a** and **b** is slightly shifted to downfield because of the inductive effect of cation on the pyridyl ring. A singlet signal of two inner protons and amine protons of **P5** are absented due to hydrogen–deuterium exchange. This hydrogen–deuterium exchange also make pyrrole protons **c** broader than usual. In addition, Mass spectra of compound **P5** exhibited molecular ion peaks at 794.782, which was consistent with the calculated value of 795.010. This indicated successful formation of compound **P5**. $^1\text{H-NMR}$ spectrum of compound **P3** and **P5** was shown in **Figure 4.4**.

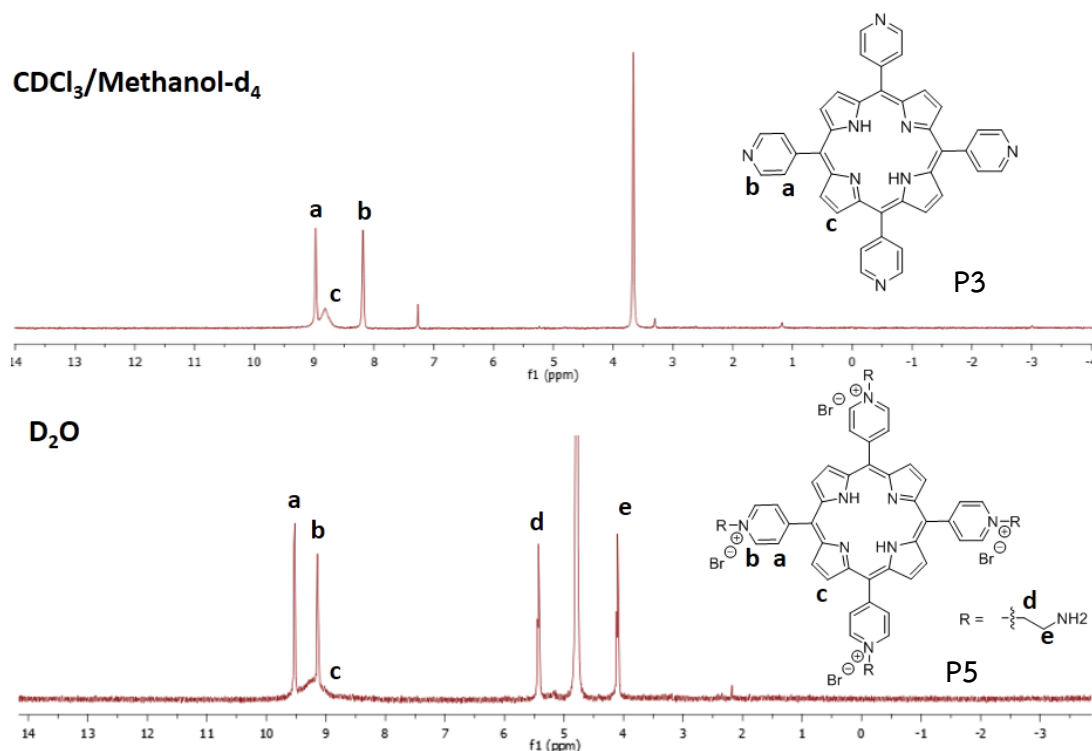


Figure 4.4: ¹H-NMR spectrum of compound **P3** and **P5**

Subsequent amidation of **P5** with lipoic acid anhydride was achieved in a mixed solvent system of H₂O and acetonitrile, affording compound **P-4Lp** as purple-brown solid in 74% yield. It should be noted that the reaction have to be done under N₂ atmosphere because the lipoyl moiety is very sensitive to air⁶⁴.

The ¹H-NMR spectrum of **P-4Lp** in D₂O was shown in **Figure 4.3**. By comparing with ¹H-NMR spectrum of compound **P5**, the formation of **P-4Lp** was confirmed by the appearance of a triplet signal of the amide protons of **P-4Lp** at δ 8.49 ppm and the lipoyl protons around δ 1-3 ppm in its ¹H-NMR spectrum as shown in **Figure 4.5**. Moreover, the MALDI-TOF mass spectrum of **P-4Lp** show the molecular ion peak [M]⁺ at m/z 1548.650, which was consistent with a calculated value of m/z 1548.222.

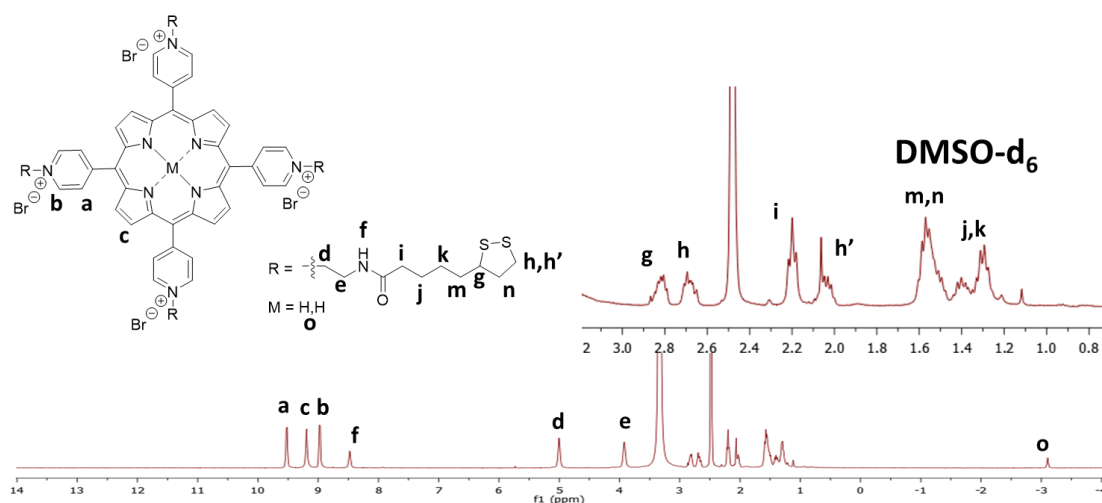


Figure 4.5: $^1\text{H-NMR}$ spectrum of compound **P-4Lp**

To obtain the desired **Mn-P-4Lp**, **P-4Lp** was metallated by manganese(II) chloride tetrahydrate in the presence of triethylamine in DMF at room temperature for 2 h leading to compound **Mn-P-4Lp** in 80% yield as dark-green solid. Triethylamine act as a base to deprotonate two inner protons of porphyrin resulting in rate acceleration in the metalation. The formation of **Mn-P-4Lp** was confirmed by UV-Visible. The maximum absorption band was shifted from 430 to 464 nm due to metal-to-ligand charge transfer (MLCT) that lower the HOMO-LUMO energy gap. In addition, disappearance of emission band of **P-4Lp** at 658 and 721 nm indicated complete formation of **Mn-P-4Lp** in the metalation step as shown in **Figure 4.6**. This quenching of fluorescence of **Mn-P-4Lp** was caused by the exchange interaction between π -electronic systems of **Mn-P-4Lp** with the unpaired d-electron of manganese ion.

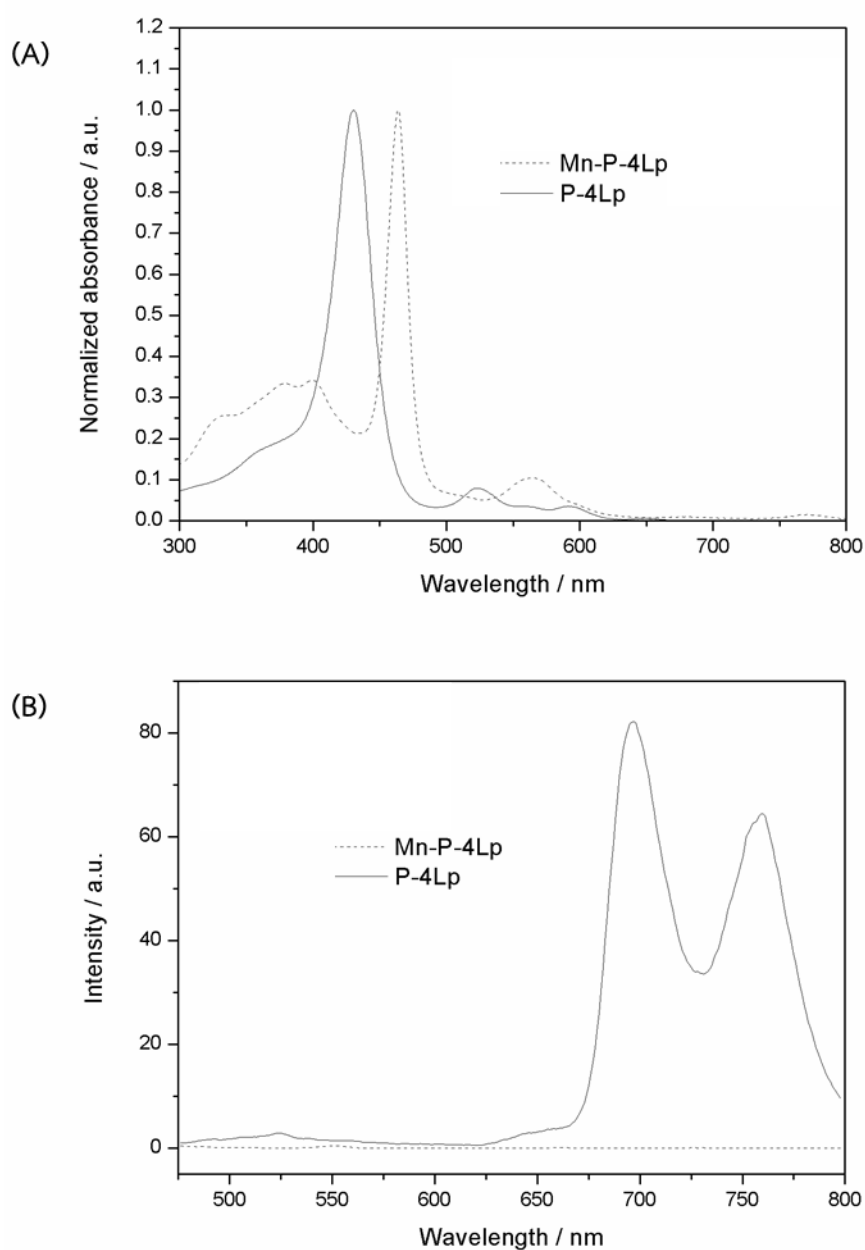


Figure 4.6: (A) Normalized UV-Vis absorption spectra of **Mn-P-4Lp** and **P-4Lp**, (B) emission spectra of **Mn-P-4Lp** and **P-4Lp**.

In order to evaluate the effect of lipoyl group in **P-4Lp** on biological activities, the cationic **TMPyP** without lipoyl group was used as benchmark compound to compare biological activities with **P-4Lp**, following a literature reported previously⁵⁹. **TMPyP** was accomplished by treatment compound **P1** with iodomethane at 50 °C for

5 h. The product was washed several times with diethyl ether and acetone, affording purple-brown solid **TMPyP** in 88% yield.

TMPyP was characterized by $^1\text{H-NMR}$ and MALDI-TOF-MS which were in good agreement with the literature reports. By comparing with $^1\text{H-NMR}$ spectrum of compound **P1**, the formation of **TMPyP** was confirmed by the appearance of a methyl proton of **TMPyP** at δ 4.73 ppm as shown in **Figure 4.7**. The $^1\text{H-NMR}$ spectrum of **TMPyP** also showed characteristic peaks of the two inner protons of porphyrin ring at δ -3.11 ppm. Moreover, the MALDI-TOF mass spectrum of **TMPyP** show the molecular ion peak $[\text{M}]^+$ at m/z 679.158, which was consistent with a calculated value of m/z 678.842.

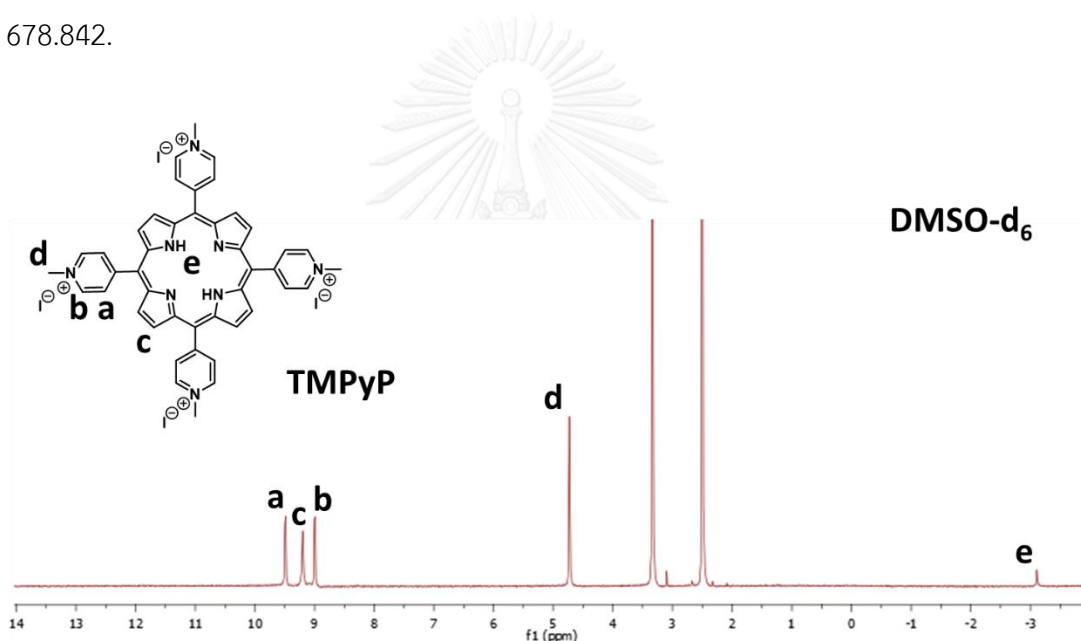


Figure 4.7: $^1\text{H-NMR}$ spectrum of **TMPyP**

4.2 Biological studies of Porphyrin derivatives

4.2.1 Cytotoxicity

The cellular cytotoxicity of lipoic acid and the porphyrin compounds **TMPyP**, **P-4Lp** and **Mn-P-4Lp** was investigated by cell viability assay on HDFa and HaCaT cells. This assay is detecting the reducing environment within viable or alive cell. By using PrestoBlue reagent, the reducing environment can convert the PrestoBlue reagent to red fluorescence dye which exhibit emission spectra at 590 nm. The experiment started by treating HDFa and HaCaT cell lines with DMEM (as a control reagent), **LA**, **TMPyP**, **P-4Lp** and **Mn-P-4Lp** at concentration of 25, 50, 100 and 150 mg/L for 24 h in 96-well plates. Then, PrestoBlue reagent was added into cell and incubated for 30 min. Finally, the fluorescence emission spectra was measured at room temperature at an excitation wavelength of 560 nm and emission wavelength at 590 nm. The percentage of cell viability was calculated by normalizing the fluorescence intensity of analyte to the intensity of control. In case of the HDFa cells, the cell viability of **LA**, **TMPyP**, **P-4Lp** and **Mn-P-4Lp** was shown in **Figure 4.8**.

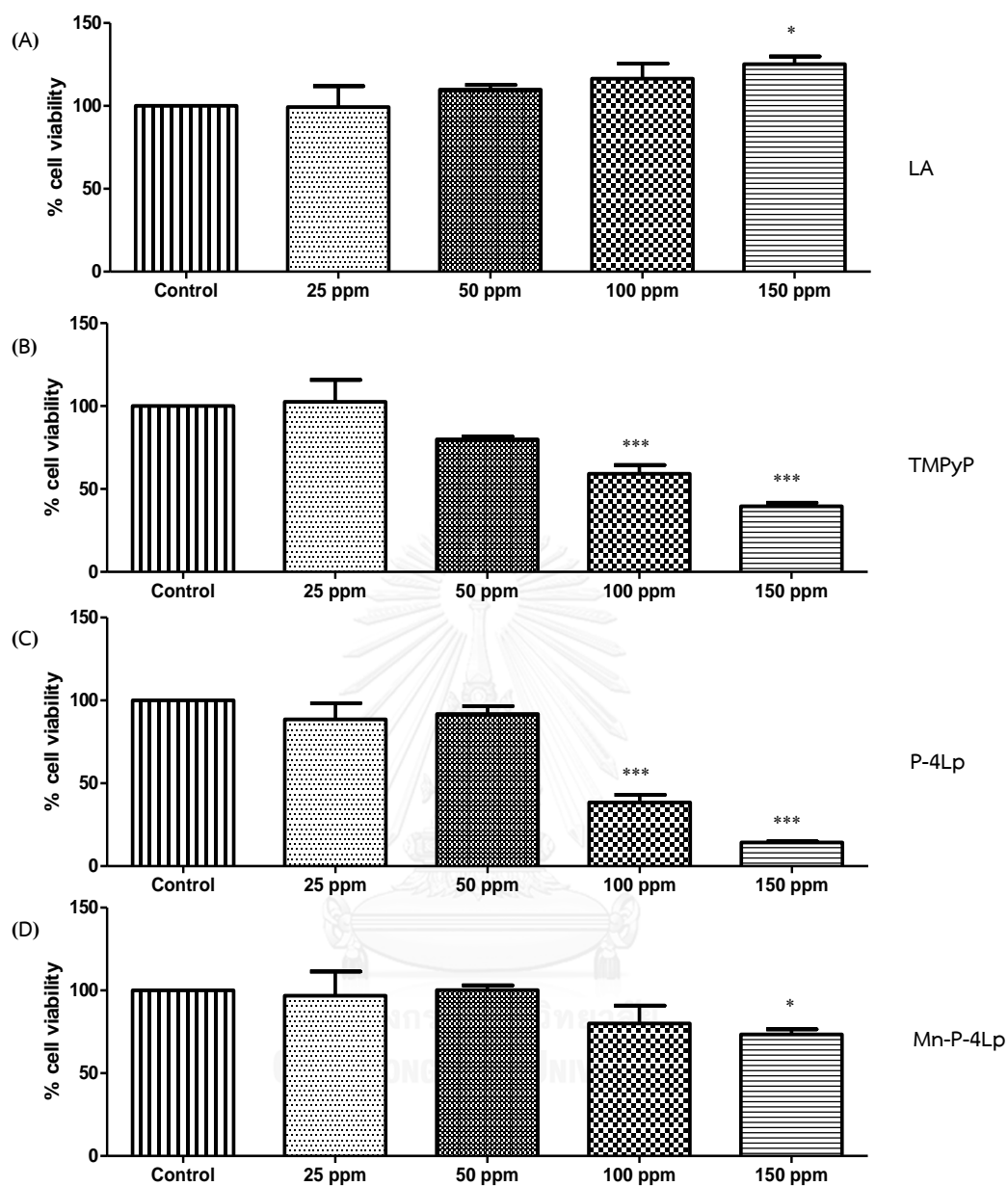


Figure 4.8: Cell viability upon the treatment of HDFa cell with (A) LA, (B) TMPyP, (C) P-4Lp, (D) Mn-P-4Lp at 25, 50, 100, 150 mg/L. (“***” indicates $p < 0.001$, “*” indicates $p < 0.05$, significant differences between control and each treatment group).

The cell viability of the HDFa cell treated with **LA** from 25 mg/L to 100 mg/L did not significantly change as compared to controls (**Figure 4.8 (A)**). While treatment of HDFa cell with 150 mg/L of **LA** showed significantly increase ($p < 0.05$) in cell viability. Moreover, **LA** was found to have IC_{50} more than 150 mg/L against HDFa cells. This result indicated that **LA** exhibited low cytotoxicity and may slightly increase enzymatic activity that caused cell to proliferate more than control⁶⁵.

Figure 4.8 (B) shows that the cell viability of the HDFa cells did not significantly change after being treated with **TMPyP** at 25 and 50 mg/L, compared with the control group. While at the concentration of 100 and 150 mg/L of **TMPyP**, decreasing of the cell viability became significant ($p < 0.001$). This results indicated that **TMPyP** exhibited cytotoxicity at high concentration. In addition, IC_{50} of **TMPyP** against HDFa cells was in the range of 100–150 mg/L.

In a similar manner as **TMPyP**, the cell viability of the HDFa cells did not significantly change when being treated with **P-4Lp** at the concentration of 25 and 50 mg/L (**Figure 4.8 (C)**). However, at the concentrations of 100 and 150 mg/L of **P-4Lp**, dramatically decrease in the cell viability of the HDFa cells was observed. This results indicated that **P-4Lp** at high concentration exhibited cytotoxicity. Moreover, **P-4Lp** was found to have IC_{50} value in the range of 50–100 mg/L against HDFa cells.

Furthermore, treatment of HDFa cells with 25 to 100 mg/L of **Mn-P-4Lp** did not affect cell viability (**Figure 4.8 (D)**). While HDFa cells treated with 150 mg/L of **Mn-P-4Lp** showed significantly decrease in cell viability ($p < 0.05$) as compared to controls. This results indicated that **Mn-P-4Lp** exhibited cytotoxicity to the HDFa cells at high concentration. In addition, **Mn-P-4Lp** was found to have IC_{50} more than 150 mg/L against HDFa cells.

The effect of the introduction of the porphyrin unit on the cell viability of the HDFa cells can be determined by the comparison of the results of **LA** and those of **P-4Lp**. **LA** had the IC_{50} value more than 150 mg/L, while **P-4Lp** exhibited the IC_{50} around 50–100 mg/L. This results indicated that the introduction of the porphyrin unit induced the cytotoxicity against HDFa cells.

In addition, the effect of lipoyl group on cell viability of the HDFa cells can be determine by the comparison between IC_{50} value of **TMPyP** and **P-4Lp**. **TMPyP** exhibited the IC_{50} of 100–150 mg/L, while **P-4Lp** showed the IC_{50} of 50–100 mg/L. This informed that the attachment of lipoyl group to porphyrin increased the cytotoxicity against HDFa cells.

Moreover, the effect of the introduction of the Mn-chelation of the porphyrin unit on the cell viability of the HDFa cells can be determined by the comparison of the results of **P-4Lp** and those of **Mn-P-4Lp**. **P-4Lp** exhibited the IC_{50} around 50–100 mg/L, while **Mn-P-4Lp** had the IC_{50} value more than 150 mg/L. This indicated that the introduction of the Mn-chelation of the porphyrin unit can decrease cytotoxicity against HDFa cells. According to previous report, this decreasing in cytotoxicity possibly related to their essential role in development, activation of certain metalloenzymes, energy metabolism, immunological system function⁶⁶.

In case of the HaCaT cells, the cell viability of **LA**, **TMPyP**, **P-4Lp** and **Mn-P-4Lp** was shown in **Figure 4.9**.

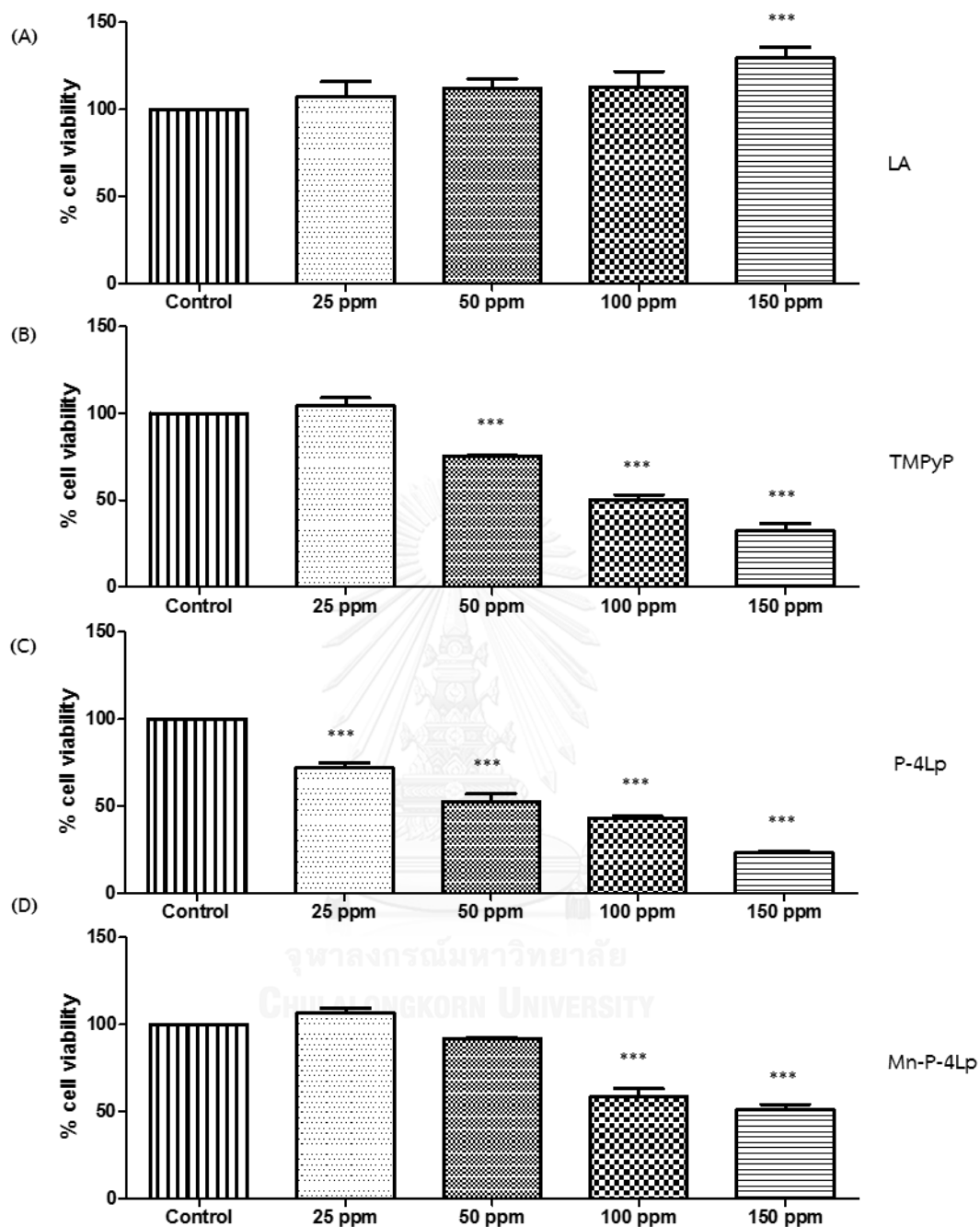


Figure 4.9: Cell viability upon the treatment of HaCaT cell with (A) LA, (B) TMPyP, (C) P-4Lp, (D) Mn-P-4Lp at 25, 50, 100, 150 mg/L. (“***” indicates $p < 0.001$, “*” indicates $p < 0.05$, significant differences between control and each treatment group).

The cell viability of the HaCaT cell treated with **LA** from 25 mg/L to 100 mg/L did not significantly change as compared to controls (**Figure 4.9 (A)**). While treatment of HaCaT cell with 150 mg/L of **LA** showed significantly increase ($p < 0.001$) in cell viability. Moreover, **LA** was found to have IC_{50} more than 150 mg/L against HaCaT cells. This result indicated that **LA** exhibited low cytotoxicity and proliferation of the HaCaT cells at high concentration.

Figure 4.9 (B) shows that the cell viability of the HaCaT cells did not significantly change after being treated with **TMPyP** at 25 mg/L, compared with the control group. While at the concentration of 50 to 150 mg/L of **TMPyP**, decreasing of the cell viability became significant ($p < 0.001$). These results indicated that **TMPyP** exhibited cytotoxicity at high concentration. In addition, IC_{50} of **TMPyP** against HaCaT cells was in the range of 100–150 mg/L.

As shown in **Figure 4.9 (C)**, the cell viability of the HaCaT cells dramatically decreased when being treated with **P-4Lp** at the concentration of 25 to 150 mg/L ($p < 0.001$). This results indicated that **P-4Lp** exhibited cytotoxicity. Moreover, **P-4Lp** was found to have IC_{50} value in the range of 50–100 mg/L against HaCaT cells.

Furthermore, treatment of HaCaT cells with 25 and 50 mg/L of **Mn-P-4Lp** did not affect cell viability (**Figure 4.9 (D)**). While HaCaT cells treated with 100 and 150 mg/L of **Mn-P-4Lp** showed significantly decrease in cell viability ($p < 0.001$) as compared to controls. This results indicated that **Mn-P-4Lp** exhibited cytotoxicity to the HaCaT cells at high concentration. In addition, **Mn-P-4Lp** was found to have IC_{50} more than 150 mg/L against HaCaT cells.

The effect of the introduction of the porphyrin unit on the cell viability of the HaCaT cells can be determined by the comparison of the results of **LA** and those of **P-4Lp**. **LA** had the IC_{50} value more than 150 mg/L, while **P-4Lp** exhibited the IC_{50} around 50–100 mg/L. This results indicated that the introduction of the porphyrin unit induced the cytotoxicity against HaCaT cells.

In addition, the effect of lipoyl group on cell viability of the HaCaT cells can be determined by the comparison between IC_{50} value of **TMPyP** and **P-4Lp**. **TMPyP** exhibited the IC_{50} of 100–150 mg/L, while **P-4Lp** showed the IC_{50} of 50–100 mg/L. This informed that the attachment of lipoyl group to porphyrin increased the cytotoxicity against HaCaT cells.

Moreover, the effect of the introduction of the Mn-chelation of the porphyrin unit on the cell viability of the HaCaT cells can be determined by the comparison of the results of **P-4Lp** and those of **Mn-P-4Lp**. **P-4Lp** exhibited the IC_{50} around 50–100 mg/L, while **Mn-P-4Lp** had the IC_{50} value more than 150 mg/L. This indicated that the introduction of the Mn-chelation of the porphyrin unit can decrease cytotoxicity against HaCaT cells due to their essential role in development, activation of certain metalloenzymes, energy metabolism, immunological system function⁶⁶.

According to above-mentioned IC_{50} results, the concentration of 25 and 50 mg/L of all compounds of interest was chosen for the ROS generation assay in both types of cells.

4.2.2 Antioxidant Activity

Antioxidant activity of lipoic acid and the porphyrin compounds **TMPyP**, **P-4Lp** and **Mn-P-4Lp** was investigated by ROS generation assay on HDFa and HaCaT cells. The assay used to measure ROS within cell using H_2DCFDA reagent. The non-fluorescent H_2DCFDA diffuses through cells membrane then H_2DCFDA is converted to the highly fluorescent 2',7'-dichlorofluorescein (DCF) by ROS. The experiment started by treating HDFa and HaCaT cell lines with DMEM (as a control reagent), **LA**, **TMPyP**, **P-4Lp** and **Mn-P-4Lp** at concentration of 25 and 50 mg/L for 24 h in 96-well plates. Then, H_2DCFDA reagent was added into plates and incubated for 30 min at 37°C in the dark. Finally, the cells were treated with H_2O_2 to induce ROS generation and the fluorescence was measured using a microplate reader with excitation at 485 nm and emission at 528 nm every 10 min until 1 h. The percentage of ROS generation was calculated by normalizing the fluorescence intensity of analyte to the intensity of control. The formation of DCF by H_2O_2 was shown in **Figure 4.10**.

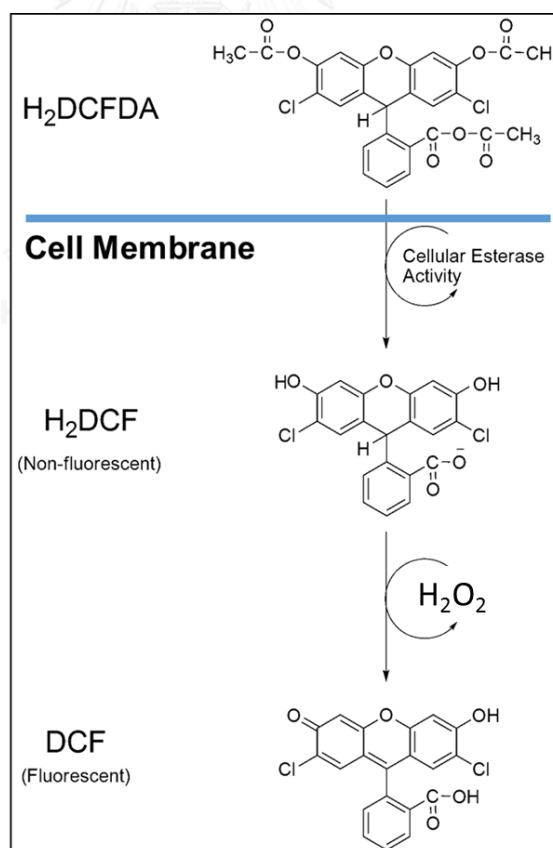


Figure 4.10: Formation of fluorescent Compound DCF by H_2O_2 in cell.

4.2.2.1 ROS generation in the HDFa cells

In case of treating HDFa cells with H_2O_2 (for 0 min to 60 min), treatment of cells with **LA** at the concentration of 25 mg/L did not change the ROS generation. While treatment of cells with **LA** at the concentration of 50 mg/L seemed to decrease ROS generation with no significant comparing to the control (DMEM) as shown in **Figure 4.11**. This indicated that **LA** seemed to exhibit antioxidant activity toward HDFa cells. Since the ROS generations of cells when treating with **LA** at the concentration of 25 mg/L were always higher than that of 50 mg/L, **LA** was considered to have dose-dependent effect in the ROS generation.

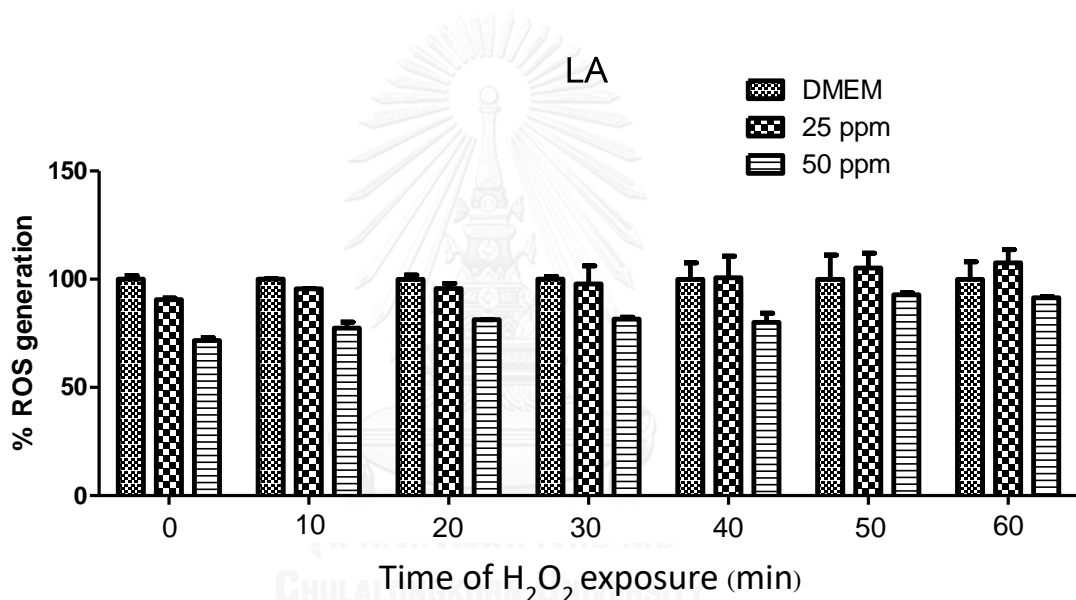


Figure 4.11: ROS generation observed in the HDFa cells upon the treatment of DMEM and **LA** at the concentration of 25 and 50 mg/L for 24 h then HDFa cells was treated with H_2O_2 for 0, 10, 20, 30, 40, 50 and 60 min.

The treatment of HDFa cells with **TMPyP** at the concentration of 25 and 50 mg/L did not affect the ROS generation both before and after treatment with H_2O_2 comparing to the control (**Figure 4.12**). This implied that **TMPyP** did not have dose dependent effect on ROS generation and exhibited no antioxidant activity toward HaCaT cells.

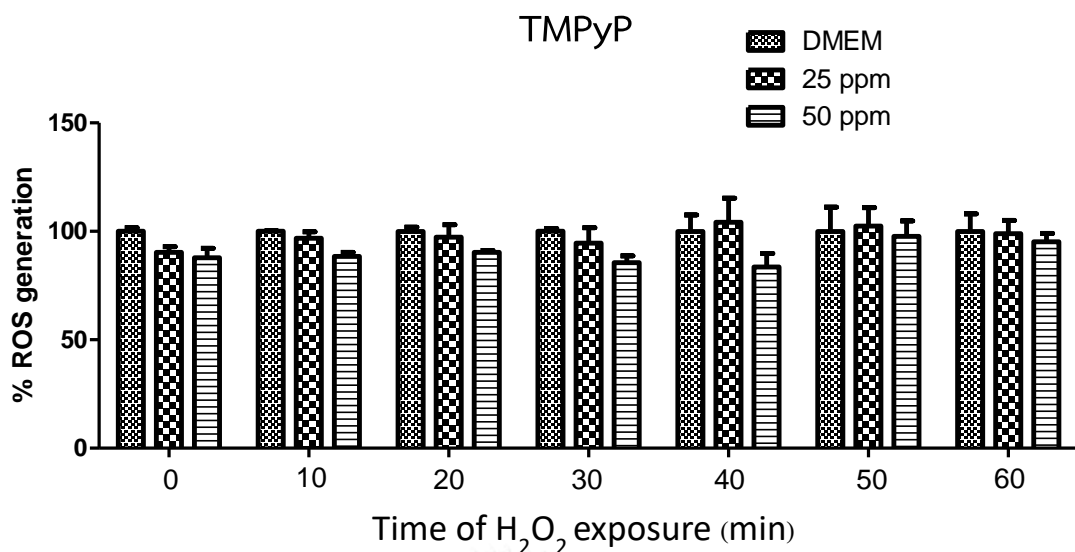


Figure 4.12: ROS generation observed in the HDFa cells upon the treatment of DMEM and TMPyP at the concentration of 25 and 50 mg/L for 24 h then HDFa cells was treated with H₂O₂ for 0, 10, 20, 30, 40, 50 and 60 min.

In the similar manner as TMPyP, the treatment of HDFa cells with P-4Lp at the concentration of 25 and 50 mg/L did not affect the ROS generation both before and after treatment with H₂O₂ comparing to the control (Figure 4.13). This indicated that that P-4Lp did not have dose dependent effect on ROS generation and exhibited no antioxidant activity toward HaCaT cells.

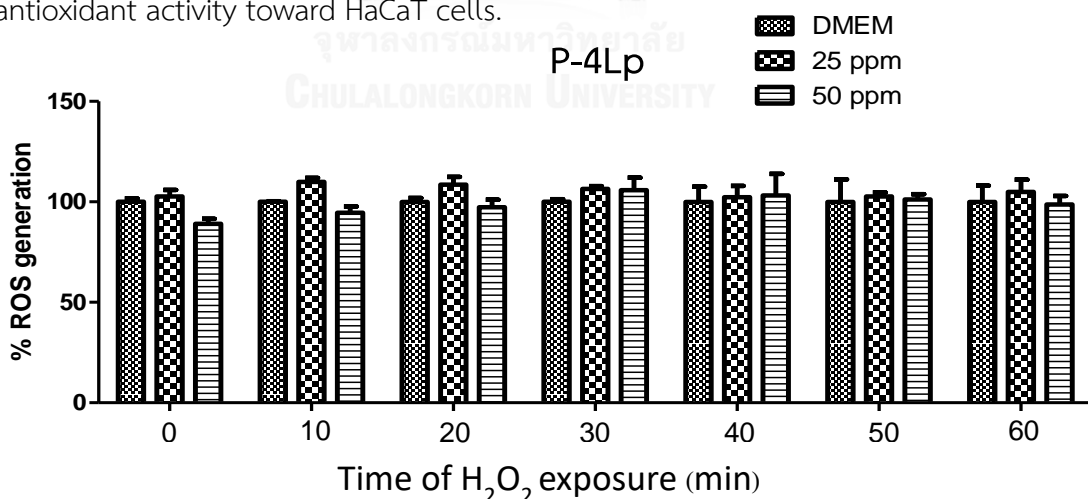


Figure 4.13: ROS generation observed in the HDFa cells upon the treatment of DMEM and P-4Lp at the concentration of 25 and 50 mg/L for 24 h then HDFa cells was treated with H₂O₂ for 0, 10, 20, 30, 40, 50 and 60 min.

The ROS generation observed for the HDFa cells treated with **Mn-P-4Lp** at the concentration of 25 and 50 mg/L, and then treated with H₂O₂ for 10 to 60 min is shown in Figure 4.14.

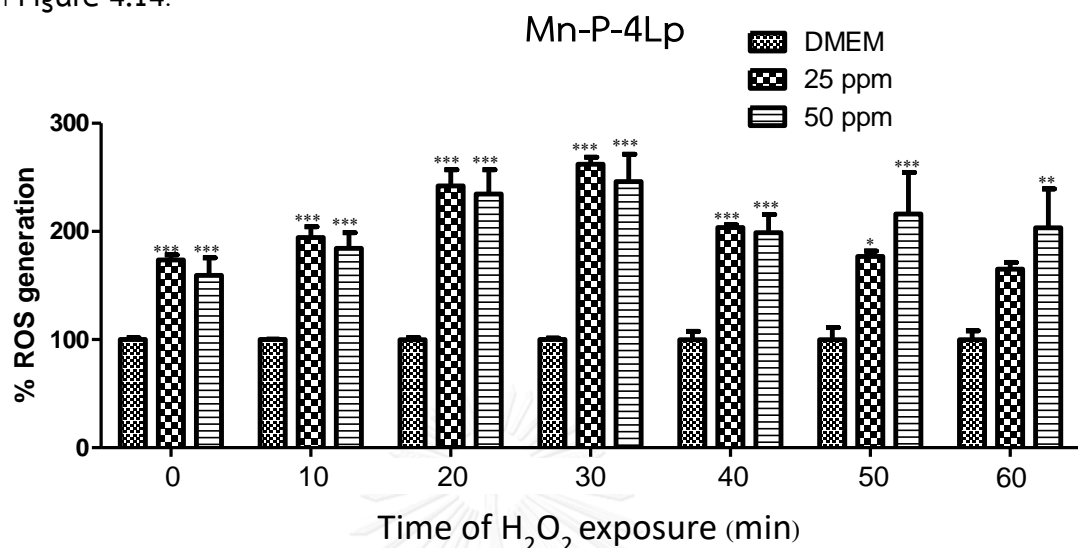


Figure 4.14: ROS generation observed in the HDFa cells upon the treatment of DMEM and **Mn-P-4Lp** at the concentration of 25 and 50 mg/L for 24 h then HDFa cells was treated with H₂O₂ for 0, 10, 20, 30, 40, 50 and 60 min (“***” indicates p < 0.001, “**” indicates p < 0.01 and “*” indicates p < 0.05).

In the absence of H₂O₂ (at 0 min), the treatment of HDFa cells with **Mn-P-4Lp** at the concentration of 25 mg/L significantly increased ROS generation. After the cells were treated with H₂O₂ for 10 to 30 min, the ROS generation was slightly increased. Then, the ROS generation gradually decreased at 40 to 60 min of the H₂O₂ exposure. However, at 60 min of the H₂O₂ exposure, the ROS generation observed in the cells was still higher than the control batch. This indicated that **Mn-P-4Lp** induced ROS generation instead of scavenging ROS toward HDFa cells, but seemed to be able to scavenge ROS from external source like H₂O₂ addition. Similar results were obtained when 50 mg/L of **Mn-P-4Lp** was used. The similar ROS generation between 25 and 50 mg/L of **Mn-P-4Lp** indicated that **Mn-P-4Lp** has no dose-dependent effect in the ROS generation.

The effect of the introduction of the porphyrin unit on the ROS generation of the HDFa cells can be determined by the comparison of the ROS generation between LA and P-4Lp (Figure 4.15). At the concentration of 25 mg/L, the treatment of the cells with both LA and P-4Lp did not show significant difference in the ROS generation. However, at the concentration of 50 mg/L, the treatment of the cells with P-4Lp exhibited significant increase in the ROS generation (at 0 to 20 min of the H₂O₂ exposure), compared with those of LA. This results indicated that the introduction of the porphyrin unit slightly affect the ROS generation of the HDFa cells.

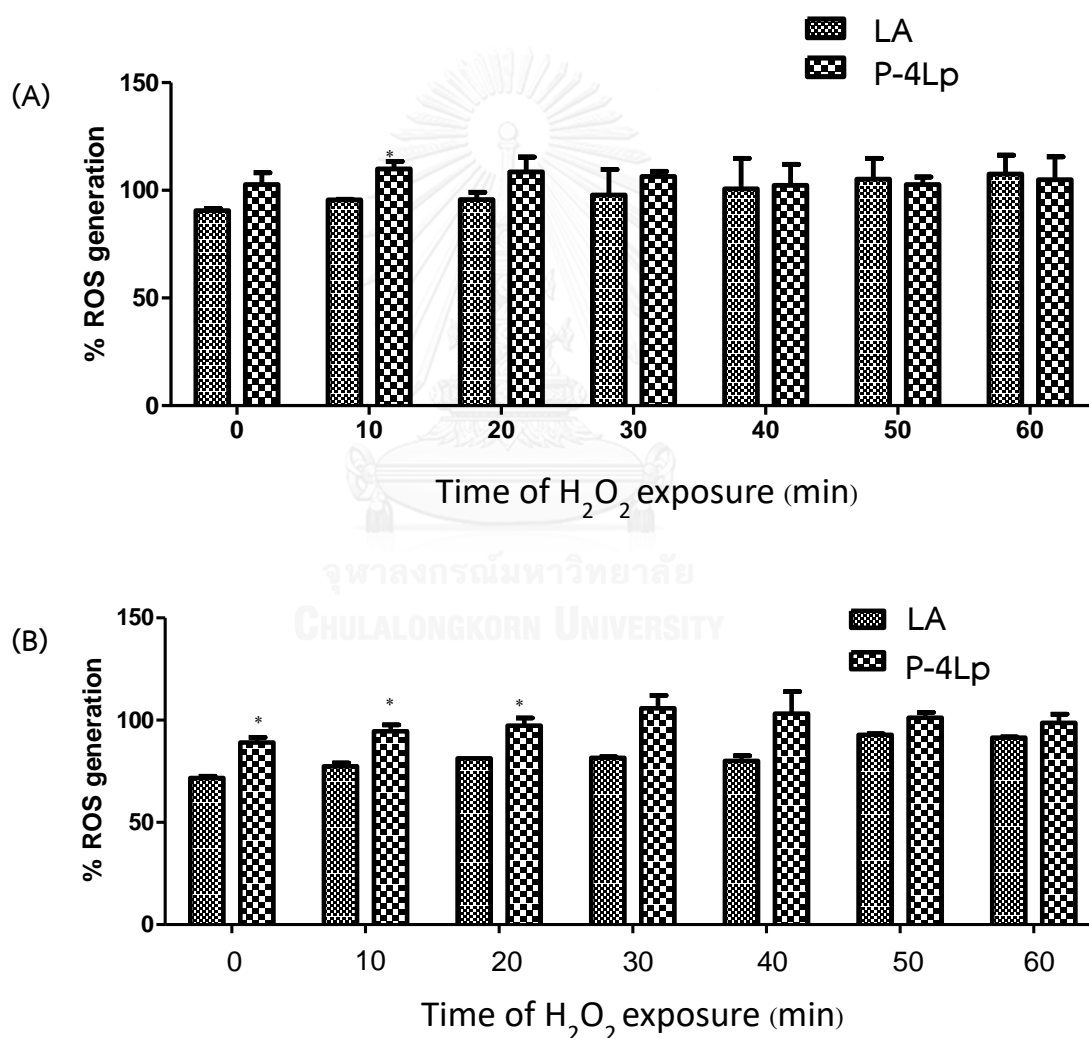


Figure 4.15: The ROS generation observed in the HDFa cells upon the treatment with LA and P-Lp at the concentration of (A) 25 mg/L and (B) 50 mg/L for 24 h, followed by the treatment with H₂O₂ for 0, 10, 20, 30, 40, 50 and 60 min.

The effect of the introduction of lipoyl unit on the ROS generation of the HDFa cells can be determined by the comparison of the ROS generation between **TMPyP** and **P-4Lp** (Figure 4.16). The treatment of the HDFa cells with both **TMPyP** and **P-4Lp** at the concentration of 25 and 50 mg/L did not show significant difference in the ROS generation both before and after the exposure to H_2O_2 . This results indicated that the introduction of lipoyl unit on the porphyrin did not significantly affect the ROS generation in the HDFa cells.

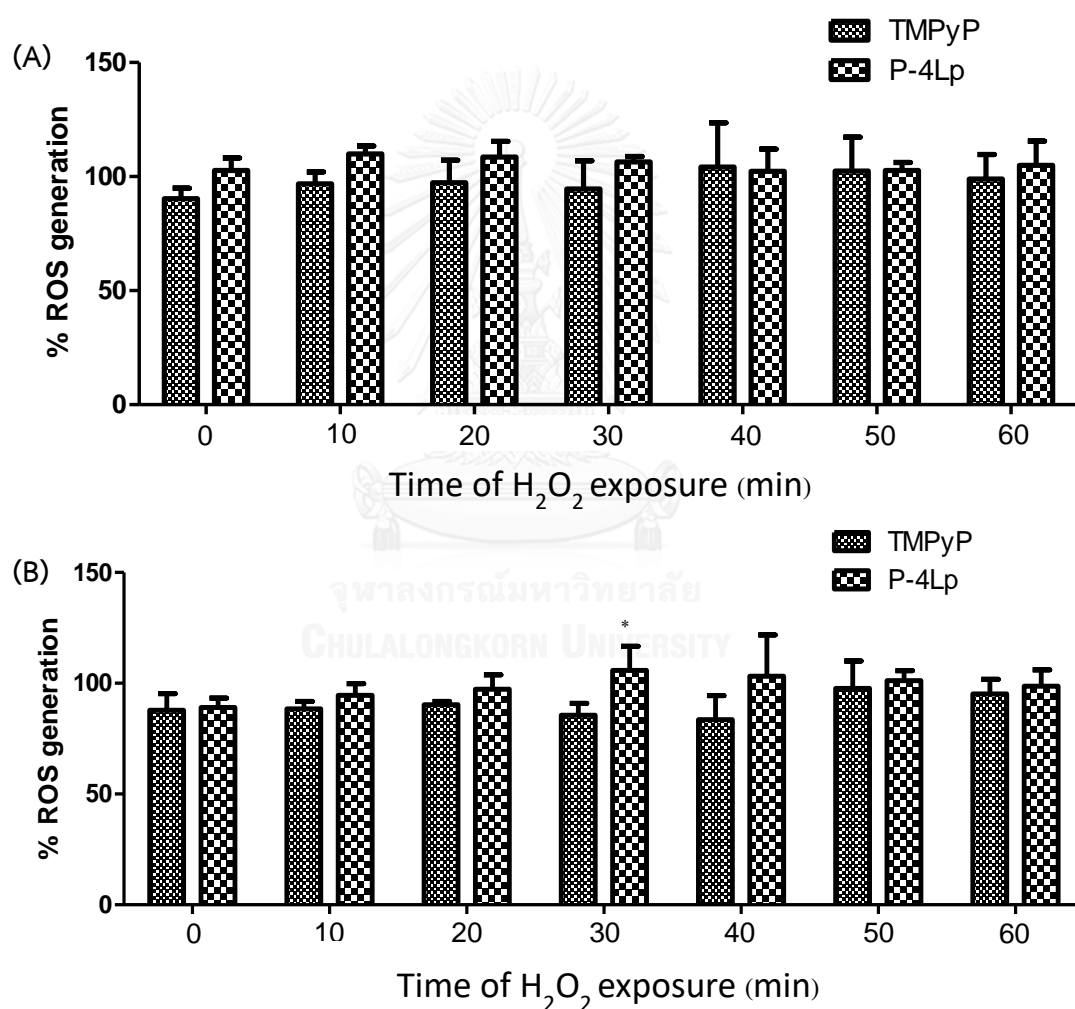


Figure 4.16: The ROS generation observed in the HDFa cells upon the treatment with **TMPyP** and **P-Lp** at the concentration of (A) 25 mg/L and (B) 50 mg/L for 24 h, followed by the treatment with H_2O_2 for 0, 10, 20, 30, 40, 50 and 60 min.

The effect of the introduction of the Mn-chelation in the porphyrin unit on the ROS generation of the HDFa cells can be determined by the comparison of the ROS generation between **P-4Lp** and those of **Mn-P-4Lp** as shown in **Figure 4.17**.

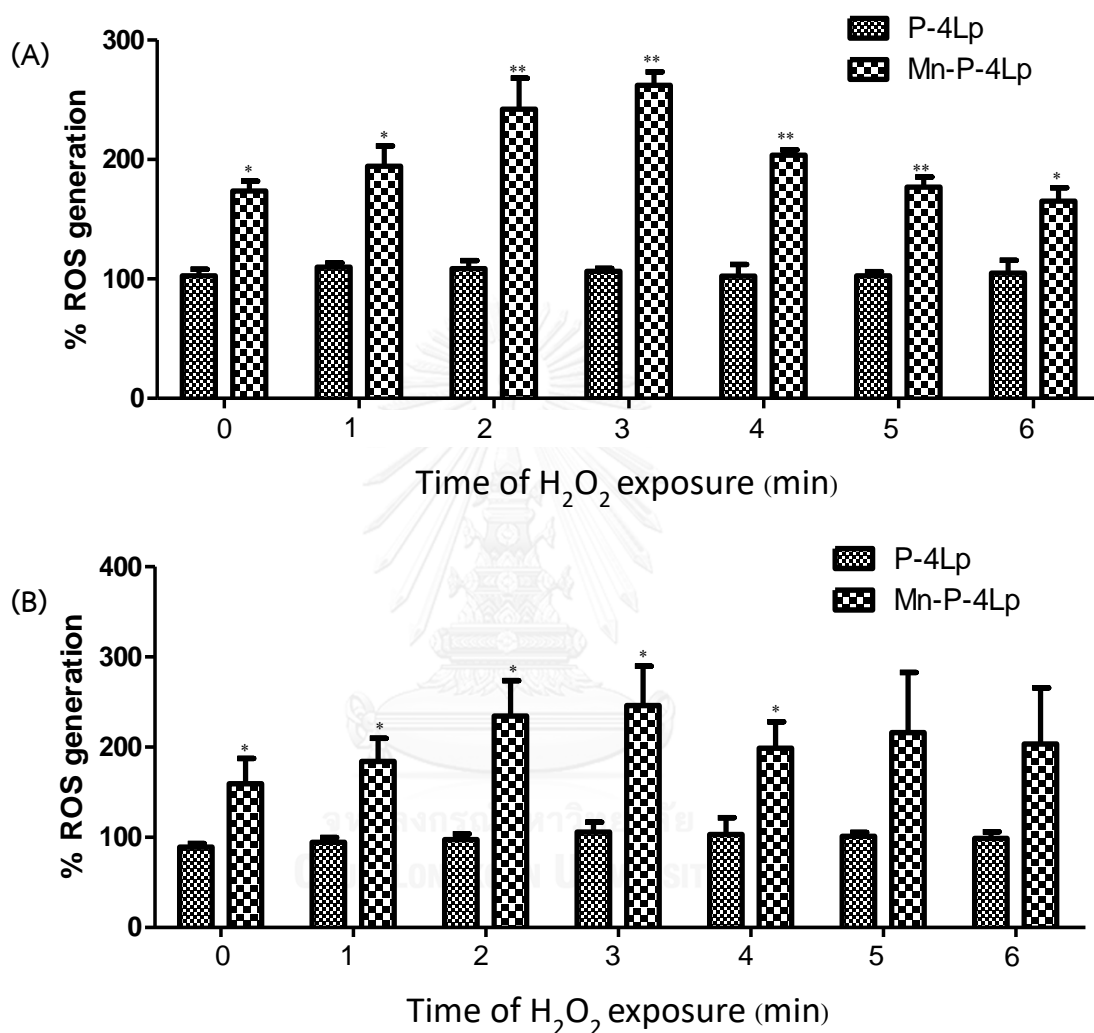
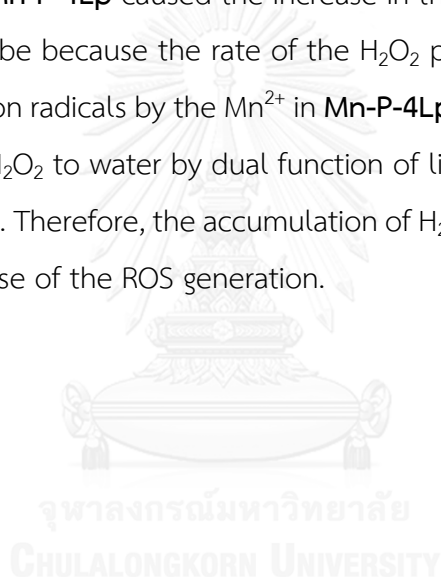


Figure 4.17: ROS generation observed in the HDFa cells upon the treatment of **P-4Lp** and **Mn-P-4Lp** at the concentration of 25 mg/L (A) and 50 mg/L (B) for 24 h then HDFa cells was treated with H_2O_2 for 0, 10, 20, 30, 40, 50 and 60 min (“***” indicates $p < 0.01$ and “*” indicates $p < 0.05$).

In the absence of H_2O_2 (at 0 min), the treatment of HaCaT cells with **P-4Lp** and **Mn-P-4Lp** at the concentration of 25 and 50 mg/L showed significantly different in ROS generation. After the cells were treated with H_2O_2 for 10 to 30 min, the difference in

ROS generation was significantly increased. After that, the difference in ROS generation gradually decreased at 40 to 60 min of the H₂O₂ exposure. Following a previous report⁶⁷ where Mn(II)-porphyrin unit was conjugated with catalase to form a catalyst that could reduce superoxide anion radicals to H₂O₂ by the function of Mn²⁺ and could reduce H₂O₂ further to water under the catalysis of catalase. In a similar manner, the Mn(II)-porphyrin unit in Mn-P-4Lp is expected to reduce the superoxide anion radicals and its lipoyl group is expected to convert the resulting H₂O₂ to water. Lipoic acid has an importance role in inducing elevation of glutathione level in the cell²⁸ that involves the conversion of H₂O₂ to water⁶⁸. However, our results in this section indicated that the Mn-chelation of **Mn-P-4Lp** caused the increase in the ROS generation in the HDFa cells. This is likely to be because the rate of the H₂O₂ production from the reduction of the superoxide anion radicals by the Mn²⁺ in **Mn-P-4Lp** is higher than the conversion rate of the resulting H₂O₂ to water by dual function of lipoyl moiety in **Mn-P-4Lp** and glutathione in the cell. Therefore, the accumulation of H₂O₂ in the HDFa cells occurred, resulting in the increase of the ROS generation.



4.2.2.2 ROS generation in the HaCaT cells

The ROS generation observed for the HaCaT cells treated with **LA** at the concentration of 25 and 50 mg/L, and then with H₂O₂ for 10–60 min is shown in **Figure 4.18**.

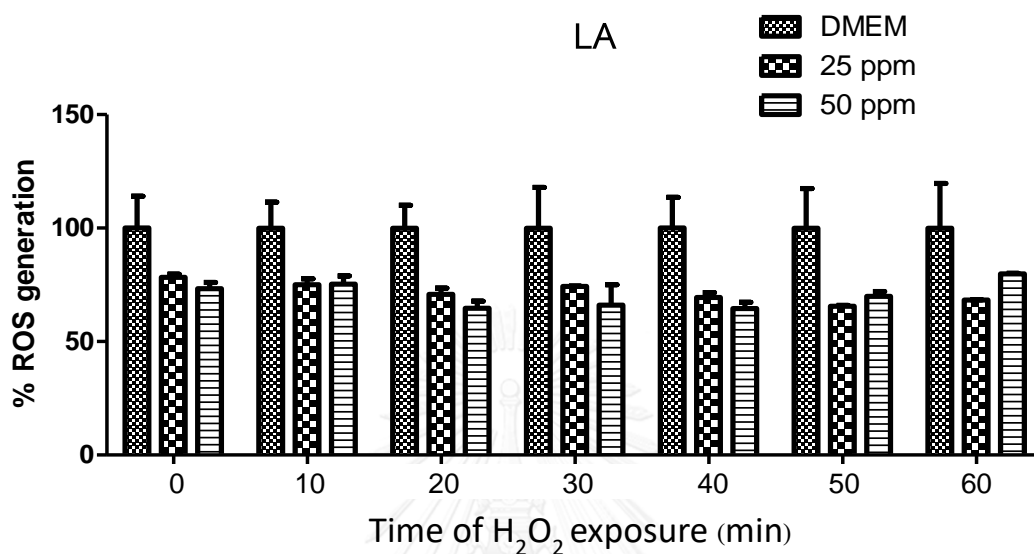


Figure 4.18: ROS generation observed in the HaCaT cells upon the treatment of DMEM and **LA** at the concentration of 25 and 50 mg/L for 24 h then HaCaT cells was treated with H₂O₂ for 0, 10, 20, 30, 40, 50 and 60 min.

In case of treating HaCaT cells with H₂O₂ (for 0 min to 60 min), treatment of cells with **LA** at the concentration of 25 mg/L decrease the ROS generation with no significant ($P > 0.05$) comparing to the control (DMEM). This indicated that **LA** seemed to exhibit antioxidant activity toward HaCaT cells. Similar results were obtained when 50 mg/L of **LA** was used. The similar ROS generation between 25 and 50 mg/L of **LA** indicated that **LA** have no dose-dependent effect in the ROS generation.

The ROS generation observed for the HaCaT cells treated with **TMPyP** at the concentration of 25 and 50 mg/L, and then with H₂O₂ for 10–60 min is shown in **Figure 4.19**.

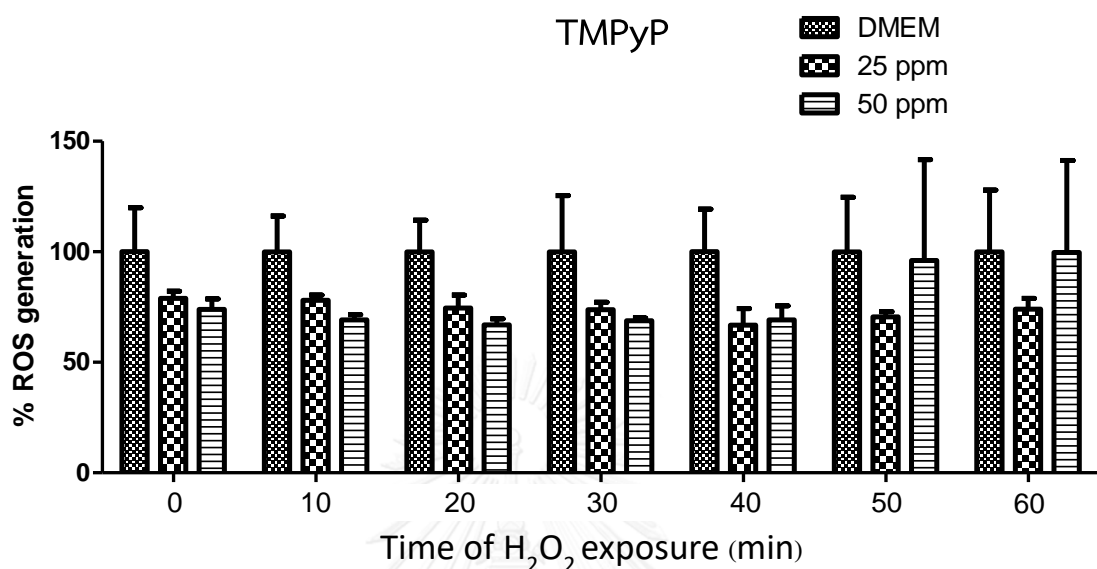


Figure 4.19: ROS generation observed in the HaCaT cells upon the treatment of DMEM and **TMPyP** at the concentration of 25 and 50 mg/L for 24 h then HaCaT cells was treated with H₂O₂ for 0, 10, 20, 30, 40, 50 and 60 min.

In the similar manner as **LA**, the treatment of HaCaT cells with **TMPyP** at the concentration of 25 and 50 mg/L decreased ROS generation both before and after treatment of H₂O₂ with no significant ($P > 0.05$) comparing to the control. This implied that **TMPyP** seem to exhibit antioxidant activity toward HaCaT cells. With the similar ROS generation between 25 and 50 mg/L of **TMPyP**, **TMPyP** was found to have no dose-dependent effect in the ROS generation.

The ROS generation observed for the HaCaT cells treated with **P-4Lp** at the concentration of 25 and 50 mg/L, and then with H₂O₂ for 10–60 min is shown in **Figure 4.20**.

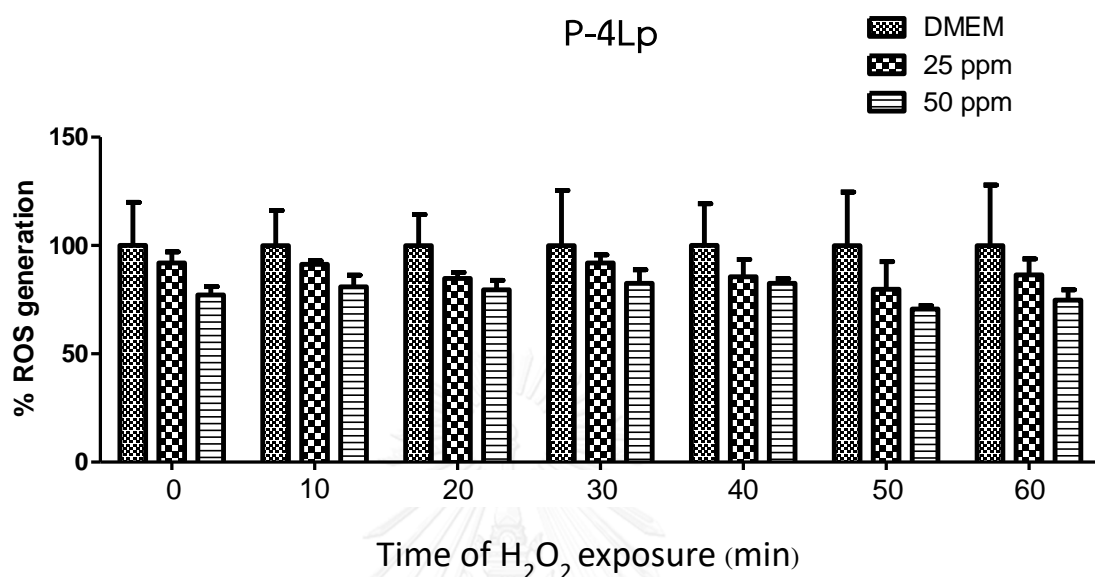


Figure 4.20: ROS generation observed in the HaCaT cells upon the treatment of DMEM and **P-4Lp** at the concentration of 25 and 50 mg/L for 24 h then HaCaT cells was treated with H₂O₂ for 0, 10, 20, 30, 40, 50 and 60 min.

For the case where the HaCaT cells were treated only with **P-4Lp** at concentration of 25 mg/L (at 0 to 60 min of the H₂O₂ exposure), the decrease in the ROS generation, compared with the control experiment, was observed. The same results were obtained when the concentration of 50 mg/L of **P-4Lp** was used. This indicated that **P-4Lp** seemed to exhibit antioxidant activity toward HaCaT cells. Since the ROS generation of cell when treating with **P-4Lp** at the concentration of 25 mg/L is always higher than that of 50 mg/L, **P-4Lp** was considered to have dose-dependent effect in the ROS generation.

The ROS generation observed for the HaCaT cells treated with **Mn-P-4Lp** at the concentration of 25 and 50 mg/L, and then with H₂O₂ for 10–60 min is shown in **Figure 4.21**.

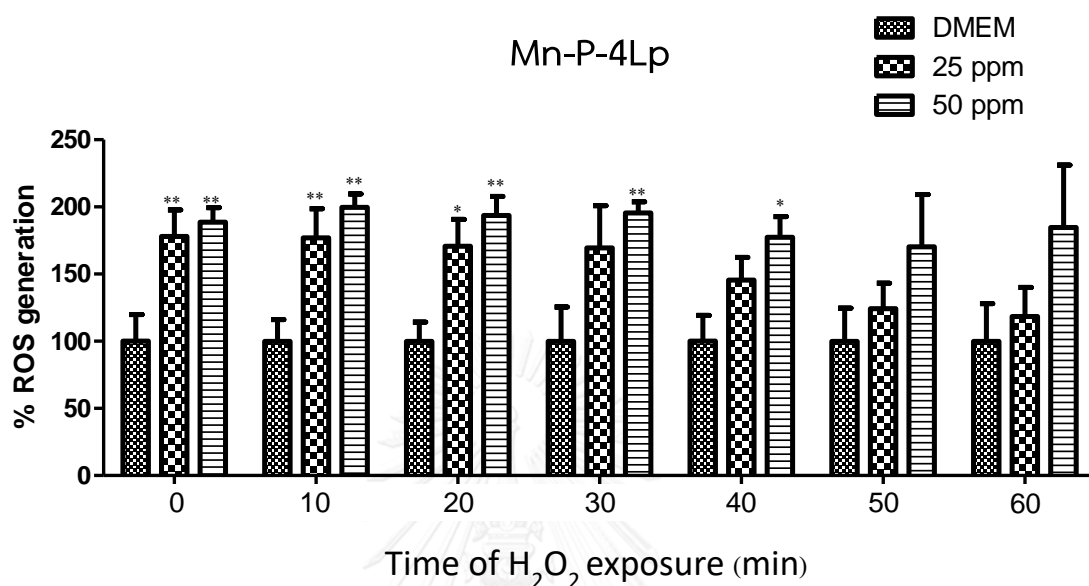


Figure 4.21: ROS generation observed in the HaCaT cells upon the treatment of DMEM and **Mn-P-4Lp** at the concentration of 25 and 50 mg/L for 24 h then HaCaT cells was treated with H₂O₂ for 0, 10, 20, 30, 40, 50 and 60 min (“**” indicates $p < 0.01$ and “*” indicates $p < 0.05$).

In the absence of H₂O₂ (at 0 min), the treatment of HaCaT cells with **Mn-P-4Lp** at the concentration of 25 mg/L significantly increased the ROS generation. After the cells were treated with H₂O₂ for 10 to 30 min, no change in the ROS generation was observed. Then, the ROS generation gradually decreased at 40 to 60 min of the H₂O₂ exposure. However, at 60 min of the H₂O₂ exposure, the ROS generation observed in the cells was still higher than the control batch. This indicated that **Mn-P-4Lp** induced ROS generation instead of scavenging ROS toward the HDFa cells, but seemed to be able to scavenge ROS from external source like H₂O₂ addition. Similar results were obtained when 50 mg/L of **Mn-P-4Lp** was used. Since the ROS generation of cells when treating with **Mn-P-4Lp** at the concentration of 50 mg/L is always higher than

that of 25 mg/L, Mn-P-4Lp was considered to have dose-dependent effect in the ROS generation of HaCaT cells.

The effect of the introduction of the porphyrin unit on the ROS generation of the HaCaT cells can be determined by the comparison of the ROS generation between LA and P-4Lp (Figure 4.22). The treatment of the HaCaT cells with both LA and P-4Lp at the concentration of 25 and 50 mg/L did not show significant difference in the ROS generation both before and after the exposure to H₂O₂. This results indicated that the introduction of the porphyrin unit slightly affect the ROS generation of the HaCaT cells.

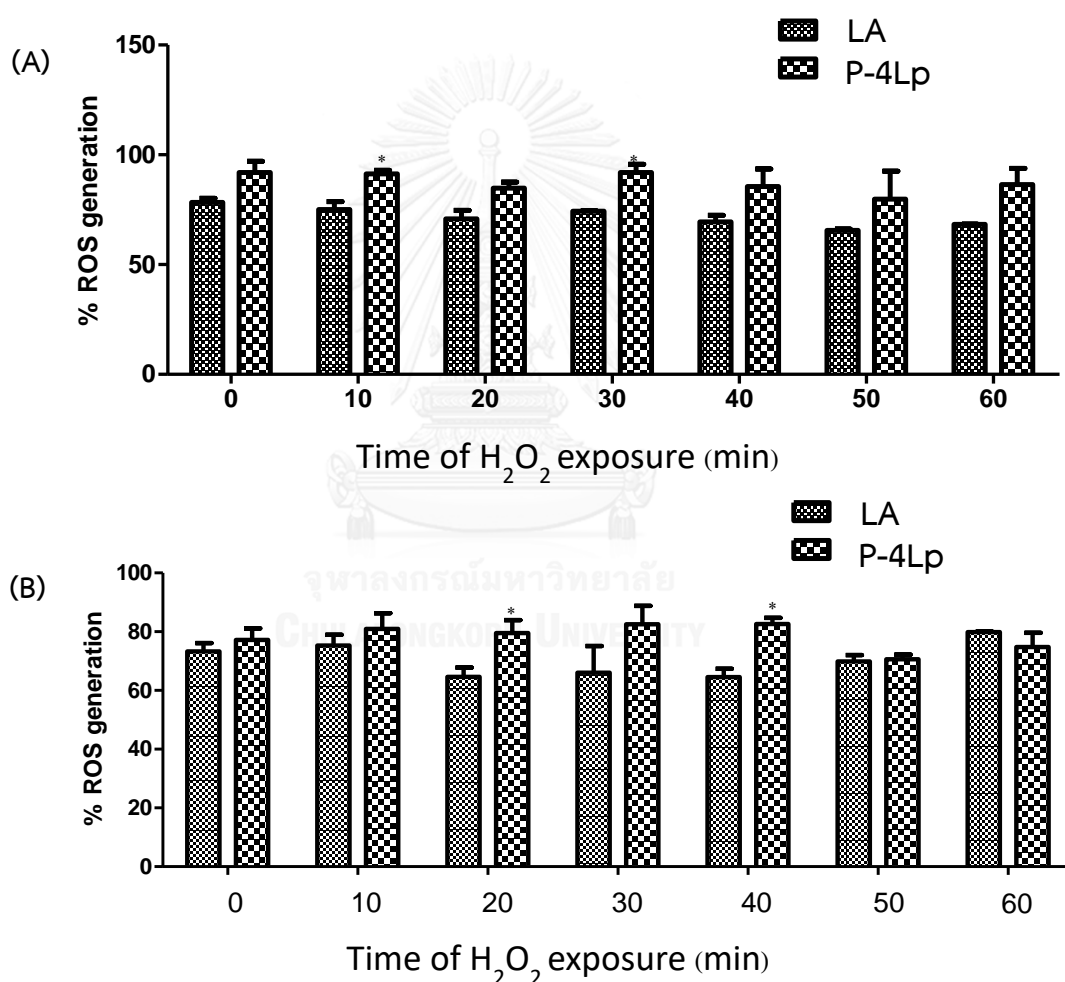


Figure 4.22: The ROS generation observed in the HaCaT cells upon the treatment with LA and P-Lp at the concentration of (A) 25 mg/L and (B) 50 mg/L for 24 h, followed by the treatment with H₂O₂ for 0, 10, 20, 30, 40, 50 and 60 min.

The effect of the introduction of lipoyl unit on the ROS generation of the HaCaT cells can be determined by the comparison of the ROS generation between **TMPyP** and **P-4Lp** (Figure 4.23). The treatment of the HaCaT cells with both **TMPyP** and **P-4Lp** at the concentration of 25 and 50 mg/L did not show significant difference in the ROS generation both before and after the exposure to H_2O_2 . This results indicated that the introduction of lipoyl unit on porphyrin did not significantly affect the ROS generation of the HaCaT cells.

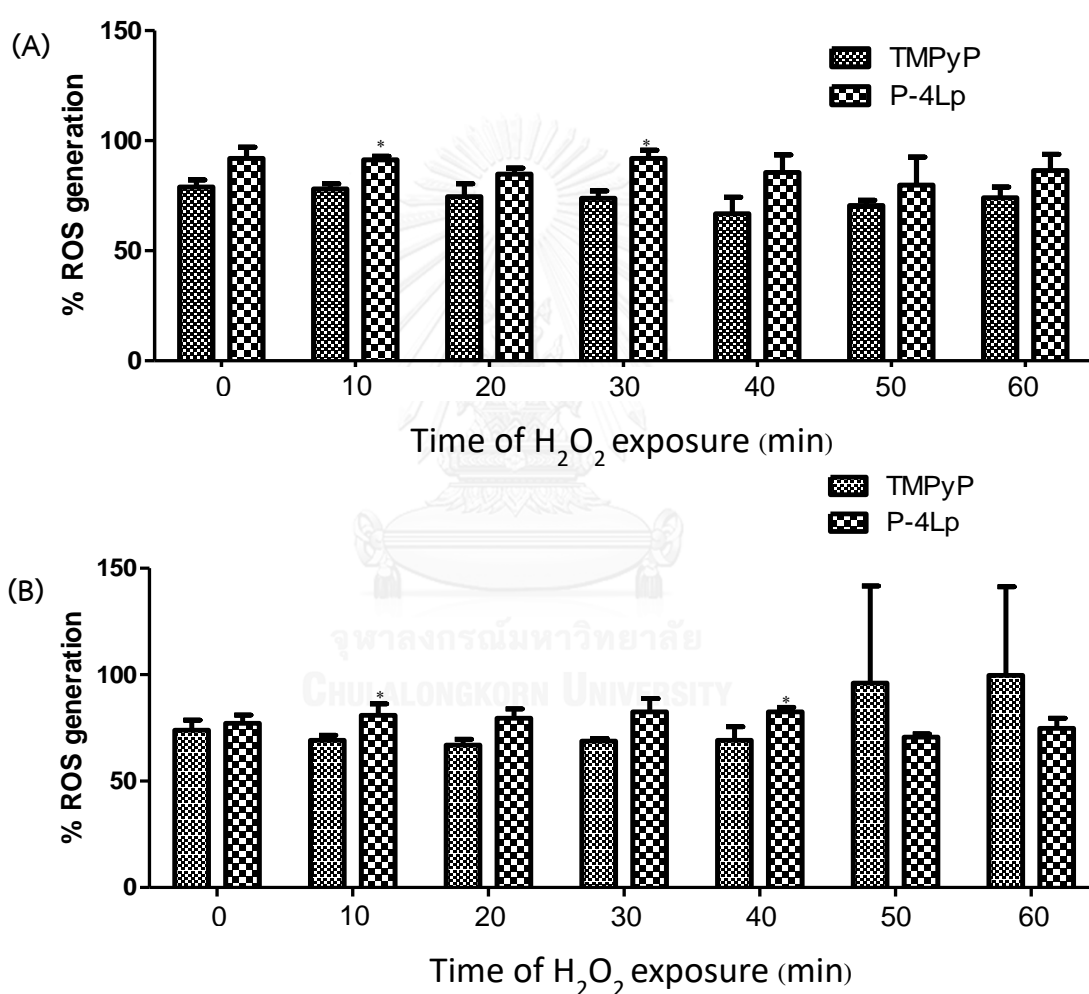


Figure 4.23: ROS generation observed in the HaCaT cells upon the treatment of **TMPyP** and **P-4Lp** at the concentration of 25 mg/L (A) and 50 mg/L (B) for 24 h then HaCaT cells was treated with H_2O_2 for 0, 10, 20, 30, 40, 50 and 60 min (“*” indicates $p < 0.05$).

The effect of the introduction of the Mn-chelation in the porphyrin unit on the ROS generation of the HaCaT cells can be determined by the comparison of the ROS generation between P-4Lp and those of Mn-P-4Lp as shown in Figure 4.24.

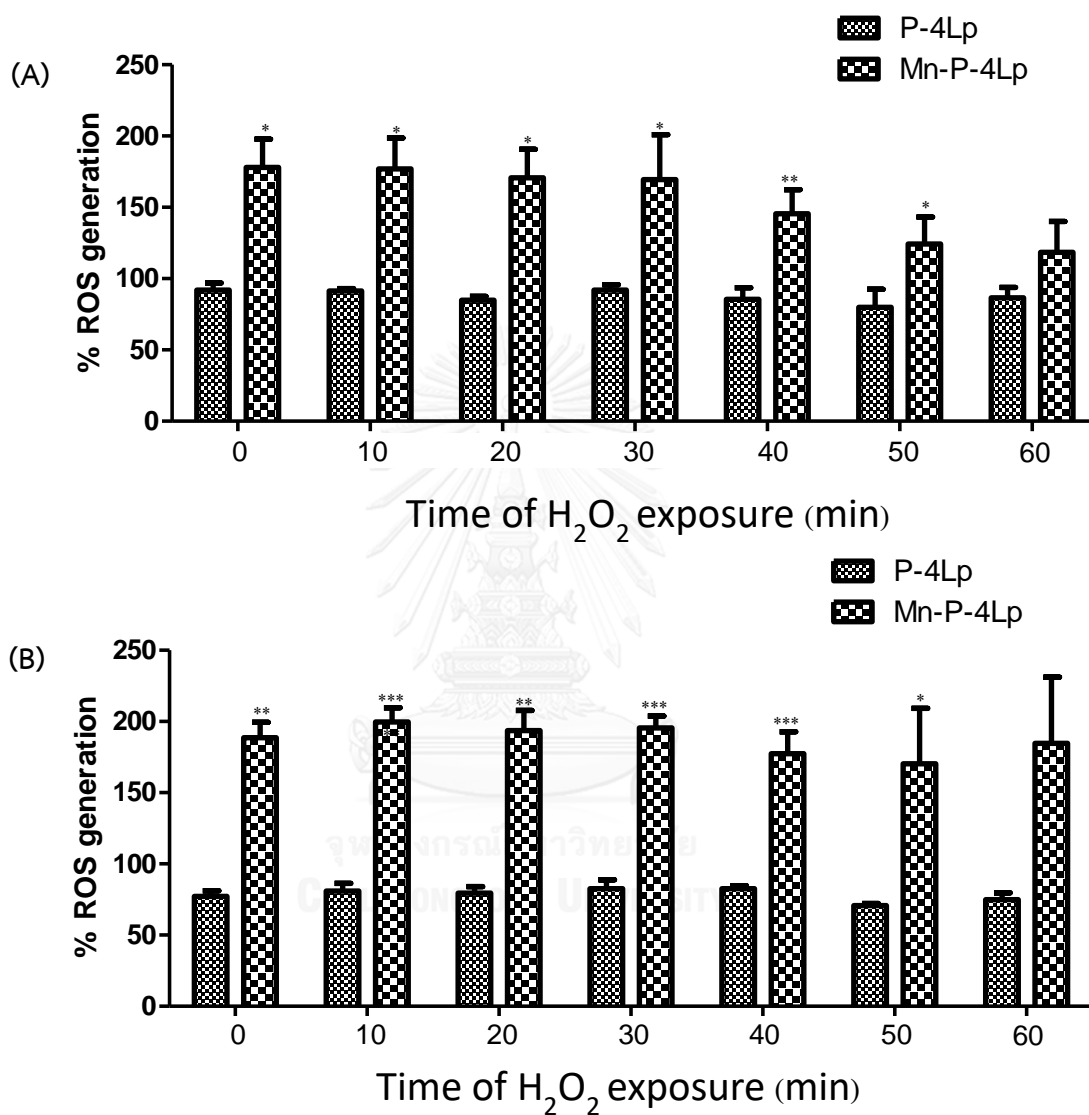


Figure 4.24: ROS generation observed in the HaCaT cells upon the treatment of P-4Lp and Mn-P-4Lp at the concentration of 25 mg/L (A) and 50 mg/L (B) for 24 h then HaCaT cells was treated with H₂O₂ for 0, 10, 20, 30, 40, 50 and 60 min (“***” indicates p < 0.001, “**” indicates p < 0.01 and “*” indicates p < 0.05).

In the absence of H_2O_2 (at 0 min), the treatment of HaCaT cells with **P-4Lp** and **Mn-P-4Lp** at the concentration of 25 and 50 mg/L showed significantly different in ROS generation. After the cells were treated with H_2O_2 for 10 to 30 min, no change in the different in ROS generation was observed. Then, the different in ROS generation gradually decreased at 40 to 60 min of the H_2O_2 exposure. This results indicated that the Mn-chelation of the porphyrin unit dramatically increased ROS generation in HaCaT cells in the similar manner as mentioned for the HDFa cells in Section 4.2.2.1.



4.2.3 Mitochondria targeting evaluation

In this studies, the evidence for mitochondria targeting was confirmed by cell imaging by LSM 800 confocal microscope. In order to indicate position of cells, nucleus of the HaCaT cells were stained with Hoechst 33342 dye as seen in the blue region in **Figure 4.25**.

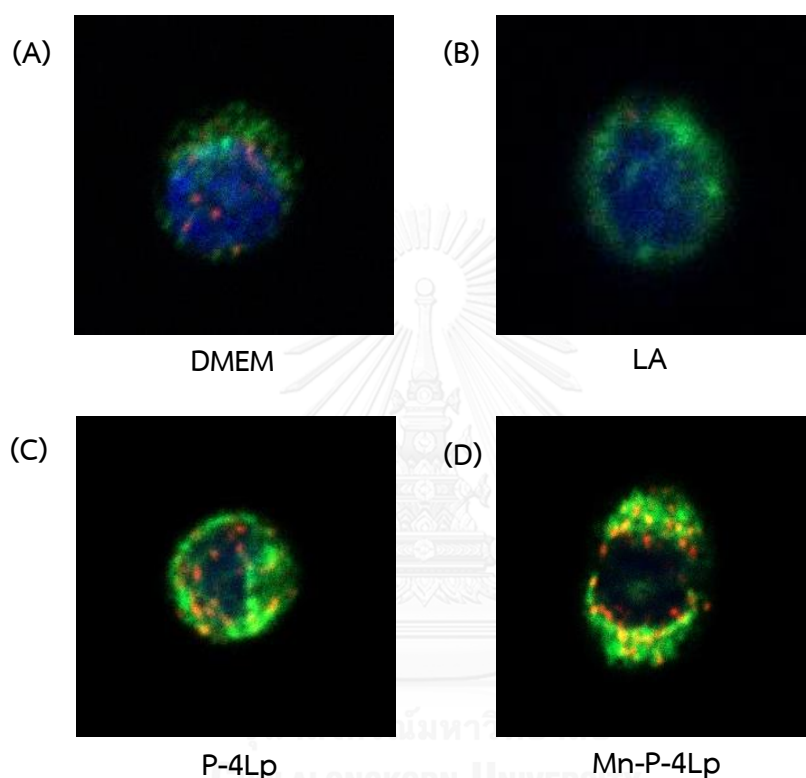
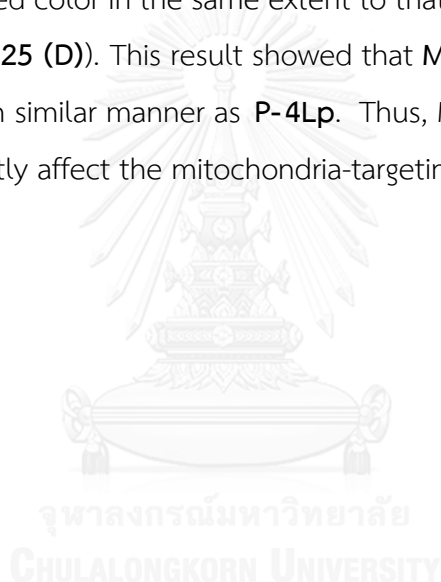


Figure 4.25: Images of the HaCaT cells treated by (A) DMEM, (B) LA, (C) P-4Lp, (D) Mn-P-4Lp.

After JC-1 dye was loaded into HaCaT cells, JC-1 exists as a monomer which exhibits green fluorescence in the aqueous component of the cytoplasm of a cell. In the other hand, some JC-1 dye can enter the mitochondrial matrix where it accumulates. When the critical concentration of JC-1 dye is exceeded, JC-1 dye spontaneously forms the *J*-aggregates which exhibits intense red fluorescence. **Figure 4.25 (A)** shows that the images of the HaCaT cells treated with only DMEM (control) mainly exhibited green fluorescence with red fluorescence at some parts. Indicating that JC-1 is slightly accumulated in mitochondria. When treated cells with **LA**, the images also mainly exhibited green (**Figure 4.25 (B)**). The fluorescence color from cells

treated with **LA** is quite similar with the result when treated cells with DMEM. This indicated that **LA** does not affect mitochondrial membrane potential or it cannot be accumulated in mitochondria. On the contrary, **Figure 4.25 (C)** shows that the images of the cells treated with **P-4Lp** exhibits higher intensity of red fluorescence comparing to the cells treated with **LA**. This results suggested that **P-4Lp** can be highly accumulated in the mitochondria than **LA** because of the appearance of the porphyrin unit in **P-4Lp**. This is likely to be an effect of positive charges on the porphyrin ring which attach to negative charges of mitochondrial inner membrane which is consistent with the previous report⁶⁹. Moreover, when treated cells with **Mn-P-4Lp**, the images exhibited green and red color in the same extent to that observed in the cells treated with **P-4Lp**. (**Figure 4.25 (D)**). This result showed that **Mn-P-4Lp** can be accumulated in the mitochondria in similar manner as **P-4Lp**. Thus, Mn-chelation in the porphyrin unit did not significantly affect the mitochondria-targeting ability of **P-4Lp**.



CHAPTER V

CONCLUSION

The new water-soluble porphyrin derivatives bearing the lipoyl *meso*-substituents with and without manganese at the center of porphyrin ring were successfully synthesized. Synthesis of these compounds proceeded from amidation reaction between porphyrin unit and lipoic anhydride, followed by Mn-metallation with $\text{MnCl}_2 \cdot 4\text{H}_2\text{O}$. This synthesis was accomplished in an overall yield of 5% and 4% for **P-4Lp** and **Mn-P-4Lp**, respectively. The resulting compounds were characterized by ^1H -NMR and ^{13}C -NMR spectroscopy, mass spectrometry, and UV-visible and fluorescence spectrophotometry. Absorption maxima of these compounds were observed at 430 nm for **P-4Lp** and 464 nm for **Mn-P-4Lp**. Upon excitation at the maximum absorption, two emission peaks of **P-4Lp** were found at 658 and 721 nm whereas no emission band of **Mn-P-4Lp** was observed. The biological studies of the compounds of interest (**LA**, **TMPyP**, **P-4Lp** and **Mn-P-4Lp**) were performed in HDFa and HaCaT cell lines. The effects of the introduction of the porphyrin unit, the presence of lipoyl and Mn-chelation on the porphyrin unit on cytotoxicity and antioxidant activity in HaCaT and HDFa cells were determined by cell viability assay and the ROS generation assay. The results showed that the introduction of the porphyrin unit and the presence of lipoyl on the porphyrin unit increased cell cytotoxicity, but did not affect antioxidant activity in both kinds of cells. While the Mn-chelation on the porphyrin unit decreased cell cytotoxicity, but no significant change in the antioxidant activity in those cells was observed. In mitochondria-targeting evaluation, the target porphyrin derivative exhibited accumulation specifically in the mitochondria. This result indicated that the introduction of the porphyrin unit increases mitochondria-targeted activity.

REFERENCES

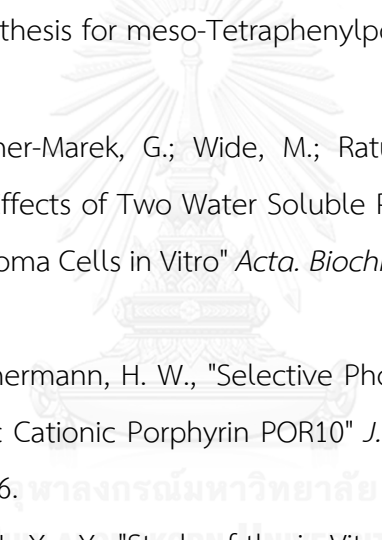
1. Bahorun, T.; Soobrattee, M.; Luximon-Ramma, V.; Aruoma, O., "Free Radicals and Antioxidants in Cardiovascular Health and Disease" *IJMU* **2006**, *1*, 1-17.
2. (a) Brambilla, D.; Mancuso, C.; Scuderi, M. R.; Bosco, P.; Cantarella, G.; Lempereur, L.; Di Benedetto, G.; Pezzino, S.; Bernardini, R., "The Role of Antioxidant Supplement in Immune System, Neoplastic, and Neurodegenerative Disorders: A Point of View for an Assessment of the Risk/Benefit Profile" *Nutrition journal* **2008**, *7*, 29; (b) Lagouge, M.; Larsson, N. G., "The Role of Mitochondrial DNA Mutations and Free Radicals in Disease and Ageing" *J. Intern. Med.* **2013**, *273* (6), 529-43; (c) Young, I. S.; Woodside, J. V., "Antioxidants in Health and Disease" *J. Clin. Pathol.* **2001**, *54*, 176-186.
3. (a) Qi, H.; Zhang, Q.; Zhao, T.; Chen, R.; Zhang, H.; Niu, X.; Li, Z., "Antioxidant Activity of Different Sulfate Content Derivatives of Polysaccharide Extracted from *Ulva Pertusa* (Chlorophyta) in Vitro" *International journal of biological macromolecules* **2005**, *37* (4), 195-9; (b) Shalaby, E. A.; Shanab, S. M. M., "Antioxidant Compounds, Assays of Determination and Mode of Action" *AJPP*. **2013**, *7*(10), 528-539.
4. (a) Maitarad, P.; Namuangruk, S.; Zhang, D.; Shi, L.; Li, H.; Huang, L.; Boekfa, B.; Ehara, M., "Metal-porphyrin: A Potential Catalyst for Direct Decomposition of N(2)O by Theoretical Reaction Mechanism Investigation" *Environmental science & technology* **2014**, *48* (12), 7101-10; (b) Smith, P. D.; James, B. R.; Dolphin, D. H., "Structural Aspects and Coordination Chemistry of Metal Porphyrin Complexes with Emphasis on Axial Ligand Binding to Carbon Donors and Mono- and Diatomic Nitrogen and Oxygen Donors" *Coord. Chem. Rev.* **1981**, *39*, 31-75.
5. (a) Dezhampanah, H.; Bordbar, A. K.; Tangestaninejad, S., "Thermodynamic Investigation of Manganese(III)5-(1-(4-carboxybutyl)pyridinium-4-yl) 10,15,20-Tris-(1-methylpyridinium-4-yl)porphyrin with Calf Thymus DNA" *J. Porphyr. Phthalocyanines*. **2009**, *13*, 964-972; (b) Romera, C.; Sabater, L.; Garofalo, A.; I,

- M. D.; Pratviel, G., "Interaction of Cationic Nickel and Manganese Porphyrins with the Minor Groove of DNA" *Inorg. Chem.* **2010**, *49* (18), 8558-67.
6. (a) Asayama, S.; Kawamura, E.; Nagaoka, S.; Kawakami, H., "Design of Manganese Porphyrin Modified with Mitochondrial Signal Peptide for a New Antioxidant" *Mol. Pharm.* **2006**, *3*(4), 468-470; (b) Kos, I.; Reboucas, J. S.; DeFreitas-Silva, G.; Salvemini, D.; Vujaskovic, Z.; Dewhirst, M. W.; Spasojevic, I.; Batinic-Haberle, I., "Lipophilicity of Potent Porphyrin-Based Antioxidants: Comparison of Ortho and Meta Isomers of Mn(III) N-alkylpyridylporphyrins" *Free radical biology & medicine* **2009**, *47* (1), 72-8.
 7. Moon, H. S., "Chemopreventive Effects of Alpha Lipoic Acid on Obesity-Related Cancers" *Annals of nutrition & metabolism* **2016**, *68* (2), 137-44.
 8. Biewenga, G.; M., G. R. M.; Haenen.; Bast, A., "The Pharmacology of the Antioxidant Lipoic Acid" *Gen. Pharmacol.* **1997**, *29* (3), 315-331.
 9. Mentese, E.; Yilmaz, F.; Baltas, N.; Bekircan, O.; Kahveci, B., "Synthesis and Antioxidant Activities of Some New Triheterocyclic Compounds Containing Benzimidazole, Thiophene, and 1,2,4-Triazole Rings" *Journal of enzyme inhibition and medicinal chemistry* **2015**, *30* (3), 435-41.
 10. (a) Kumar, D.; Chandra Shekar, K. P.; Mishra, B.; Kurihara, R.; Ogura, M.; Ito, T., "Cationic Porphyrin-Quinoxaline Conjugate as a Photochemically Triggered Novel Cytotoxic Agent" *Bioorganic & medicinal chemistry letters* **2013**, *23* (11), 3221-4; (b) Rodriguez, R.; Redman, R., "Balancing the Generation and Elimination of Reactive Oxygen Species" *Proceedings of the National Academy of Sciences of the United States of America* **2005**, *102* (9), 3175-6.
 11. (a) Mishra, B. P.; Badade, Z. G.; Anand, B. K.; Lingidi, J. L.; Jaiswal, S., "8-Hydroxydeoxyguanosine (8-OHdG) Levels in Urinary Samples of Pesticide Sprayers on Exposure to Organophosphorus Pesticides" *Int. J. Clin. Trials.* **2015**, *2* (3), 59; (b) Pham-Huy, L. A.; He, H.; Pham-Huy, C., "Free Radicals, Antioxidants in Disease and Health" *Int. J. Biomed. Sci.* **2008**, *4* (2), 89-96.
 12. (a) Koutsilieris, E.; Scheller, C.; Grunblatt, E.; Nara, K.; Li, J.; Riederer, P., "Free Radicals in Parkinson's Disease" *Journal of neurology* **2002**, *249* Suppl 2, I11-5; (b) Markesbery, W. R.; Lovell, M. A., "DNA Oxidation in Alzheimer's Disease"

- Antioxid. Redox Signal.* **2006**, *8*, 2039-2045; (c) Maxwell, R. J. S.; Lip, Y. H. G., "Free Radicals and Antioxidants in Cardiovascular Disease" *Br. J. Clin. Pharmacol.* **1997**, *44*, 307-317; (d) Steinberg, D., "Low Density Lipoprotein Oxidation and Its Pathobiological Significance" *J. Biol. Chem.* **1997**, *272*, 20963-20966; (e) Yeh, J. Y.; Hsieh, L. H.; Wu, K. T.; Tsai, C. F., "Antioxidant Properties and Antioxidant Compounds of Various Extracts from the Edible Basidiomycete *Grifola Frondosa* (Maitake)" *Molecules* **2011**, *16* (4), 3197-211.
13. Barbara, S. B.; Earl, R. S., "Protein Oxidation in Aging, Disease, and Oxidative Stress" *J. Biol. Chem.* **1997**, *272* (33), 20313-20316.
 14. Schneider, C., "An Update on Products and Mechanisms of Lipid Peroxidation" *Molecular nutrition & food research* **2009**, *53* (3), 315-21.
 15. Brandes, N.; Schmitt, S.; Jakob, U., "Thiol-Based Redox Switches in Eukaryotic Proteins" *Antioxid. Redox Signal.* **2009**, *11*, 997-1014.
 16. Cooke, M. S.; Evans, M. D.; Dizdaroglu, M.; Lunec, J., "Oxidative DNA Damage: Mechanisms, Mutation, and Disease" *FASEB* **2003**, *17* (10), 1195-214.
 17. (a) ADELMAN, R.; SAUL, L. R.; Ames, B. N., "Oxidative Damage to DNA: Relation to Species Metabolic Rate and Life Span" *Proc. Natl. Acad. Sci. USA* **1988**, *85*, 2706-2708; (b) Ames, B. N., "Dietary Carcinogens and Anticarcinogens" *Science* **1983**, *221*, 1256-1264.
 18. Lobo, V.; Patil, A.; Phatak, A.; Chandra, N., "Free Radicals, Antioxidants and Functional Foods: Impact on Human Health" *Pharmacognosy reviews* **2010**, *4* (8), 118-26.
 19. Rahman, K., "Studies on Free Radicals, Antioxidants, and Co-factors" *Clin. Interv. Aging.* **2007**, *2* (2), 219-236.
 20. Townsend, D. M.; Tew, K. D.; Tapiero, H., "The Importance of Glutathione in Human Disease" *Biomed. Pharmacother.* **2003**, *57* (3-4), 145-155.
 21. Donnerstag, B.; Ohlenschlager, G.; Cinatl, J.; Amrania, M.; Hofmann, D.; Flindt, S.; Treusch, G.; Trlgera, L., "Reduced Glutathione and S-acetylglutathione as Selective Apoptosisinducing Agents in Cancer Therapy" *Cancer Lett.* **1996**, *110*, 63-70.

22. Mezzetti, F.; De Vero, L.; Giudici, P., "Evolved *Saccharomyces Cerevisiae* Wine Strains with Enhanced Glutathione Production Obtained by an Evolution-Based Strategy" *FEMS yeast research* **2014**, *14* (6), 977-87.
23. Aw, Y. T., "Cellular Redox: A Modulator of Intestinal Epithelial Cell Proliferation" *News. Physiol. Sci.* **2003**, *18*, 201-204.
24. Procopio, A.; Alcaro, S.; Cundari, S.; Nino, A.; Ortuso, F.; Sacchetta, P.; Pennelli, A.; Sindona, G., "Molecular Modeling, Synthesis, and Preliminary Biological Evaluation of Glutathione-S-Transferase Inhibitors as Potential Therapeutic Agents" *J. Med. Chem.* **2005**, *48*, 6084-6089.
25. Falck, J. R.; Sangras, B.; Capdevila, J. H., "Preparation of N-tBoc L-glutathione Dimethyl and Di-tert-butyl Esters: Versatile Synthetic Building Blocks" *Bioorganic & medicinal chemistry* **2007**, *15* (2), 1062-6.
26. Katritzky, A.; Abo- Dya, N.; Tala, S.; Ghazvini-Zadeh, E.; Bajaj, K.; El-Feky, S., "Efficient and Selective Syntheses of S-Acyl and N-Acyl Glutathiones" *Synlett.* **2010**, *9*, 1337-1340.
27. Carr, W. D.; Salinthon, S., "*Lipoic Acid, Inflammation and Diseases of the Nervous System*" **2014**; Vol. *102*, p 2349-2368.
28. Moini, H.; Packer, L.; Saris, N.-E. L., "Antioxidant and Prooxidant Activities of α -Lipoic Acid and Dihydrolipoic Acid" *Toxicol. Appl. Pharmacol.* **2002**, *182* (1), 84-90.
29. Carlson, A. D.; Smith, R. A.; Fischer, J. S.; Young, L. K.; Packer, L., "The Plasma Pharmacokinetics of R-(+)-Lipoic Acid Administered as Sodium R-(+)-Lipoate to Healthy Human Subjects" *Altern. Med. Rev.* **2007**, *12*, 343-351.
30. Park, S.; Karunakaran, U.; Jeoung, N.; Jeon, J.-H.; Lee, I.-K., "Physiological Effect and Therapeutic Application of Alpha Lipoic Acid" *Curr. Med. Chem.* **2014**, *21* (32), 3636-3645.
31. Gurkan, A. S.; Karabay, A.; Buyukbingol, Z.; Adejare, A.; Buyukbingol, E., "Syntheses of Novel Indole Lipoic Acid Derivatives and Their Antioxidant Effects on Lipid Peroxidation" *Archiv der Pharmazie* **2005**, *338* (2-3), 67-73.
32. Melagraki, G.; Afantitis, A.; Igglessi-Markopoulou, O.; Detsi, A.; Koufaki, M.; Kontogiorgis, C.; Hadjipavlou-Litina, D. J., "Synthesis and Evaluation of the

- Antioxidant and Anti-inflammatory Activity of Novel Coumarin-3-aminoamides and Their Alpha-Lipoic Acid Adducts" *Eur. J. Med. Chem.* **2009**, *44* (7), 3020-6.
33. Koufaki, M.; Detsi, A.; Theodorou, E.; Kiziridi, C.; Calogeropoulou, T.; Vassilopoulos, A.; Kourounakis, A. P.; Rekka, E.; Kourounakis, P. N.; Gaitanaki, C.; Papazafiri, P., "Synthesis of Chroman Analogues of Lipoic Acid and Evaluation of Their Activity Against Reperfusion Arrhythmias" *Bioorg. Med. Chem.* **2004**, *12* (18), 4835-41.
34. Scheer, H.; Katz, J. J., "Nuclear Magnetic Resonance Spectroscopy of Porphyrins and Metalloporphyrins" Elsevier Scientific Publishing Company **1975**; p 399-910.
35. (a) Ivanov, A. S.; Boldyrev, A. I., "Deciphering Aromaticity in Porphyrinoids via Adaptive Natural Density Partitioning" *Org. Biomol. Chem.* **2014**, *12* (32), 6145-50; (b) Saito, S.; Osuka, A., "Expanded Porphyrins: Intriguing Structures, Electronic Properties, and Reactivities" *Angew. Chem. Int. Ed.* **2011**, *50* (19), 4342-73.
36. Josefsen, L. B.; Boyle, R. W., "Photodynamic Therapy and the Development of Metal-Based Photosensitisers" *Metal-based drugs* **2008**, *2008*, 276109.
37. (a) Haruyama, T.; Asayama, S.; Kawakami, H., "Highly Amphiphilic Manganese Porphyrin for the Mitochondrial Targeting Antioxidant" *J. Biochem* **2010**, *147* (2), 153-6; (b) Schoonover, M.; Kerwin, S. M., "G-quadruplex DNA Cleavage Preference and Identification of a Perylene Diimide G-quadruplex Photocleavage Agent Using a Rapid Fluorescent Assay" *Bioorg. Med. Chem.* **2012**, *20* (24), 6904-18.
38. Wasielewski, M. R.; Johnson, D. G.; Niemczyk, M. P.; Gaines, G. L.; O'Neil, M. P.; Svec, W. A., "Chlorophyll-Porphyrin Heterodimers with Orthogonal π Systems: Solvent Polarity Dependent Photophysics" *J. Am. Chem. Soc.* **1990**, *112* (18), 6482-6488.
39. Kabe, Y.; Ohmori, M.; Shinouchi, K.; Tsuboi, Y.; Hirao, S.; Azuma, M.; Watanabe, H.; Okura, I.; Handa, H., "Porphyrin Accumulation in Mitochondria is Mediated by 2-Oxoglutarate Carrier" *J. Biol. Chem.* **2006**, *281* (42), 31729-35.
40. Kawai, C.; Araujo-Chaves, J. C.; Magrini, T.; Sanches, C. O.; Pinto, S. M.; Martinho, H.; Daghasanli, N.; Nantes, I. L., "Photodamage in a Mitochondrial Membrane

- Model Modulated by the Topology of Cationic and Anionic Meso-Tetrakis Porphyrin Free Bases" *J. Photochem. Photobiol.* **2014**, *90* (3), 596-608.
41. (a) Batinic´-Haberle, I.; Spasojevic´, I.; Hambright, P.; Benov, L.; Crumbliss, L. A.; Fridovich, I., "Relationship Among Redox Potentials, Proton Dissociation Constants of Pyrrolic Nitrogens, and in Vivo and in Vitro Superoxide Dismutating Activities of Manganese(III) and Iron(III) Water-Soluble Porphyrins" *Inorg. Chem.* **1999**, *38*, 4011-4022; (b) Terziev, L.; Dancheva, V.; Shopova, V.; Stavreva, G., "Antioxidant Effect of MnTE-2-PyP on Lung in Asthma Mice Model" *Scientific World J.* **2012**, *2012*, 379360.
 42. Adler, A. D.; Longo, F. R.; Finarelli, J. D.; Goldmacher, J.; Assour, J.; Korsakoff, L., "A Simplified Synthesis for meso-Tetraphenylporphine" *J. Org. Chem.* **1967**, *32*, 476.
 43. Szurko, A.; Krämer-Marek, G.; Wide, M.; Ratuszna, A.; Habdas, J.; Kuś, P., "Photodynamic Effects of Two Water Soluble Porphyrins Evaluated on Human Malignant Melanoma Cells in Vitro" *Acta. Biochimica. Polonica.* **2003**, *50*, 1165–1174.
 44. Cernay, T.; Zimmermann, H. W., "Selective Photosensitization of Mitochondria by the Lipophilic Cationic Porphyrin POR10" *J. Photochem. Photobiol. B, Biol.* **1996**, *34*, 191-196. 
 45. (a) Li, W.; Zhou, J.; Xu, Y., "Study of the in Vitro Cytotoxicity Testing of Medical Devices" *Biomed. Rep.* **2015**, *3* (5), 617-620; (b) Martin, J. S., *Mammalian Cell Viability*. AO Research Institute Davos, Davos Platz, Switzerland.
 46. Boncler, M.; Rozalski, M.; Krajewska, U.; Podsedek, A.; Watala, C., "Comparison of PrestoBlue and MTT Assays of Cellular Viability in the Assessment of Anti-Proliferative Effects of Plant Extracts on Human Endothelial cells" *J. Pharmacol. Toxicol. Methods* **2014**, *69* (1), 9-16.
 47. Tarpey, M.; David, A. W.; Matthew, B. G., "Methods for Detection of Reactive Metabolites of Oxygen and Nitrogen: in Vitro and in Vivo Considerations" *Am. J. Physiol. Regul. Integr. Comp. Physiol.* **2004**, *286*, 431-444.

48. Ayala, A.; Munoz, M. F.; Arguelles, S., "Lipid Peroxidation: Production, Metabolism, and Signaling Mechanisms of Malondialdehyde and 4-hydroxy-2-nonenal" *Oxid. Med. Cell. Longev.* **2014**, 2014, 360438.
49. WILLIAM, A. P.; STANLEY, J. P.; BLAIR, E., "Autoxidation of Polyunsaturated Fatty Acids" II. A Suggested Mechanism for the Formation of TBA-Reactive Materials from Prostaglandin-like Endoperoxides" *LIPIDS.* **1976**, 11 (5), 370-379.
50. Armstrong, D., "*Advanced Protocols in Oxidative Stress II*".
51. (a) Benipal, B.; Lash, L. H., "Modulation of Mitochondrial Glutathione Status and Cellular Energetics in Primary Cultures of Proximal Tubular Cells From Remnant Kidney of Uninephrectomized Rats" *Biochem. Pharmacol.* **2013**, 85 (9), 1379-88; (b) Lowes, D. A.; Thottakam, B. M.; Webster, N. R.; Murphy, M. P.; Galley, H. F., "The Mitochondria-Targeted Antioxidant MitoQ Protects Against Organ Damage in a Lipopolysaccharide-Peptidoglycan Model of Sepsis" *Free. Radic. Biol. Med.* **2008**, 45 (11), 1559-65.
52. Sheu, S. S.; Nauduri, D.; Anders, M. W., "Targeting Antioxidants to Mitochondria: a New Therapeutic Direction" *BBA* **2006**, 1762 (2), 256-65.
53. Perry, S. W.; Norman, J. P.; Barbieri, J.; Brown, E. B.; Gelbard, H. A., "Mitochondrial Membrane Potential Probes and the Proton Gradient: a Practical Usage Guide" *Biotechniques* **2011**, 50 (2), 98-115.
54. Sato, N.; Fujimura, T.; Shimada, T.; Tani, T.; Takagi, S., "J-aggregate Formation Behavior of a Cationic Cyanine Dye on Inorganic Layered Material" *Tetrahedron Lett.* **2015**, 56 (22), 2902-2905.
55. Peng, C.-L.; Lai, P.-S.; Chang, C.-C.; Lou, P.-J.; Shieh, M.-J., "The Synthesis and Photodynamic Properties of meso-Substituted, Cationic Porphyrin Derivatives in HeLa cells" *Dyes Pigm.* **2010**, 84 (1), 140-147.
56. Zakavi, S.; Mojarrad, A. G.; Yazdely, T. M., "Facile Purification of meso-Tetra(pyridyl)porphyrins and Detection of Unreacted Porphyrin upon Metallation of meso-Tetra(aryl) porphyrins" *Macroheterocycles.* **2012**, 5 (1), 67-71.

57. Basel, Y.; Hassner, A., "Imidazole and Trifluoroethanol as Efficient and Mild Reagents for Destruction of Excess Di-tert-butyl Dicarboxylate [(BOC)₂O]" *Synthesis* **2001**, *4*, 550-552.
58. Liu, F.; Wang, M.; Wang, Z.; Zhang, X., "Polymerized Surface Micelles Formed Under Mild Conditions" *Chem. Commun. (Camb.)* **2006**, (15), 1610-2.
59. Gomes, M. C.; Woranovicz-Barreira, S. M.; Faustino, M. A.; Fernandes, R.; Neves, M. G.; Tome, A. C.; Gomes, N. C.; Almeida, A.; Cavaleiro, J. A.; Cunha, A.; Tome, J. P., "Photodynamic Inactivation of *Penicillium Chrysogenum* Conidia by Cationic Porphyrins" *Photochem. Photobiol. Sci.* **2011**, *10* (11), 1735-43.
60. Makpol, S.; Jam, F. A.; Khor, S. C.; Ismail, Z.; Mohd Yusof, Y. A.; Ngah, W. Z., "Comparative Effects of Biodynes, Tocotrienol-Rich Fraction, and Tocopherol in Enhancing Collagen Synthesis and Inhibiting Collagen Degradation in Stress-Induced Premature Senescence Model of Human Diploid Fibroblasts" *Oxid. Med. Cell. Longev.* **2013**, *2013*, 298574.
61. Wu, D.; Yotnda, P., "Production and Detection of Reactive Oxygen Species (ROS) in cancers". *JoVE* **2011**, *57*, 3357.
62. Nelson, J. D. "Stable, Water-Insoluble r-(+)-.Alpha.-Lipoic Acid Salt Useful for the Treatment of Diabetes Mellitus and its Co-morbidities" 24 Oct **2008**, *2008*.
63. Qasim, M. "Why Do My MTT Assay Results Sometimes Show Cell Viability of More Than 100%, or More Than the Control?".
https://www.researchgate.net/post/Why_do_my_MTT_assay_results_sometimes_show_cell_viability_of_more_than_100_or_more_than_the_control.
64. Avila, S. D.; Puntel, L. R.; Aschner, M., "*Toxicological Profile for Manganese*" U.S. Department of Health and Human Services Public Health Service: **2000**.
65. Avila, S. D.; Puntel, L. R.; Aschner, M., "*Dietary Reference Intakes: Vitamin A, Vitamin K, Arsenic, Boron, Chromium, Copper, Iodine, Iron, Manganese, Molybdenum, Nickel, Silicon, Vanadium, and Zinc*" Medicine, National Academy Press, Washington DC: **2011**.
66. Worley, G. C.; Bombick, D.; Allen, W. J.; Suber, R. L.; Aschner, M., "Effects of Manganese on Oxidative Stress in CATH.a Cells" *NeuroToxicology* **2002**, *23* 159-164.

67. Asayama, S.; Mori, T.; Nagaoka, S.; Kawakami, H., "Chemical Modification of Manganese Porphyrins with Biomolecules for New Functional Antioxidants" *J. Biomater. Sci. Polym. Ed.* **2003**, *14* (11), 1169-1179.
68. Castello, G.; Costantini, S.; Scala, S., "Targeting the Inflammation in HCV-Associated Hepatocellular Carcinoma: A Role in the Prevention and Treatment" *J. Transl. Med.* **2010**, *8*, 109.
69. Batinic-Haberle, I.; Tovmasyan, A.; Spasojevic, I., "An Educational Overview of the Chemistry, Biochemistry and Therapeutic Aspects of Mn Porphyrins--From Superoxide Dismutation to H₂O₂-Driven Pathways" *Redox Biol.* **2015**, *5*, 43-65.





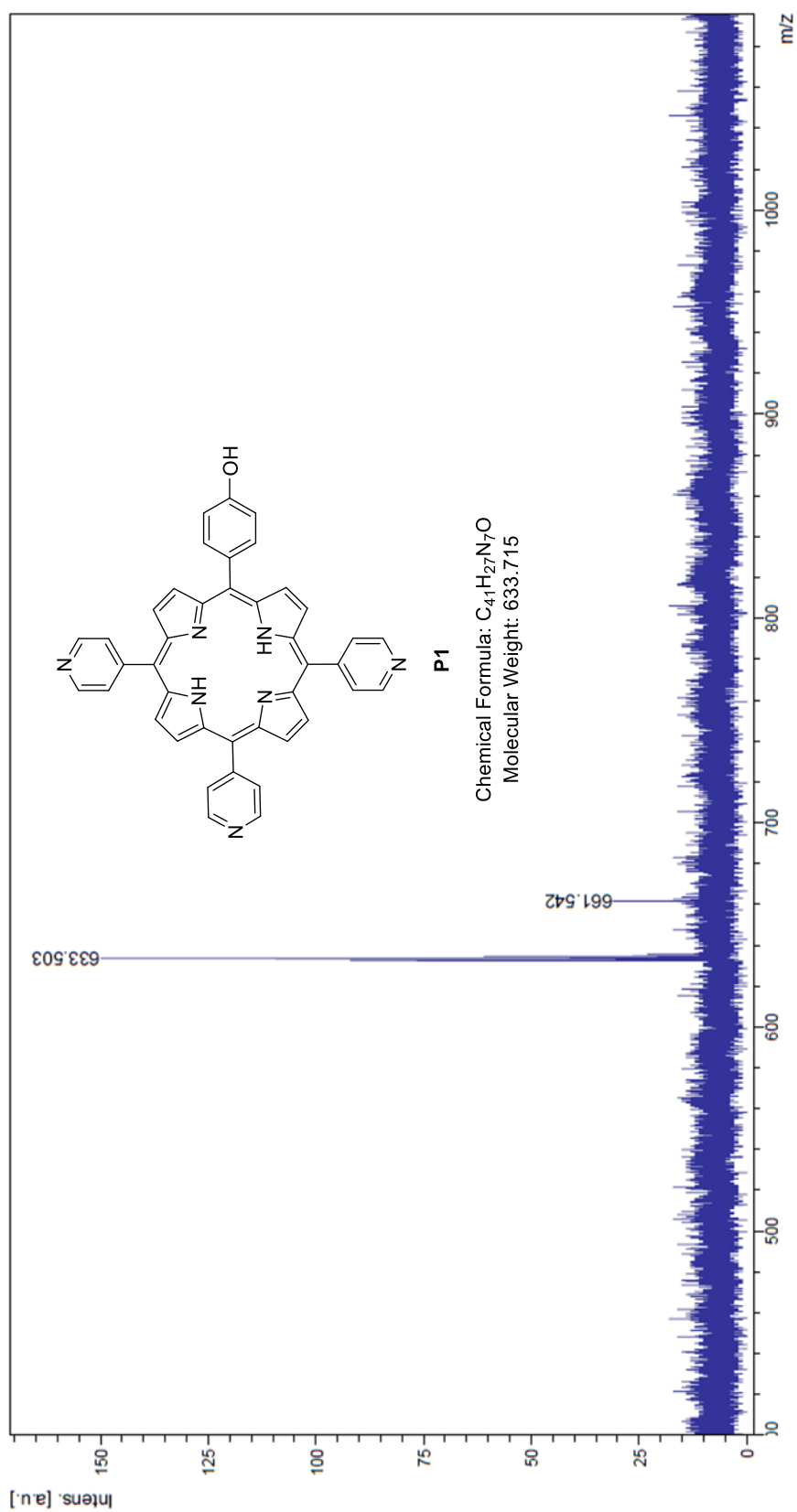


Figure A1: MALDI-TOF-MS of compound P1

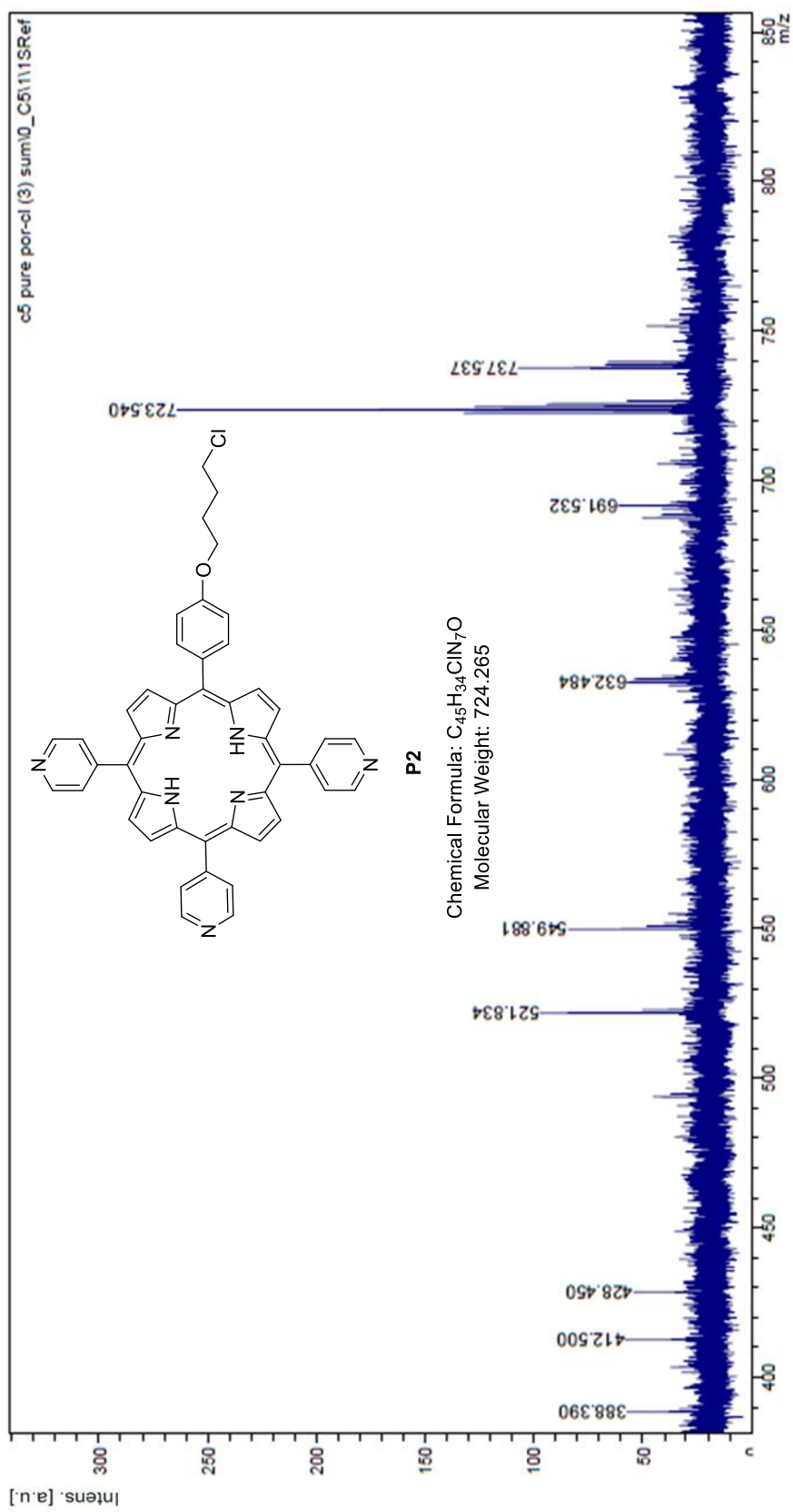


Figure A2: MALDI-TOF-MS of compound P2

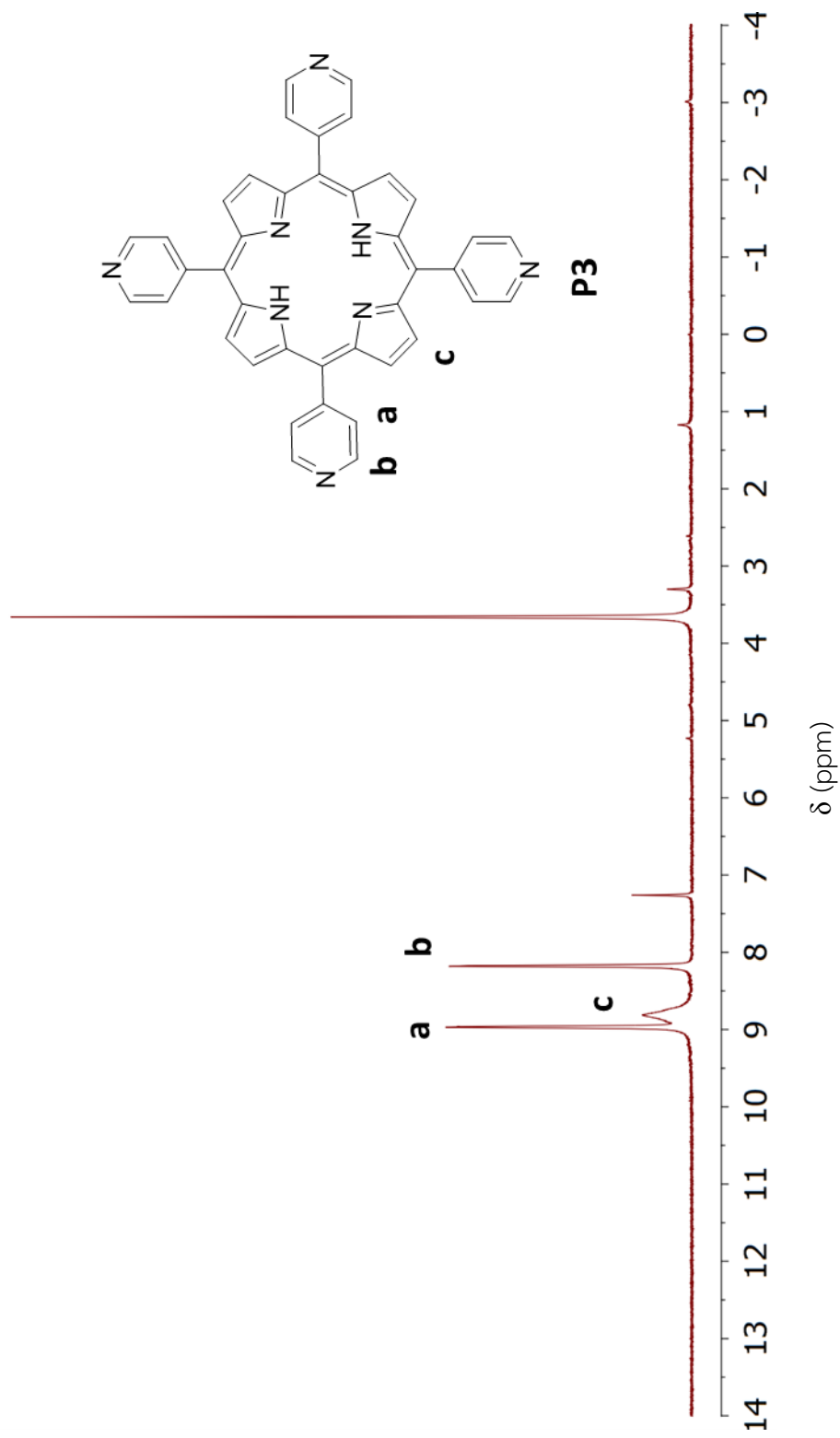


Figure A3: $^1\text{H-NMR}$ spectrum of compound **P3** in $\text{CDCl}_3/\text{MeOD}$

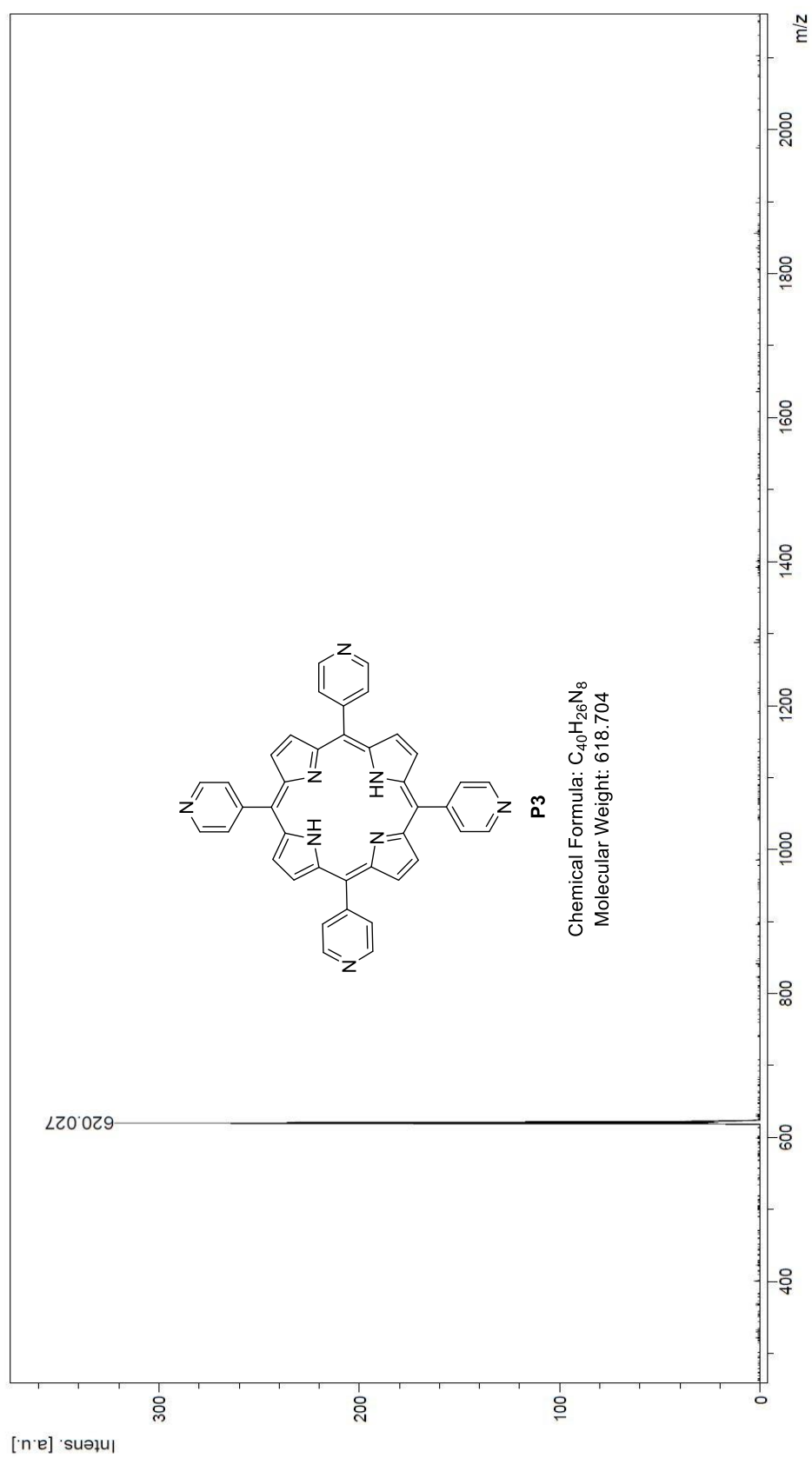


Figure A4: MALDI-TOF-MS of compound P3

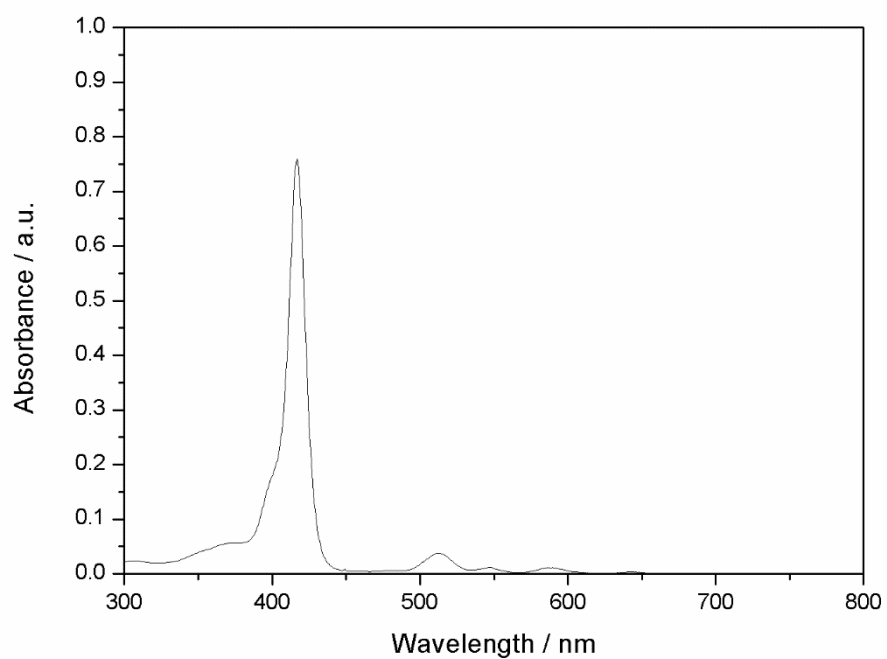


Figure A5: Absorption spectrum of compound P3 in CHCl₃/MeOH

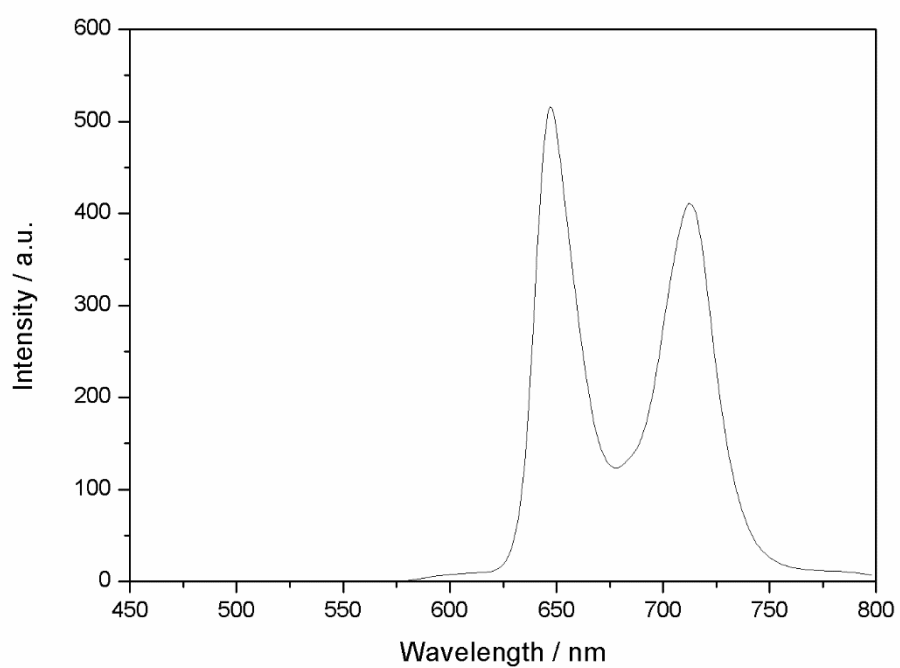


Figure A6: Emission spectrum of compound P3 in CHCl₃/MeOH

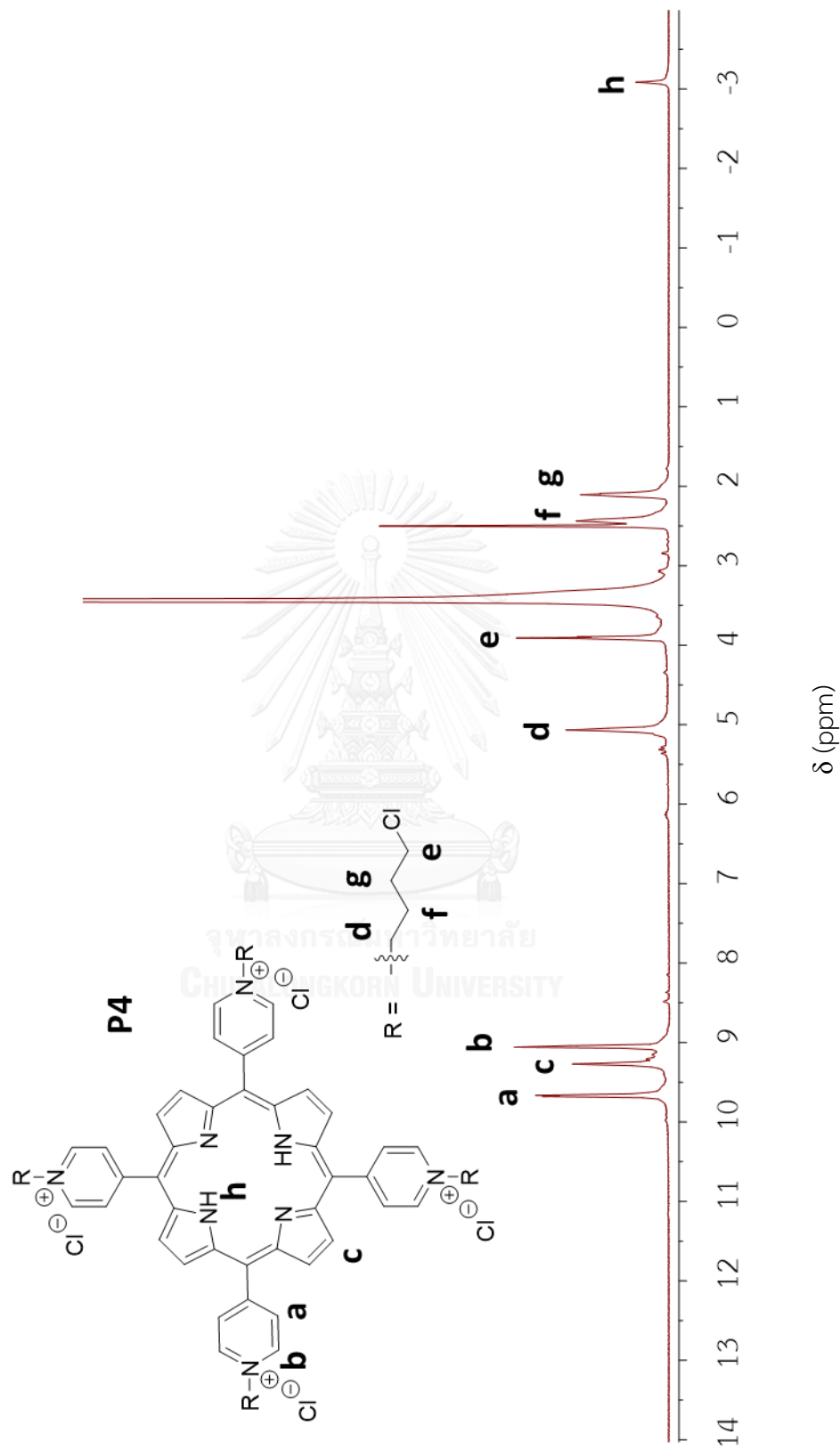


Figure A7: $^1\text{H-NMR}$ spectrum of compound **P4** in DMSO-d_6

Mass Spectrum List Report

Analysis Info

Analysis Name OSCU5703040011.d
Method MKE_tune_wide_20130204.m
Sample Name Por-Cl
Por-Cl

Acquisition Parameter

Source Type	ESI	Ion Polarity	Positive
Scan Range	n/a	Capillary Exit	300.0 V
Scan Begin	50 m/z	Hexapole RF	400.0 V
Scan End	3000 m/z	Skimmer 1	45.0 V
		Hexapole 1	25.0 V

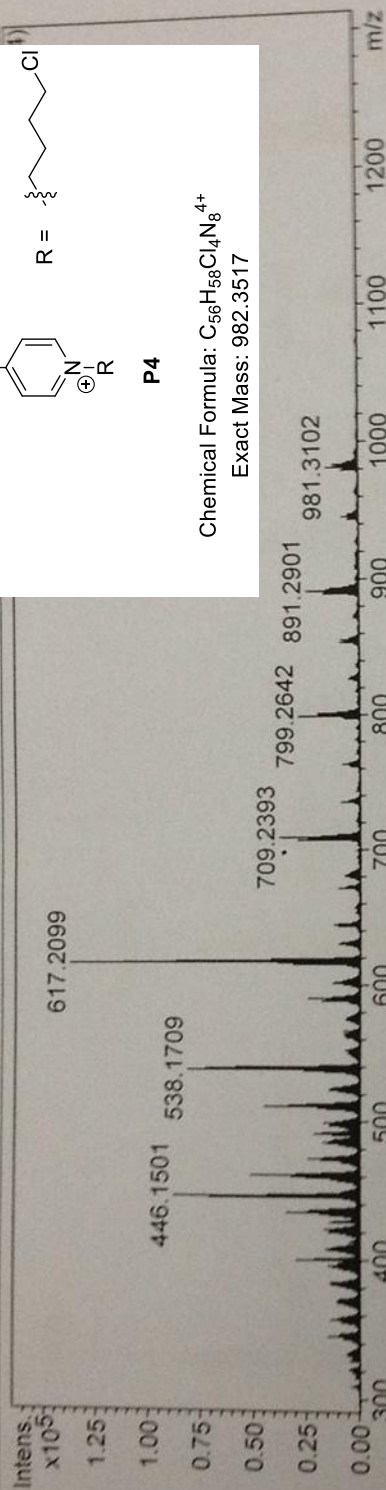


Figure A8: HR-ESI-MS of compound P4

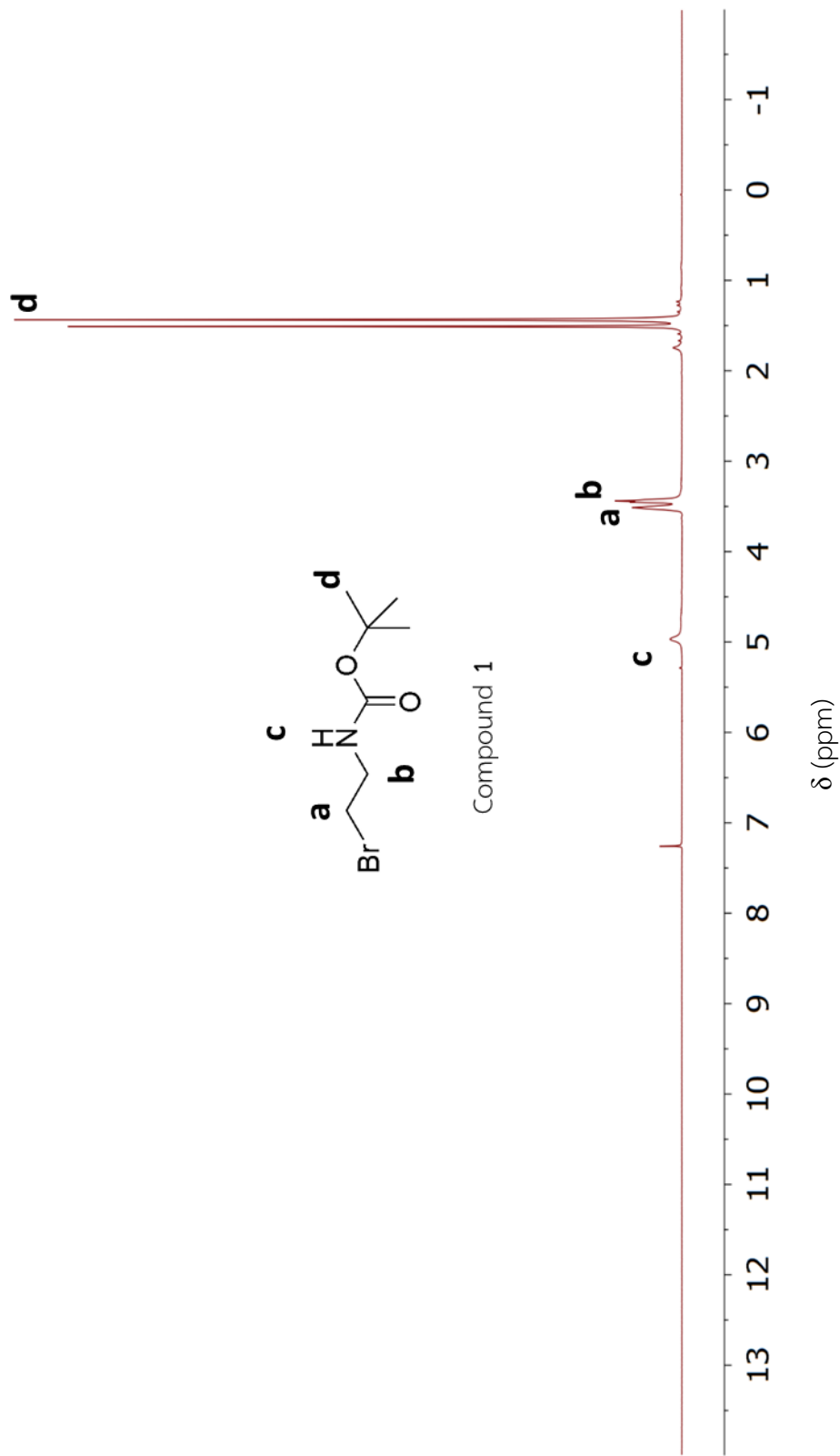


Figure A9: ¹H-NMR spectrum of compound **1** in CDCl₃

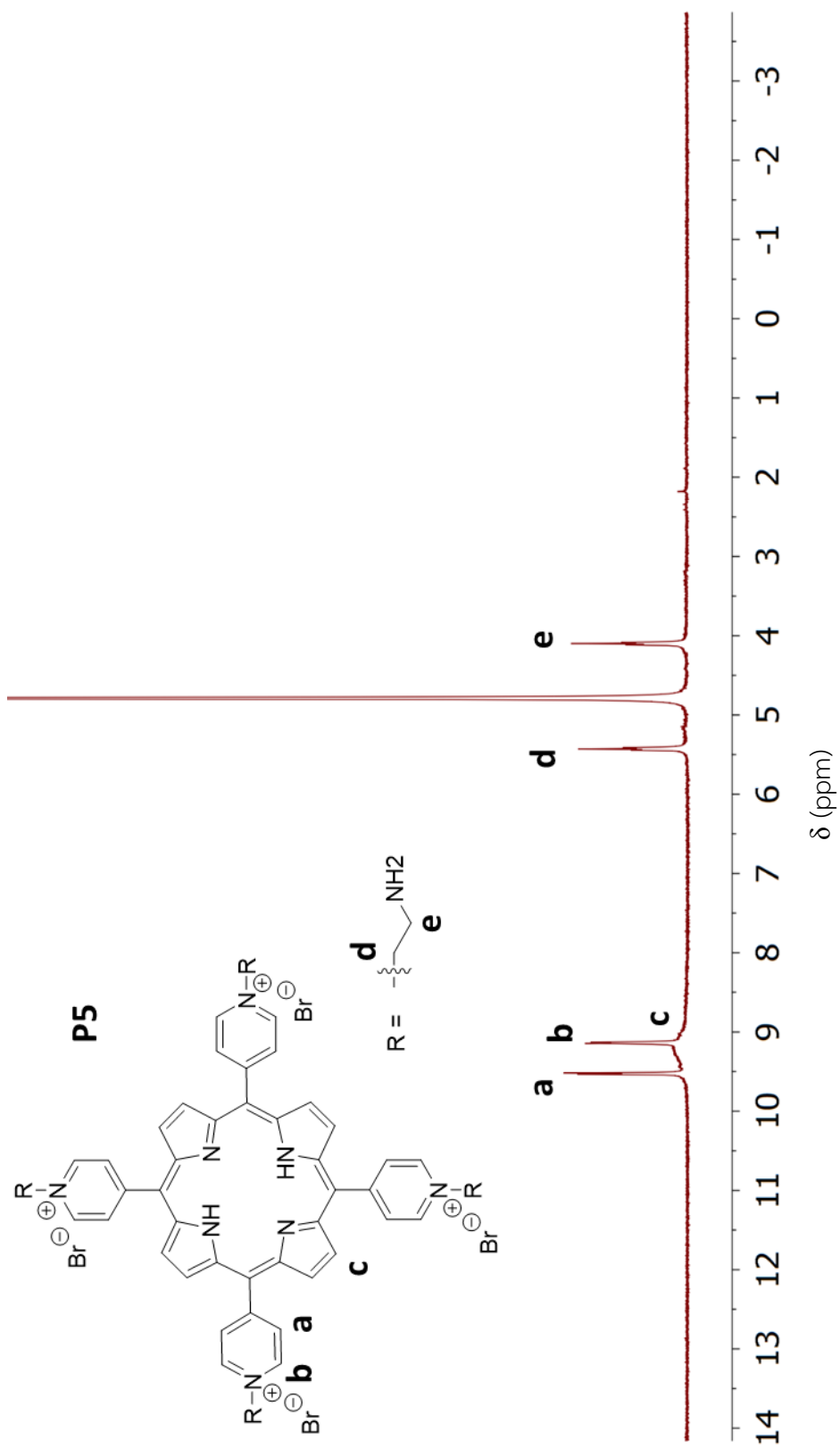


Figure A10: $^1\text{H-NMR}$ spectrum of compound P5 in D_2O

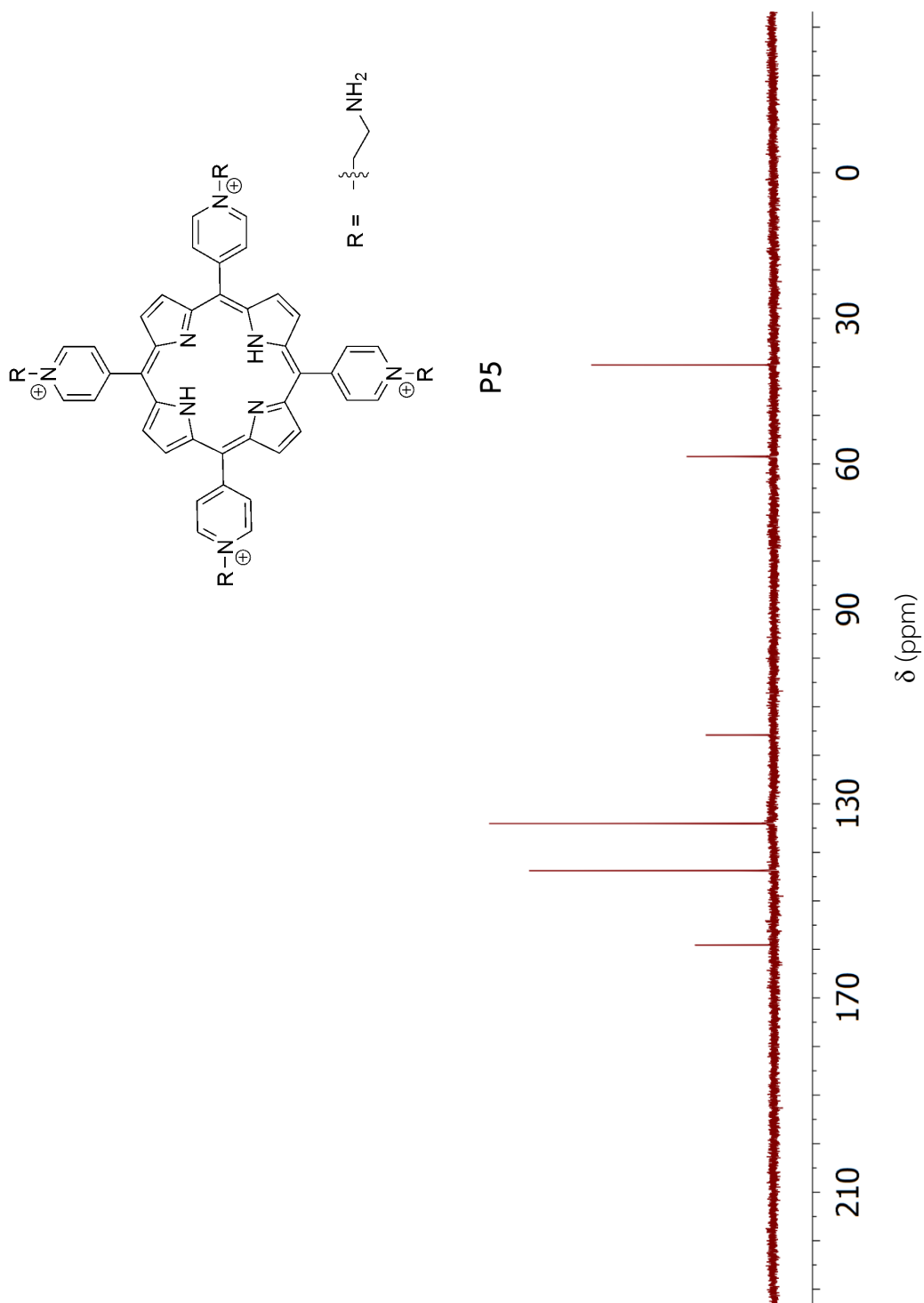


Figure A11: $^{13}\text{C-NMR}$ spectrum of compound **P5** in D_2O

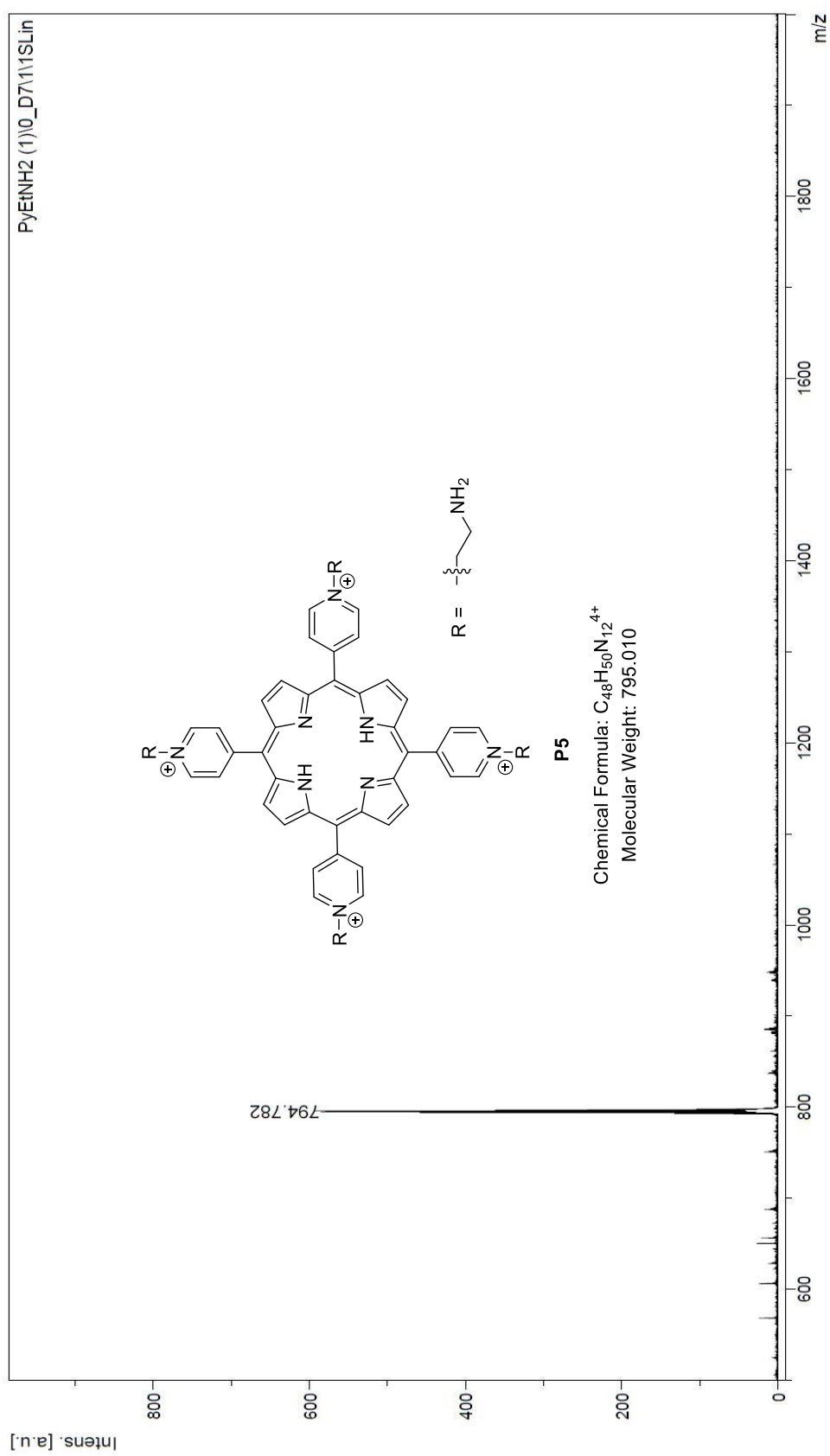


Figure A12: MALDI-TOF-MS of compound P5

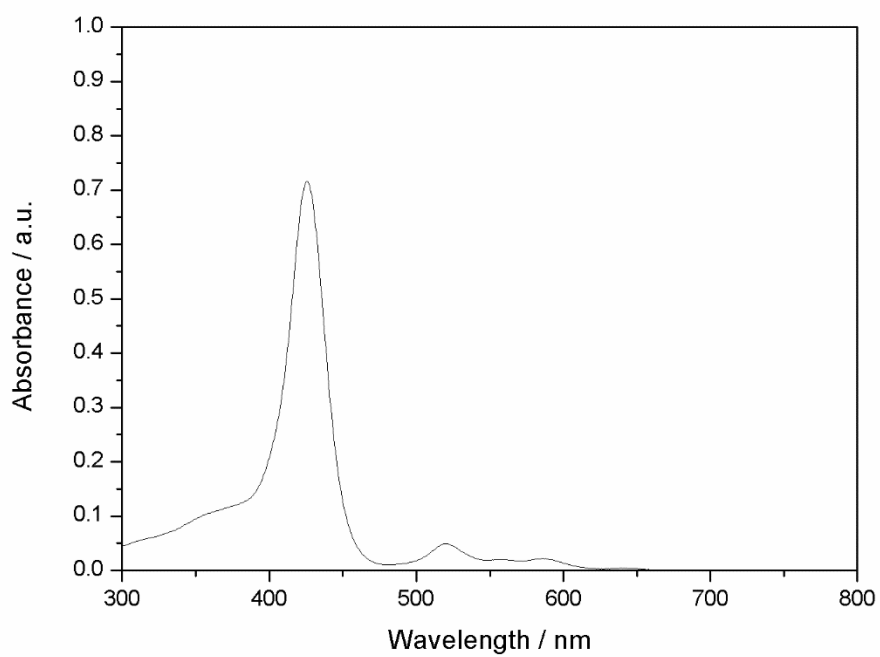


Figure A13: Absorption spectrum of compound P5 in D₂O

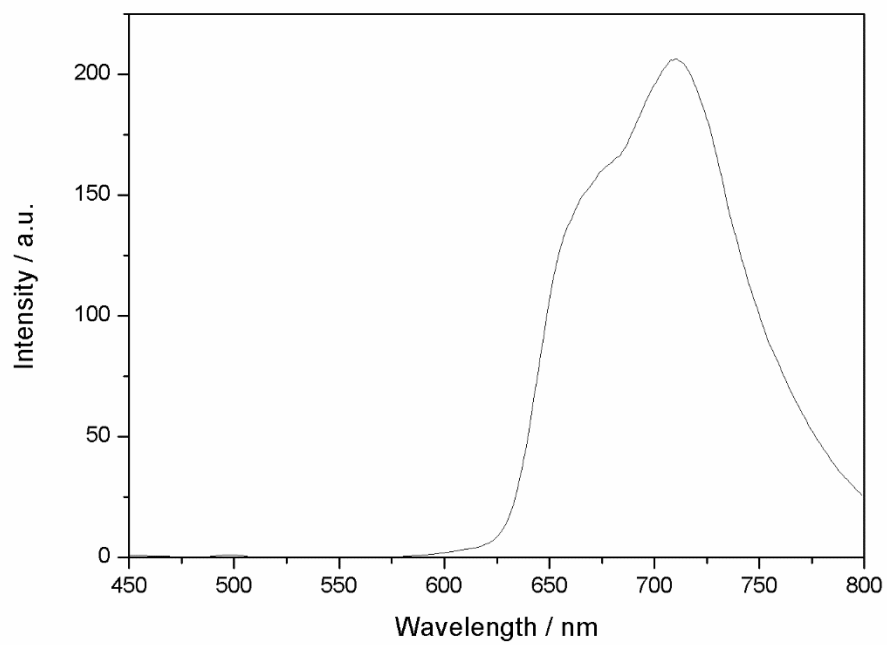


Figure A14: Emission spectrum of compound P5 in D₂O

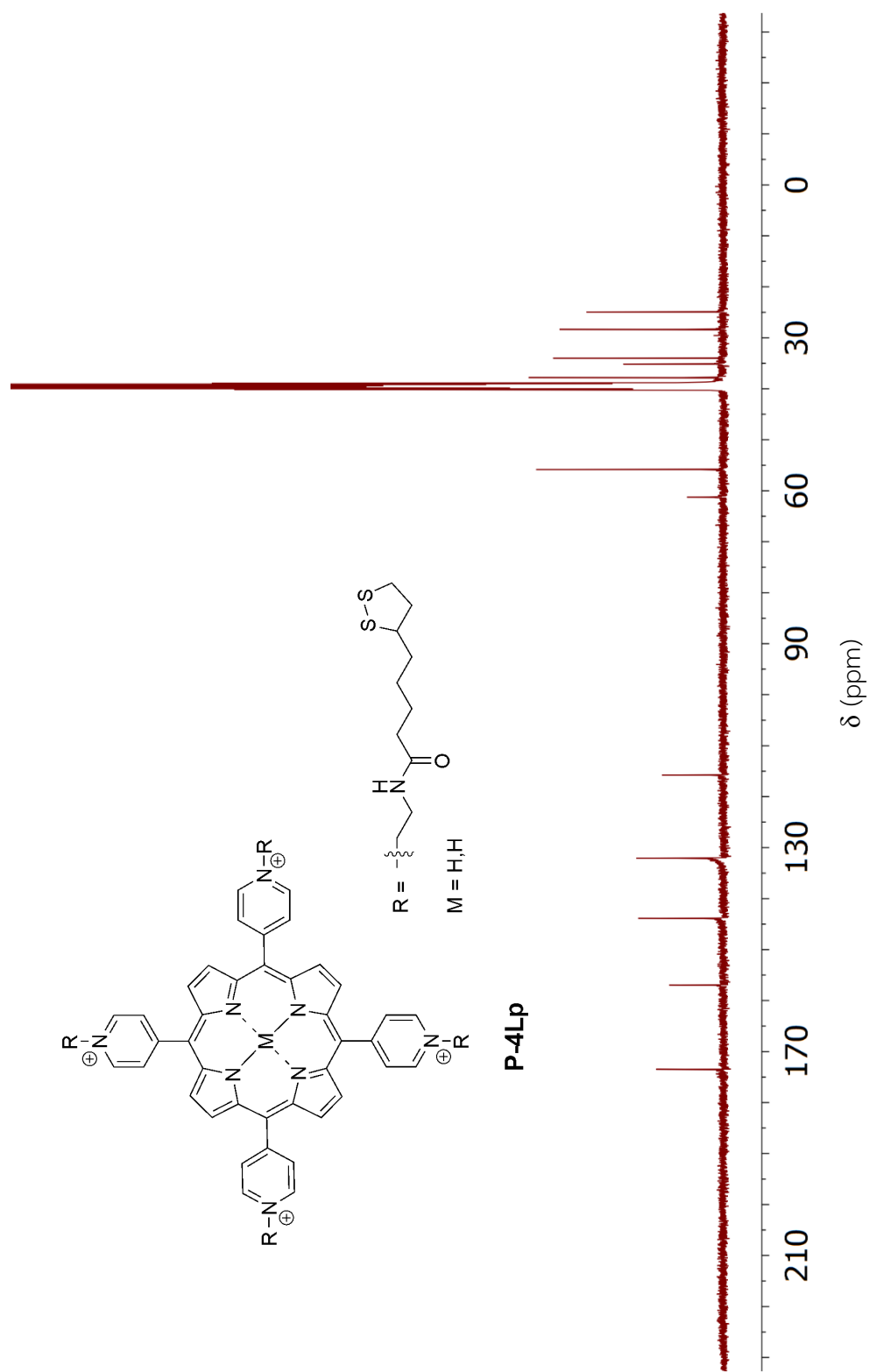


Figure A17: ¹³C-NMR spectrum of P-4Lp in DMSO

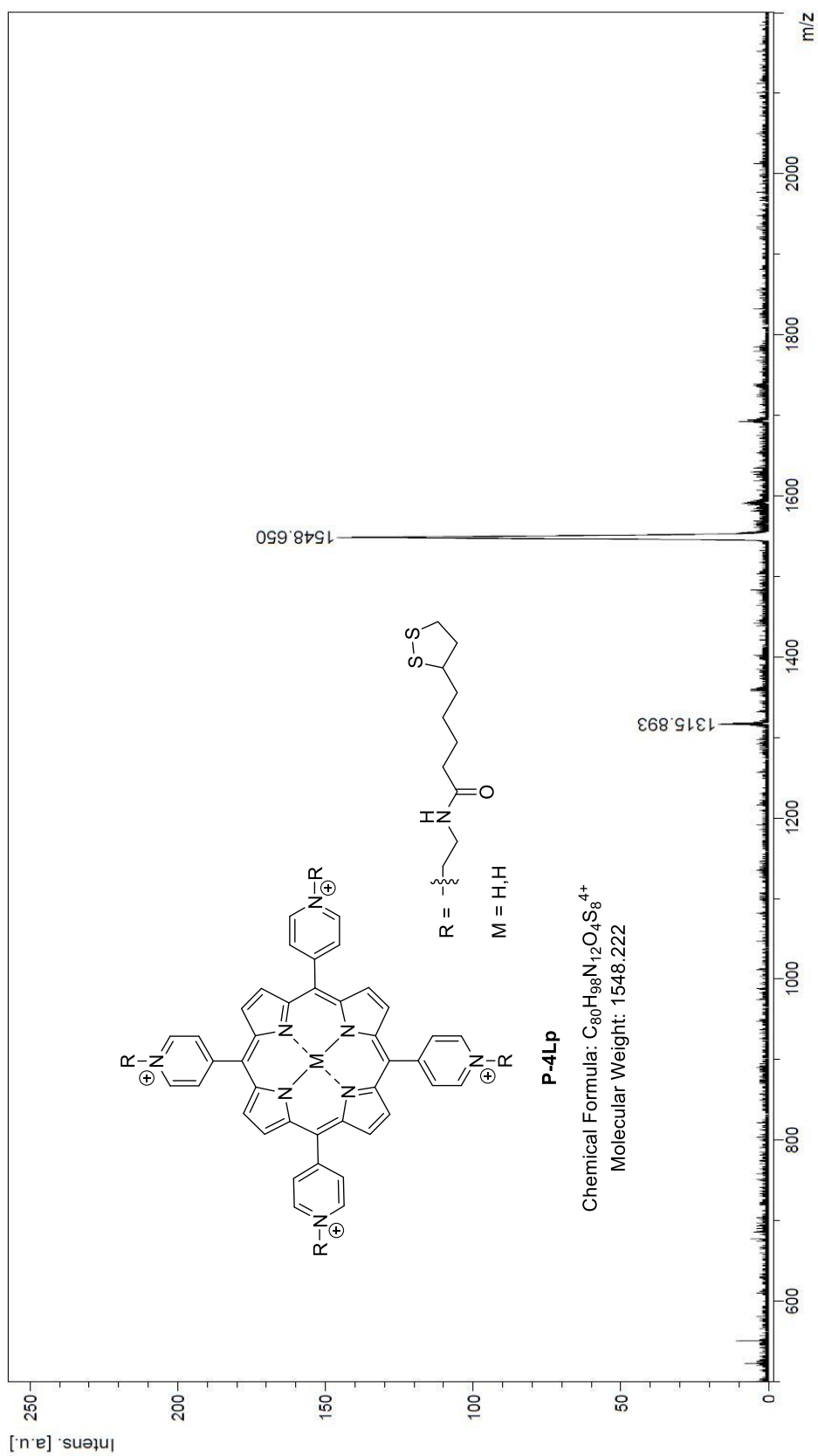


Figure A18: MALDI-TOF-MS of P-4Lp

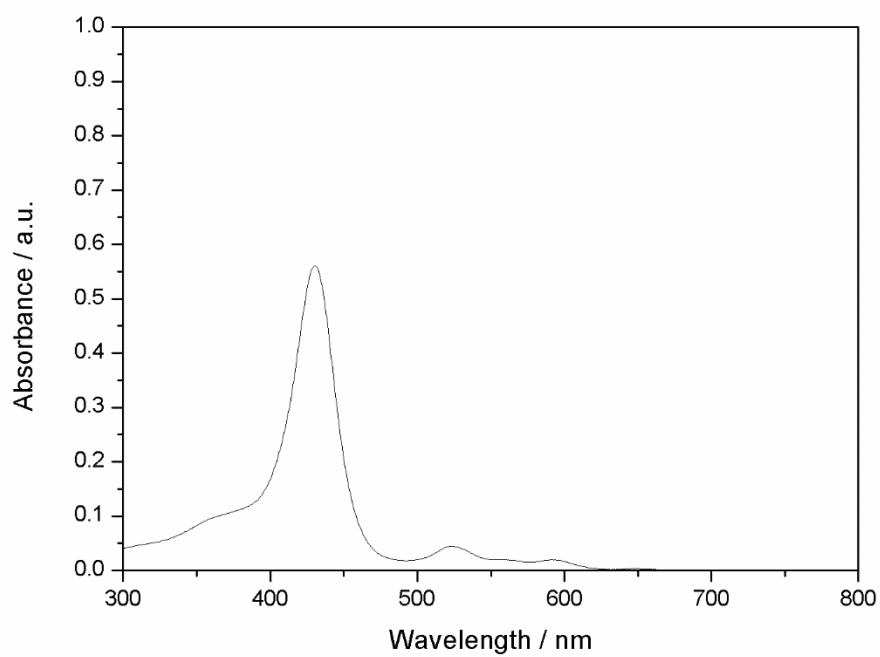


Figure A19: Absorption spectrum of P-4Lp in D₂O

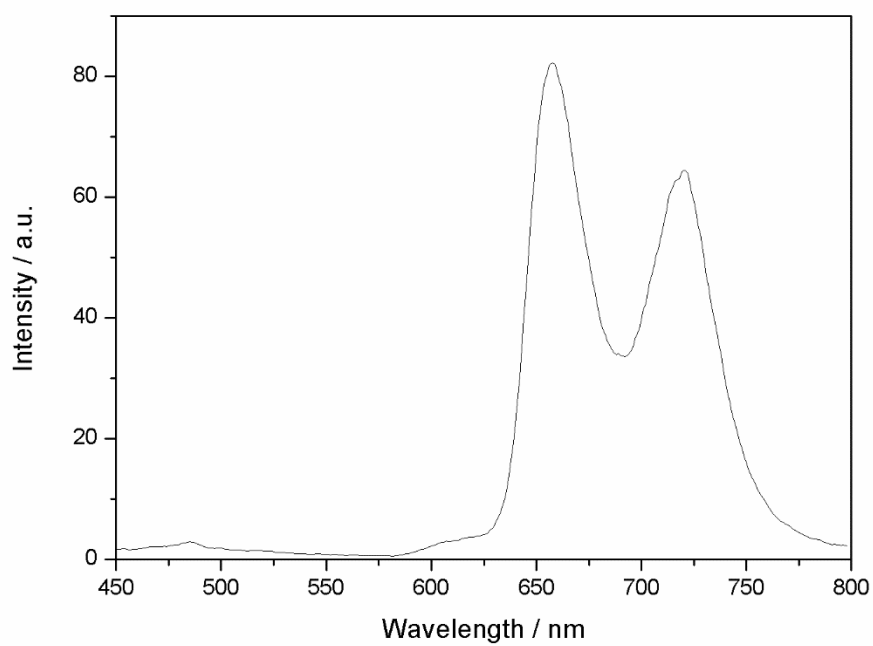


Figure A20: Emission spectrum of P-4Lp in D₂O

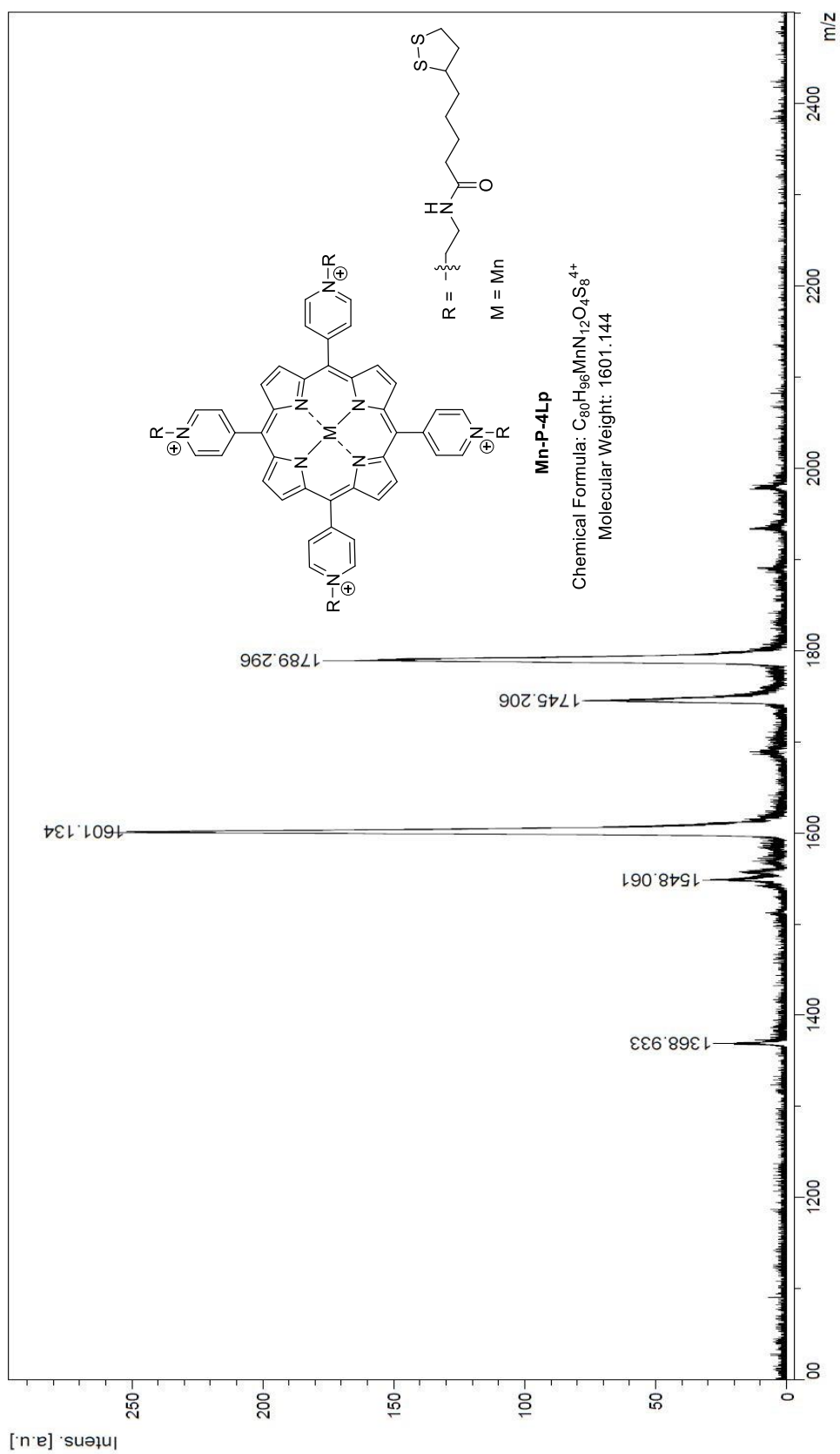


Figure A21: MALDI-TOF-MS of Mn-P-4Lp

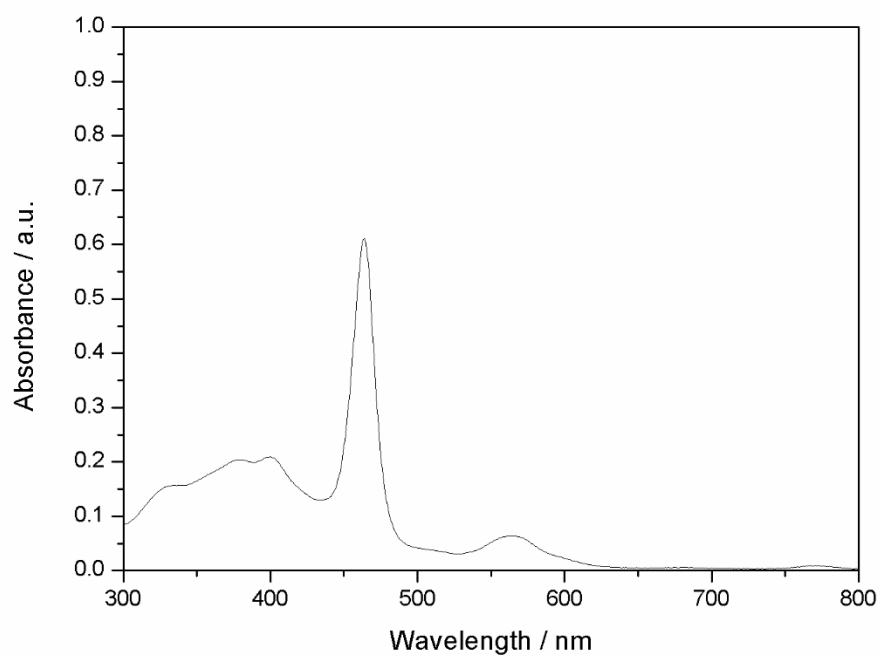
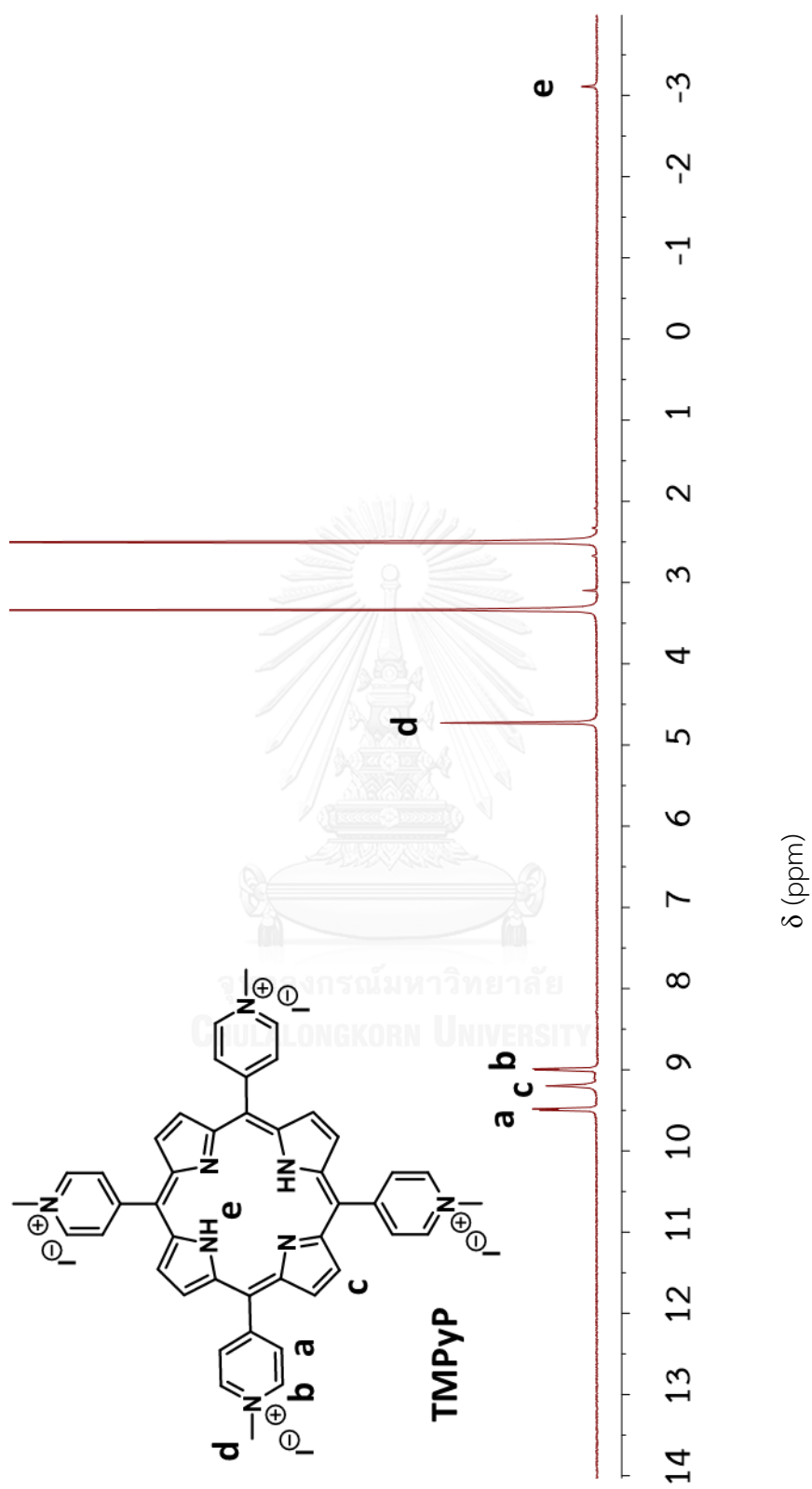


Figure A22: Absorption spectrum of Mn-P-4Lp in D₂O



Figure A23: $^1\text{H-NMR}$ spectrum of TMPyP in DMSO

VITA

Mr. Apiratt Thitimom was born on November 8, 1983 in Bangkok, Thailand. He received a Bachelor's Degree of Science, majoring in Chemistry from Faculty of Science, Chulalongkorn University in 2006. He also got a Master Degree program in Chemistry, majoring in Organic Chemistry, Faculty of Science, Chulalongkorn University, in 2010. He had presented his research on "Colorimetric Detection of DNA by Chemically Treated Silver Nanoparticles: A Preliminary Evaluation" Pure and Applied Chemistry International Conference (PACCON), Ubon Ratchathani University, 21-23 January 2010. After that, he graduated with Ph.D. degree in Organic chemistry at Chulalongkorn University in academic year 2016. During all of his studies periods, he got a scholarship from the development and promotion of science and technology talents project (DPST) scholarship (2002-2016) for financial support.